NBS TECHNICAL NOTE

463

Mössbauer Effect Study Of Magnetic Ordering in Copper-Rich Cu-Ni-Fe Alloys

U.S. DEPARTMENT OF COMMERCE
National Bureau of Standards

NATIONAL BUREAU OF STANDARDS

The National Bureau of Standards[1] was established by an act of Congress March 3, 1901. Today, in addition to serving as the Nation's central measurement laboratory, the Bureau is a principal focal point in the Federal Government for assuring maximum application of the physical and engineering sciences to the advancement of technology in industry and commerce. To this end the Bureau conducts research and provides central national services in three broad program areas and provides central national services in a fourth. These are: (1) basic measurements and standards, (2) materials measurements and standards, (3) technological measurements and standards, and (4) transfer of technology.

The Bureau comprises the Institute for Basic Standards, the Institute for Materials Research, the Institute for Applied Technology, and the Center for Radiation Research.

THE INSTITUTE FOR BASIC STANDARDS provides the central basis within the United States of a complete and consistent system of physical measurement, coordinates that system with the measurement systems of other nations, and furnishes essential services leading to accurate and uniform physical measurements throughout the Nation's scientific community, industry, and commerce. The Institute consists of an Office of Standard Reference Data and a group of divisions organized by the following areas of science and engineering:

Applied Mathematics—Electricity—Metrology—Mechanics—Heat—Atomic Physics—Cryogenics[2]—Radio Physics[2]—Radio Engineering[2]—Astrophysics[2]—Time and Frequency.[2]

THE INSTITUTE FOR MATERIALS RESEARCH conducts materials research leading to methods, standards of measurement, and data needed by industry, commerce, educational institutions, and government. The Institute also provides advisory and research services to other government agencies. The Institute consists of an Office of Standard Reference Materials and a group of divisions organized by the following areas of materials research:

Analytical Chemistry—Polymers—Metallurgy — Inorganic Materials — Physical Chemistry.

THE INSTITUTE FOR APPLIED TECHNOLOGY provides for the creation of appropriate opportunities for the use and application of technology within the Federal Government and within the civilian sector of American industry. The primary functions of the Institute may be broadly classified as programs relating to technological measurements and standards and techniques for the transfer of technology. The Institute consists of a Clearinghouse for Scientific and Technical Information,[3] a Center for Computer Sciences and Technology, and a group of technical divisions and offices organized by the following fields of technology:

Building Research—Electronic Instrumentation — Technical Analysis — Product Evaluation—Invention and Innovation— Weights and Measures — Engineering Standards—Vehicle Systems Research.

THE CENTER FOR RADIATION RESEARCH engages in research, measurement, and application of radiation to the solution of Bureau mission problems and the problems of other agencies and institutions. The Center for Radiation Research consists of the following divisions:

Reactor Radiation—Linac Radiation—Applied Radiation—Nuclear Radiation.

---

[1] Headquarters and Laboratories at Gaithersburg, Maryland, unless otherwise noted; mailing address Washington, D. C. 20234.
[2] Located at Boulder, Colorado 80302.
[3] Located at 5285 Port Royal Road, Springfield, Virginia 22151.

UNITED STATES DEPARTMENT OF COMMERCE
C. R. Smith, Secretary
NATIONAL BUREAU OF STANDARDS • A. V. Astin, Director

TECHNICAL NOTE 463

ISSUED AUGUST 1968

Mössbauer Effect Study of Magnetic Ordering in Copper-Rich Cu-Ni-Fe Alloys

L.J. Swartzendruber

Metallurgy Division
Institute for Materials Research
National Bureau of Standards
Washington, D.C. 20234

Sponsored by the Department of the Interior
Office of Saline Water, Contract No. 14-01-0001-1091

For sale by the Superintendent of Documents, U.S. Government Printing Office, Washington, D.C., 20402
Price $1.25.

ABSTRACT

The ^{57}Fe Mössbauer effect has been observed in a series of copper rich Cu-Ni-Fe alloys, and for two samples of gold rich Au-Fe. At low temperatures most of these alloys order magnetically and the Mössbauer effect spectra develop typical six-line hyperfine field structure. For dissolved Fe the room temperature Cu-Fe and Au-Fe spectra consist of a doublet superimposed on a central line. In Cu-Ni-Fe the spectra at room temperature consist of a doublet with no evidence of a central line when the Ni concentration is above 10 atomic percent. The doublet separations at room temperature (and their estimated uncertainties) are 0.69 $\pm$ 0.02, 0.58 $\pm$ 0.02 and 0.22 $\pm$ 0.04 mm/sec in Au-Fe, Cu-Fe, and Cu-Ni-Fe respectively. By observation of the spectra in a magnetic field the doublet structure is shown to be due to magnetic interactions between Fe and other Fe or Ni atoms. Isomer shifts, metallurgy in Cu-Ni-Fe alloys, sample preparation techniques, and the Mössbauer effect equipment developed are also discussed.

Key words: alloys; copper; nickel; iron; gold; Mössbauer effect; magnetism.

TABLE OF CONTENTS

LIST OF TABLES

LIST OF FIGURES

CHAPTER I

INTRODUCTION

Recoilless nuclear gamma-ray resonance in solids was discovered in 1958 by R. L. Mössbauer[1,2] and is generally referred to as the Mössbauer effect. Mössbauer effect spectroscopy has since proven itself a useful tool for studies in solid state physics. Many review articles and books covering the principles and applications are presently available.[3-17] The influence of the electronic environment on the nuclear gamma-ray transition energy of a Mössbauer nucleus causes observable hyperfine structure in a Mössbauer effect spectrum. The possibility of interpreting this structure in terms of the electronic and magnetic properties of the solid in which the Mössbauer nucleus is embedded is responsible for the large number of current solid state studies utilizing the Mössbauer effect.

One interesting application is the study of the formation and interaction of local moments in metals and alloys. The isotope ^{57}Fe is well suited to this study since it forms interacting local moments in many systems, has an easily observable Mössbauer effect with a narrow linewidth, and has a relatively long lifetime parent isotope (^{57}Co). The combination of nuclear properties and Mössbauer effect linewidth gives spectra in which it is possible to resolve magnetic fields on the order of a few kG. The nuclear properties of ^{57}Fe also make possible the observation of electric field gradients in a solid.

One recent application[18] of the ^{57}Fe Mössbauer effect has been

the study of the localized moment behavior of very dilute (<0.1%) Fe impurities in a series of nonmagnetic pure elements. The values for the localized moments found were in qualitative agreement with the moments derived from magnetic susceptibility measurements.[19] As the iron concentration is increased in those matrices where it forms a local moment, the interaction of these local moments brings about transitions to an ordered magnetic state at low temperature. The Mössbauer effect spectrum can be used to study the details of this transition.

Since the time Zener[20] suggested that magnetic ordering in some metals might arise from indirect magnetic coupling via the conduction electrons, there has been considerable interest in the magnetic properties of alloys in which the magnetic centers are dilute. Extensive measurements[21-25] have been performed on the Cu-Mn system by a number of techniques. Accordingly a great deal of theoretical work on magnetism in dilute alloys has been directed toward a description of this system.[26-30] The ^{57}Fe Mössbauer effect offers a sensitive technique to extend these studies to dilute magnetic alloys containing Fe.

In this thesis the ^{57}Fe Mössbauer effect was used to study Fe dissolved in copper-rich Cu-Ni alloys. Some experiments were also performed in the related AuFe system. The AuFe, CuFe and copper rich CuNiFe systems were found to possess many similarities in their magnetic behavior as observed by the Mössbauer effect. In addition to a transition to a low temperature magnetically ordered state they all appear to retain magnetic structure at higher temperatures. This magnetic structure manifests itself by the appearance of a poorly resolved doublet in the Mössbauer effect spectra of these alloys.

CHAPTER II

BACKGROUND

A. Related Measurements on Au-Fe, Cu-Fe and Cu-Ni. In their Mössbauer effect investigations of the Au-Fe system, Borg et al.[31] found magnetic transitions in alloys with as little as 0.84 atomic percent Fe. This was in disagreement with the earlier investigations of Kaufmann et al.[32,33] who concluded that AuFe alloys containing less than about 6.5% Fe were paramagnetic at all temperatures, while the more concentrated alloys appeared to have definite Curie temperatures. From the measurements of Kaufmann et al., Arrott[34] calculated a critical concentration for the Au-Fe system of 12% Fe. Sato et al.[27] took this to be in reasonable agreement with the theoretical value of 17% based on their cluster variation model for a dilute alloy with only nearest-neighbor interactions.

Lutes and Schmit[35] measured the magnetic susceptibility of several AuFe alloys and found a maximum in the reciprocal susceptibility suggestive of antiferromagnetic ordering. This interpretation is supported by the low induced moment of 0.63 μ_B per Fe atom measured by Henry[36] at 4.2°K in an applied field of 95 kG. This contrasts with the 2 μ_B per Fe atom for very dilute Fe in Au indicated by Lutes and Schmidt[35] as well as by the Mössbauer effect measurements of Kitchens et al.[37] Also, a Mössbauer effect spectrum[38] for a 5% Fe in Au alloy at 4.2°K in an applied field of 30.8 kG exhibited very little change from the spectrum observed at zero field. All these measurements indicate that, on the average, the magnetic ordering for AuFe with low

Fe concentration is antiferromagnetic. However, they do not specify the precise nature of the local ordering.

Mössbauer effect measurements[39,40] for dilute Fe in Cu have shown similar effects. However the study in Cu-Fe is more difficult due to the limited solubility of Fe, about 3% at 1000°C compared to about 60% for Fe in Au. It appears[40] that the ordering temperature is higher in Cu-Fe than in Au-Fe for equal Fe concentrations. However, in contrast to the Au-Fe system, the Mössbauer spectra in Cu-Fe remain complicated and unresolved well below the magnetic transition temperature. As pointed out by Housley[41] this is not expected from a model which utilizes a distribution of molecular fields which has a reasonable temperature dependence, such as the one proposed by Liu.[42]

From the measurements in Cu-Fe and Au-Fe it appears that the magnetic interaction must be longer range than first nearest neighbor, and oscillatory in sign. This is similar to the previously observed measurements in Cu-Mn alloys. Klein and Brout[28,29] have proposed a model in which the magnetic interaction couples the solute atoms within small clusters by means of an interaction of the RKKY type. This model proved successful in explaining the low temperature specific heat of Cu-Mn, Cu-Fe and Cu-Co. No well defined transition temperature exists in this model. Instead the randomly oriented moments become increasingly correlated in an antiferromagnetic manner as the temperature decreases.[43] While this is not inconsistent with the observations on the Cu-Fe system, it is not in agreement with the relatively well defined transition temperature found[39,44] for Au-Fe.

In further study of the Au-Fe system, Violet and Borg[45] found

structure in their Mössbauer effect spectra at high temperatures. This structure consisted of a doublet superimposed on a central singlet. The doublet was interpreted as being due to quadrupole effects arising from Fe-Fe pairs. The measurements made here have revealed that this doublet also exists in CuFe and Cu-Ni-Fe alloys at high temperature. It also appears that this doublet is of magnetic, rather than quadrupole origin. Since the interpretation of structure in Mössbauer effect spectra and the metallurgy of the Cu-Ni-Fe system are important to this study, they are discussed in some detail below in Sections B and C.

The properties of Cu-Ni alloys have been extensively studied by a number of techniques.[46-79] Of particular interest here are the conclusions of Goldman[49,50] and of Lang and Ehrenreich[79] that the simple rigid-band model[80] gives a poor approximation to the properties of Cu-Ni alloys. They propose a model in which d-holes are present on Ni atoms at all concentrations. Lang and Ehrenreich[79] emphasize, however, that a real justification of this model in terms of band theory for nonperiodic systems remains to be given.

B. Origin of ^{57}Fe Mössbauer Effect Line Structure. In iron the Mössbauer effect is observed for gamma-ray transitions between the ground state of the ^{57}Fe nucleus and its first excited state. The first excited state has a half life of 0.14 μ sec, a magnetic dipole moment $\mu_e = -0.155$ nuclear magnetons, a quadrupole moment $Q_e = 0.33$ b, and a spin $I_e = 3/2$. The gamma-ray transition energy to the ground state is 14.4 keV. The ^{57}Fe ground state has a spin $I_g = 1/2$ and a magnetic dipole moment $\mu_g = +0.0903$ nuclear magnetons.

The nuclear properties of ^{57}Fe allow the observation of Mössbauer effect line structure due to three interactions. The electrostatic interaction between the distributed positive charge of the nucleus and the electronic charge density that interpenetrates it gives rise to the isomer shift. The interaction between the nuclear magnetic dipole moment and the effective field at the nuclear site gives rise to magnetic hyperfine field splitting. Finally, the interaction between the nuclear electric quadrupole moment and the electric field gradient at the nuclear site gives rise to quadrupole splitting. These three interactions, along with their angular dependences and time and space fluctuations, are predominately responsible for the line structure observed in ^{57}Fe Mössbauer effect spectra.

1. Line Shapes. Mössbauer effect absorption lines are expected to be Lorentzian in shape, with a width determined by the lifetime of the excited level. However if the absorber is of finite thickness the shape of the energy distribution in the gamma-ray beam will be distorted as it passes through the absorber. This has been studied in detail by Fraunfelder et al.[81] They found that for $t < 10$ the shape of the absorption line is Lorentzian to within about 1/2% but has an increased linewidth, Γ, that can be approximated by

$$\Gamma = 2\Gamma_o\ (1.00 + 0.135t) \text{ for } 0 \leq t < 5$$
$$= 2\Gamma_o\ (1.01 + 0.145t - 0.0025\ t^2) \text{ for } 4 < t < 10 \qquad \text{II-1}$$

where $t = fn\sigma_o$ is the absorber thickness with f the recoil free fraction of the absorber, n the number of ^{57}Fe nuclei per unit area, and σ_o the resonance absorption cross section for a single nucleus.

2. Isomer Shift. This is a nuclear volume effect and results from the fact that the ground and excited states of the nucleus have different effective charge radii. The electrostatic interaction energy due to the overlap of electronic and nuclear charge is therefore different for the two levels and the γ-ray energy is shifted. Neglecting relativistic effects, one obtains for the isomer shift, s, the expression

$$s = \frac{4\pi}{5} Ze^2 \left[\left| \psi_a(o) \right|^2 - \left| \psi_s(o) \right|^2 \right] R^2 \frac{\Delta R}{R} \qquad \text{II-2}$$

where ΔR is the increase in nuclear radius of the excited state over the ground state (assumed $<< R$), Z is the nuclear charge, and $\left| \psi_a(o) \right|^2$ and $\left| \psi_s(o) \right|^2$ are the electron densities at the nuclear site in absorber and source respectively. Correction factors taking into account relativistic corrections to the electron wave functions have been given by Shirley.[82] These corrections can be as high as 30 percent for heavier nuclei. The centroid of the Mössbauer effect spectrum is also shifted by the second order Doppler effect.

Thus if a doublet is observed in a Mössbauer spectrum one possible origin is a non-homogeneous specimen. This could give Fe in two different environments, each with a different isomer shift.

3. Magnetic Hyperfine Splitting. The Hamiltonian for the interaction between the nuclear magnetic moment and a magnetic field can be written

$$H_m = - \vec{\mu}_I \cdot \vec{H}_{eff} \qquad \text{II-3}$$

where $\vec{H}_{eff}$ refers to the effective magnetic field at the nucleus. In ^{57}Fe the spin 3/2 excited level is split into four sublevels while the

spin 1/2 ground level is split into two sublevels. This gives rise to eight possible transitions, two of which are forbidden by the selection rules for M1 transitions. The six remaining transitions, along with their angular distributions are listed below in order of increasing energy:

Transition	Angular Distribution
$-3/2 \rightarrow -1/2$	$3(1 + \cos^2\theta)$
$-1/2 \rightarrow -1/2$	$4 \sin^2\theta$
$-1/2 \rightarrow +1/2$	$1 + \cos^2\theta$
$+1/2 \rightarrow -1/2$	$1 + \cos^2\theta$
$+1/2 \rightarrow +1/2$	$4 \sin^2\theta$
$+3/2 \rightarrow +1/2$	$3(1 + \cos^2\theta)$

Here θ is the angle between the magnetic field and the direction of propagation for the gamma-ray. This gives rise to the familiar six-line absorption pattern for iron metal (see Fig. III-4). A magnetic field oriented at random to the line of observation of the gamma-ray gives an intensity ratio of 3:2:1:1:2:3 for the six lines. If the magnetic field is longitudinal, i.e. points in the same direction as the direction of gamma-ray travel, the six lines will have an intensity ratio of 3:0:1:1:0:3 and only four lines will be observed. Finite thickness effects, instrumental broadening, and field distributions can serve to modify these theoretical ratios somewhat.

The effective field at the ^{57}Fe nucleus is usually large for Fe in a magnetic material below its transition temperature, -330 kG for Fe in metallic form at room temperature. The origin of this field has been discussed by Watson and Freeman[83] and by Marshall and Johnson.[84] The large value observed in iron metal is almost entirely due to core polarization.

4. Quadrupole Splitting. The Hamiltonian for the interaction between a nucleus with quadrupole moment, Q, and an electric field gradient, eq, at the nuclear site can be written

$$H_{eq} = \frac{e^2qQ}{4I(2I-1)} \left[3I_z^2 - I(I+1) + \frac{1}{2}\eta (I_+^2 + I_-^2) \right] \quad \text{II-4}$$

where

$$eq = V_{zz} = \frac{\partial^2 V}{\partial z^2} \quad \text{II-5}$$

with V the electric potential. The asymmetry parameter $\eta = (V_{xx} - V_{yy})/V_{zz}$ and $I_{\pm} = I_x \pm iI_y$. The z direction in the above Hamiltonian is taken in the direction of the principle axis of the electric field gradient. If the field gradient has axial symmetry $V_{xx} = V_{yy}$ and $\eta = 0$. Thus η is a measure of the deviation from axial symmetry. For cubic or spherical symmetry each of the $V_{ii} = 0$ and the quadrupole interaction vanishes.

Consider the case of axial symmetry. The ground state of ^{57}Fe has Q = 0 and thus is not affected. The excited state, with spin 3/2 is split into two levels with separation

$$\Delta = eQV_{zz}/2 \quad \text{II-6}$$

resulting in two possible transitions and a Mössbauer spectrum with two lines. The angular distributions for the two transitions are given by:

Transition	Angular Distribution
$\pm 3/2 \rightarrow \pm 1/2$	$1 + \cos^2\theta$
$\pm 1/2 \rightarrow \pm 1/2$	$5/3 - \cos^2\theta$

Here θ is the angle between the principal axis of the electric field gradient and the direction of gamma-ray propagation. If the electric field gradient is randomly oriented the average intensity is the same

for both transitions. However if the recoil free fraction were to have an angular dependence, the average intensity could be different for the two transitions. This would result in a Mössbauer spectrum with the appearance of an asymmetric doublet. This is generally referred to as the Goldanskii effect.[85]

The origin of electric field gradients in metals has been discussed by Watson et al.[86,87] They can be expressed as

$$q = q_{latt} (1 - \gamma_\infty) + q_{loc} (1 - R_Q) \qquad \text{II-7}$$

where q_{latt} is the field gradient due to charges outside an atomic sphere centered at the nucleus in question, and q_{loc} is the field gradient due to conduction electrons within the atomic sphere. The factors γ_∞ and R_Q are Sternheimer[88] antishielding factors. In this thesis we will not be preoccupied with the source of field gradients. Main interest will center on determining if a given interaction is of magnetic or quadrupole origin.

5. Combined Magnetic and Quadrupole. If the principal axis of the electric field gradient tensor is not in the same direction as the magnetic field, no closed form solution is possible for this case. In general the magnetic substates will be mixed by the quadrupole interaction and all eight possible transitions will be allowed, yielding complex spectra. If $e^2qQ/\mu H \ll 1$ and the electric field gradient is axially symmetric the energy levels of the excited state will be given by

$$E = -\mu_e H M_I + (-1)^{|M_I|} + 1/2 \frac{eqQ}{4} \frac{3\cos^2\theta - 1}{2} \qquad \text{II-8}$$

where θ is the angle between the magnetic field and the electric field gradient.

For the more complex situations where e^2qQ and μH are comparable and the angle between the electric field gradient tensor principal axis and the magnetic field may be at random, it is advantageous to use machine computations. Computer methods for performing such computations for a wide variety of experimental situations have been developed by Gabriel and Ruby.[89] The use of these calculations for the case of ^{57}Fe has been described in detail by Collins and Travis.[90]

6. Relaxation Effects. The effect of fluctuating magnetic fields and electric field gradients on Mössbauer effect spectra have been recently considered by a number of authors.[91-101] The presence of these relaxation effects can, for example, distort the shape of a quadrupole doublet giving it an asymmetric appearance, cause a magnetic field splitting to be observed in a paramagnetic material, and distort the shape of a six-line magnetic hyperfine pattern.

Consider ^{57}Fe in a matrix in which there are a number of unpaired electrons at the iron site giving a resultant spin S_z along the axis of quantization. The presence of this spin results in an effective field H_z at the nucleus, established mainly through the mechanism of core polarization.[87] Even in a magnetized material the spin S_z will undergo a constant motion, due to spin-spin and spin-lattice relaxation mechanisms, which can be characterized by a spin flip frequency Ω. In a magnetized material S_z will spend, on the average, more time in one direction than in the other. The magnetization is expected to be proportional to $\langle S_z \rangle$, and hence $\langle H_z \rangle$ to the magnetization. If the

spin flip frequency is much greater than the Larmor frequency $\omega_L = \mu H_z/\hbar$ then the observed energy level splitting will be proportional to $\langle H_z \rangle$ and hence to the magnetization. If the spin flip frequency is very small compared to the Larmor frequency then the observed energy level splitting will be proportional to H_z rather than to $\langle H_z \rangle$. Thus even in paramagnetic materials in which $\langle H_z \rangle = 0$ it is possible to observe a magnetic hyperfine splitting if the spin flip frequency is very low. In the intermediate case, where the spin flip frequency and Larmor frequency are of comparable magnitude, complex spectra with broad lines are expected.[91] These expected spectra are very similar to those obtained in the presence of a hyperfine field distribution.

For the case of pure Fe metal we have $H_z = -330$ kG, $\omega_L = 1.6 \times 10^8$ rad/sec for the excited state and $\omega_L = 2.8 \times 10^8$ rad/sec for the ground state. Thus if the spin relaxation time is much less than about 10^{-8} sec one expects the magnetization and observed magnetic hyperfine splitting to be proportional. In metals this is usually assumed to be the case. In pure Fe metal the careful measurements of Preston et al.[102] have shown that the observed H_z is closely proportional to the magnetization, and that there is no observable broadening of the individual lines as a function of temperature. Thus no relaxation effects are apparent in pure Fe metal. Although there are hints[45,102] that relaxation effects might be present in, for example, dilute Fe in Pd or Au, their existence for Fe in metallic form has been definitely established only in the case of large super paramagnetic precipitates.[104,105] In this case the Mössbauer effect spectra show changes over a wide temperature range. Such behavior has not been detected

in this study.

C. Metallurgy of the Cu-Ni-Fe System. Because of its importance to this study the metallurgy of the Cu-Ni-Fe ternary alloy system will be discussed briefly. This system has the simplifying feature that it contains only body-centered-cubic (bcc) and face-centered-cubic (fcc) crystal structures (with the exception of the composition Fe_3Ni which attains the ordered Cu_3Au ($L1_2$) structure). However, the metallurgy of the system is quite complex and cannot be considered to be completely understood at present. We will first consider the associated binary systems and then the ternary system. The binary and ternary diagrams are shown in Fig. II-1.

1. The Cu-Ni Binary System. The Cu-Ni binary system forms only a fcc structure and has a complete range of solid solubility.[107] Homogeneous solid solutions at any composition can be prepared by a melting, quenching, and homogenizing procedure. However, a number of studies have indicated a tendency for a small amount of clustering to occur.[108-114] The tendency towards clustering has recently been studied in a neutron diffraction experiment by Mozer et al.[115] They found that, for a $Cu_{0.525}Ni_{0.475}$ sample, furnace cooled from 1021°C, the probability of finding a Ni atom in the first coordination shell of a given Ni atom was enhanced from the random probability of 0.475 to 0.542. In the second coordination shell the probability of finding Cu atoms was enhanced. On the basis of small angle X-ray scattering a much larger clustering tendency was reported by Kirdon.[116] Thus, although the amount is an open question, it is clear that there is some tendency for clustering in Cu-Ni alloys.

2. The Fe-Ni Binary System. Face-centered-cubic γ-Fe is completely soluble[107] in nickel which is also fcc. Equilibrium is difficult to achieve in the mixed bcc and fcc (α + γ) field (Fig. II-1) since the $\alpha \underset{\rightarrow}{\leftarrow} \gamma$ transformation on heating or cooling is the martensitic type. It is possible to maintain $Fe_{70}Ni_{30}$ in the fcc phase down to about 0°C. The order-disorder transformation around $FeNi_3$ (which attains the ordered Cu_3Au structure) covers a wide range of composition, about 50-80% Ni.[117]

3. The Cu-Fe Binary System. The solubility of Fe in Cu or of Cu in Fe is small. According to the copper-rich end of the diagram[107] the solubility of iron in copper reduces from about 3.0 at.% at 1060°C to practically zero at room temperature.

Only a small amount of Fe can thus be retained in solid solution in pure Cu. At room temperature the equilibrium structure is almost pure Cu and α-Fe. Precipitation of Fe in a copper-rich Cu-Fe solid solution consists first in the formation of coherent particles (Guinier-Preston zones) of γ-Fe which can later transform to α-Fe if they reach sufficient size or if the alloy is cold worked. The formation of the γ-Fe precipitates was first suggested by Bitter et al.[118,119] on the basis of magnetic susceptibility measurements.

The realization that the initially paramagnetic Fe precipitates could be made ferromagnetic after cold working or extended aging at elevated temperatures led Smith[120] to suggest that the paramagnetic precipitate might well be fcc and coherent with the Cu matrix, while the ferromagnetic precipitate could be identified with the more stable bcc α-Fe structure.

In an attempt to confirm Smith's suggestion, Denney[121,122] studied a Cu-2.4% Fe alloy. His samples were first solution annealed at 1060°C, then quenched. The samples were then precipitation annealed at temperatures up to 800°C. Magnetization measurements revealed no ferromagnetic precipitates. After cold working at room temperature to start the $\gamma \rightarrow \alpha$ transformation the samples were again raised to the annealing temperature for one minute to complete the $\gamma \rightarrow \alpha$ transformation. The samples were now ferromagnetic and their saturation magnetization was measured in a field of 10 kG. Denney concluded that the precipitation process proceeded as a diffusion limited growth process characterized by an activation energy of 1.65 $\pm$ 0.1 eV.

The precipitation behavior of Cu-rich Cu-Fe was also studied by Newkirk[123] who combined X-ray diffraction, hardness measurements, and optical and electron microscope observations on a Cu-2.5% (wt.) Fe alloy. After solution treatment at 1050°C for one hour and quenching the sample in wire form the Debye-Scherrer X-ray patterns indicated a single fcc phase with a_o = 3.615 Å. After an anneal at 600°C for 600 hours a weak fcc phase with a_o = 3.590 Å was indicated identically oriented with a strong fcc phase with a_o = 3.616 Å. After cold working at 20°C evidence for the weak fcc phase weakened and faint bcc lines with a_o = 2.864 Å were observed.

The $\gamma \rightarrow \alpha$ martensitic transformation was further studied by Easterling and Meik-Oja[124] in a Cu-1.95 wt.% (2.21 at.%) Fe alloy using rough magnetic measurements and electron microscope observations. They showed that precipitation of the γ-phase for this composition begins

at all temperatures in the range 550 - 750°C. Nucleation was found to occur homogeneously leading to fully coherent spherical precipitates. With a prolonged precipitation anneal, γ-Fe precipitates were found to grow, lose their full coherency and take on a cubic shape. Finally, after prolonged annealing, stable γ-precipitates would nucleate from large cubic γ-precipitates or directly on dislocations of the matrix as well as at grain boundaries. The rough magnetic measurements showed a drop in magnetic force upon precipitation of γ-Fe, which would indicate, as did Bitter et al.'s measurements[118,119] that the μ_B value of γ-Fe is only a fraction of that for Fe dissolved in Cu.

4. The Ternary System. Bradley et al.[125] studied the Cu-Ni-Fe phase diagram using X-rays. The criterion used for a single phase alloy was, as in most X-ray studies, that only a pattern typical of the single phase is detected, for a two-phase alloy the superimposed lines for both phases would be detected, etc. The ternary diagram determined by Bradley et al. for slowly cooled alloys (from 900°C to 300°C at 20°C/hour) is shown in Fig. II-1. The alloys within the dotted line did not give a normal two phase pattern, but showed indications that decomposition of the original single-phase structure had already begun. The positions of the single phase boundaries at several elevated temperatures were also determined by Bradley et al.

Palmer and Wilson[126] studied the solubility of Fe in Cu-Ni alloys containing 2 to 10 percent Ni by using the metallurgical techniques of etching, magnetic colloids, and polarized light microscopy. Their results did not confirm the increased solubility hump around 10 percent Ni shown in the results of Bradley et al.[125] Their alloys contained

about 0.3% Mn as an impurity and it is not known what effect this would have on the Fe solubility. Kneller et al.[127,128] studied $Cu_{0.74}Ni_{0.24}Fe_{0.02}$ after aging at 600°C by electron microscopy and magnetic susceptibility. The results indicated that Fe-Ni rich ferromagnetic particles of essentially spherical shape were coherently and randomly precipitated in a Cu-rich paramagnetic matrix. The alloy was first solution heated at 1073°K and quenched. No precipitation for this treatment was reported. Aging for 25 minutes at 873°K was reported to produce particle sizes about 40 Å in diameter. The limit of resolution was reported to be about 20 Å diameter. This result appears consistent with the trends shown for Fe solubility in Cu-Ni alloys by Palmer and Wilson.[126]

Ham et al.[129] during a study of fatigue in Cu-Ni-Fe alloys made electron microscope observations of precipitation in Cu-17.3 Ni-17.3 Fe. The alloy was first solution treated at 1000°C and then quenched. After aging for one hour at 640°C large numbers of small precipitates less than about 250 Å in diameter were observed uniformly distributed throughout the sample. After aging 2.5 hours at 640°C a modulated structure developed with the particles appearing to be linked into a lattice of rods spaced about 250 Å apart.

Hillert et al.[130] studied the formation of side bands in the X-ray patterns of $Cu_{1-x}(Ni_{0.7}Fe_{0.3})_x$ alloys. (These side bands were first observed by Bradley et al.[125] within the dotted line region of Fig.II-1.) They interpreted their results in terms of the formation of modulated structures with periodic variations in composition brought about by the simple interchange of atoms (spinodal decomposition).

The precipitation in these $Cu_{1-x}(Ni_{0.7}Fe_{0.3})_x$ alloys was also studied by Najarajan and Flinn[131] using the Mössbauer effect. They showed that the segregation of these alloys into two phases includes, at any stage of decomposition, only two rather definite compositions and not a continuous range of compositions. They interpreted this as evidence against the formation of a modulated structure.

CHAPTER III

EXPERIMENTAL PROCEDURE

A. Sample Preparation. Samples were prepared by plating a starting foil with iron isotopically enriched in ^{57}Fe followed by diffusion and heat treatment.

The Cu-Ni starting foils were prepared from 99.999 percent Cu and 99.99 percent Ni arc melted together in the required proportions in an argon atmosphere.[132] The resulting alloys were cold rolled to thicknesses of 12 and 25 μm. Pure Cu foil and seven compositions of Cu-Ni foil were prepared. The Cu-Ni foils were analyzed chemically to determine the Ni concentration.[133] The Ni concentrations found were 0.9, 5.1, 10.7, 21.0, 33.4, 46.6, and 53.2 atomic percent. To check homogeneity, four pieces were selected at random from the 10.7% foil and each piece was analyzed chemically. The measured compositions agreed within the precision of the chemical analysis which was judged to be 0.3%. The pure Cu and Cu-Ni foils were spectrochemically analyzed for impurities.[134] Those impurities detected are listed in Table III-1. The starting foil for the Au-Fe samples was 99.99% pure Au 12 μm thick.[135]

A stock solution containing 2.0 mg/ml of Fe was prepared by dissolving a sample[136] of isotopically enriched Fe_2O_3 into hydrochloric acid. The Fe_2O_3 sample was enriched to 90.7% ^{57}Fe. The results of a spectrochemical analysis[136] of this sample is given in Table III-2. The stock solution was used to place the required amount of Fe into

the plating bath.

A depletion plating technique[137] was used to deposit the required quantity of Fe onto the surface of a foil. The plating bath was prepared in a 30 ml beaker by dissolving 0.65 g of $(NH_4)_2C_2O_4$ in about 15 ml of water. The desired amount of Fe stock solution was measured and added to the plating solution with a pipette. The pH was then adjusting to about 5 by adding dilute ammonium hydroxide. Two platinum strips, each about 1 by 3 cm, were placed on opposite sides of the beaker for use as anodes. A piece of the foil to be plated was cut to about 2 by 3 cm, cleaned by scrubbing with 0.3 μm Al_2O_3 abrasive, rinsed and masked to leave a bare central region about 1.5 cm square on both sides of the foil. This foil was then placed in the plating bath, equidistant from and parallel to the anodes. A plating current of about 0.015 amp/cm^2 was used. The solution was stirred by an electric motor which would periodically strike the wire holding the foil. The plating uniformity was checked during the initial stages of plating while the plated layer was thin enough to be transparent. Any tendency not to plate uniformly could then be seen visually. About 0.1 cm along the edge of the plated region tended to plate slightly faster than the remainder of the foil. Therefore only the central region about 1.3 cm in diameter was used for obtaining Mössbauer effect spectra.

Several tests made by weighing the amount of iron plated onto the foil showed that about 90% of the iron added to the bath was recovered. Thus, to obtain a given iron concentration, an extra 10% of iron stock solution was added to the plating bath. No chemical analysis

was made of the foils after diffusion of the plated iron. It is estimated that the iron concentrations are accurate to ± 20% of the stated concentration.

The diffusion treatment consisted of holding the plated foil at 1000°C in a hydrogen atmosphere for 16 hours. The diffusion coefficient, D, as a function of temperature is given by $D = D_0 \exp(-Q/RT)$, where Q is the activation energy, R the gas constant, and T the absolute temperature. For the diffusion of iron in Cu between 720 and 1060°C, Mullen[138] gives the values $D_0 = 1.01$ cm^2/sec and Q = 50.95 kcal/mole. Then using R = 1.99 cal/mole and the above parameters we obtain a diffusion length $L = \sqrt{Dt}$, where t is the diffusion time, of 103 μm or about four times the thickest sample used. Thus, assuming solubility and good plating uniformity, the diffusion treatment is expected to give a uniform iron concentration throughout the sample.

The heat treatments used resulted in four types of samples:

(1) "Furnace cooled" samples - cooled by turning off furnace power - After diffusion the furnace power was turned off and sample and furnace were allowed to cool together.

(2) "Quenched" samples - gas quenched from 1000°C - Following diffusion at 1000°C the foil was withdrawn rapidly from the furnace and blasted on both sides with a room temperature jet of gas containing 95 percent helium and 5 percent hydrogen.

(3) "Annealed" samples - "quenched" sample held at 650°C, then gas quenched - After diffusion and quenching from 1000°C the furnace temperature was lowered to 650°C. The foil was replaced in the furnace and retained at 650°C for 16 hours in

a hydrogen atmosphere. The foil was then withdrawn rapidly and blasted on both sides with a room temperature jet of gas containing 95 percent helium and 5 percent hydrogen.

(4) "Splat cooled" samples - rapidly quenched from the melt - This was performed following diffusion and furnace cooling. The apparatus and technique used were essentially as described by Goldstein et al.[139] and Duwez and Willens.[140] The sample was placed in a boron-nitride crucible and induction melted. Using helium gas with 5 percent hydrogen under high pressure the sample was rapidly expelled through a small hole in the crucible onto a rotating copper hearth at room temperature. Both crucible and hearth were maintained in an atmosphere of helium five percent hydrogen. The resulting sample was in the form of a flake 100 to 200 μm thick. It was etched to a thickness of about 50 μm.

Several samples prepared using the above procedures were observed metallurgically by electron-probe microanalysis.[141] An annealed sample of $Cu_{0.97}Fe_{0.03}$ showed iron segregated into small particles less than about 2.0 μm in diameter. An annealed sample of $Cu_{0.94}Fe_{0.06}$ showed iron segregated into particles with diameters up to about 6 μm. Quenched samples of both $Cu_{0.97}Fe_{0.03}$ and $Cu_{0.94}Fe_{0.06}$ indicated homogeneously distributed iron. In both a quenched and an annealed sample of $(Cu_{0.90}Ni_{0.10})_{0.92}Fe_{0.08}$ no segregation of either iron or nickel could be detected by the electron probe. Fig. III-1 shows electron-probe scans of three of these samples.

Sources were prepared[142] by plating ^{57}Co onto a matrix and diffusing

at 950°C in an argon atmosphere, followed with quenching by flushing the furnace with room temperature argon gas. Two single line sources were used for studying absorbers, one had 10 mCi ^{57}Co in Pd and the other 50 mCi ^{57}Co in Pd. No difference in the Mössbauer effect linewidth for these two sources was detected. One source for study was prepared with 5 mCi ^{57}Co in a $Cu_{0.97}Ni_{0.33}$ matrix.

B. Mössbauer Effect Spectrometer. A variety of designs[143-153] for Mössbauer effect spectrometers have been published. The spectrometer used here was of the constant acceleration electro-mechanical feedback type. In such a spectrometer, which is velocity controlled, a problem arises because the system does not respond to a shift in its neutral position. This is often overcome by letting a fairly stiff suspension spring determine the neutral position. If this is done the total linear displacement of the driving rod must be small, requiring a rather high fundamental vibration frequency. When driving a source on the end of a long rod some of these higher frequency harmonics might excite acoustic vibration modes in the rod, thereby degrading the observed spectra. If, however, the neutral position is held fixed by the use of a position sensor such as a limit switch or photocell, a very weak driving rod support spring can be used, resulting in a much lower fundamental vibration frequency. Good velocity fidelity can then be obtained with a lower overall frequency response. A suitable system of this type has been described by Reugg et al.[152] and their design is the one used here. Several modifications were made aimed at reducing drift and increasing velocity fidelity when driving a gamma-ray source at the end of a long vertical rod. Those details not given below are

essentially as described by Reugg et al.[152,153]

For reference, a block diagram of the entire system is shown in Fig. III-2. To give additional drive power the Doppler-effect modulator was fabricated using two speakers[154], one on each end of the velocity transducer. A schematic of the modified section of the driver electronics is shown in Fig. III-3. This circuit is dc coupled and hence very sensitive to voltage drifts. Components and circuits were selected to reduce this drift and also to provide the best possible linearity. A stable reference voltage, V_r, is provided by the Zener diode D11. Any drift of this reference voltage results in a proportional drift in the velocity calibration of the spectrometer. The diode selected had a Zener voltage of 9.3 volts and a temperature coefficient of 0.005% per °C. A sawtooth ramp voltage, applied to J10, is added to the reference voltage through the operational amplifier A10 to provide a velocity sweep waveform. The source of this ramp voltage is provided by the multichannel analyzer as a voltage proportional to the channel address number when the analyzer is operating in the multichannel scaling mode. Overall linearity will suffer if this ramp voltage is not at least as linear as the velocity transducer. The multichannel analyzer for this system was modified to have a linearity of 0.1% in this respect. The potentiometer R14 is used to vary the total number of channels used to accumulate the spectrum. Potentiometer R15 varies the total velocity range. If the multichannel analyzer ramp voltage is accurately zero for channel one there will be no interaction between the two potentiometer settings. The velocity transducer[155] L1 had a rated sensitivity of 23.5 mV sec/mm and a linearity of better than 0.1% over a displacement range of one cm.

Wertheim[156] has commented that the velocity calibration of Doppler-effect modulators has been an unexpected challenge to the experimentalist and no attempt was made here to obtain absolute calibration. The procedure used was to calibrate the velocity scale using the data given by Preston et al.[102] for pure iron metal. A sample was prepared from iron with a purity of 99.99% crushed to a -200 mesh powder. Enough powder was bound in a lucite disc to give an areal density of ^{57}Fe of 0.32 mg/cm^2. This sample was used for all subsequent calibrations.

A spectrum of the iron calibration sample after a 14 hour run with a 10 mCi Pd(^{57}Co) source is shown in Fig. III-4. A listing of the line positions, widths, and areas is given in Table III-3. Assuming the data of Preston et al.[102] is correct, the linearity of the spectrometer is better than $\pm$ 0.01 mm/sec.

The theoretical linewidths given in Table III-3 are based on the formula given by Fraunfelder et al.[81] for the linewidth of an absorber with finite thickness (Eq. II-1). Based on the lifetime of the excited nuclear state of ^{57}Fe, $2\Gamma_0 \simeq 0.194$ mm/sec. For computing the theoretical linewidths in Table III-3 the value $\sigma_0 = 2.42 \times 10^{-18}$ cm^2 given by Hanna and Preston[157] was used. Instrumental broadening of the linewidths is seen to be small, about 0.007 mm/sec for lines 3 and 4, increasing to 0.020 mm/sec for lines 1 and 6.

Calibrations over a period of about a year showed that long term drifts in the velocity calibration were on the order of one percent

per month. To retain an accuracy of better than one percent in the velocity scale, calibration runs were made at least once a week.

C. Magnet and Dewar System. Two dewars were used for obtaining spectra at low temperatures, one a fixed temperature dewar and the other a variable temperature dewar with provision for obtaining spectra in the presence of an externally applied magnetic field.

The fixed temperature dewar is shown in Fig. III-5. The sample is immersed in liquid nitrogen or liquid helium contained in the inner well. The dewar body is basically that described by Hersh[158] except the inner well was not narrowed at the top but continued straight. This reduces the holding time for liquid helium somewhat but was necessary to prevent vibration of the sample. The magnetic field at the sample due to the bar magnets used is negligible. The liquid capacity of the inner well was 800 ml and gave a holding time of eight to ten hours for liquid helium.

The equipment used to obtain spectra in the presence of an externally applied longitudinal field[159] is shown in Fig. III-6. The temperature of the source and absorber are controlled independently. The source and Doppler-effect modulator share a common vacuum. This removes the need for the double bellows type of arrangement usually required to transmit the source motion into the dewar. The source chamber and sample holder are shown in more detail in Fig. III-7. The sample is held at the temperature of the sample holder by helium exchange gas trapped inside the sample holder.

D. Data Analysis. Many of the spectra obtained in this study were analyzed by the use of computerized least squares fitting techniques. The techniques used were adapted from the computer programs of Polinger et al.[160] and Chrisman and Tumollilo.[161] Three types of curves were used in fitting the experimental data. The first was a sum of separate Lorentzian shaped lines, the second a six-line hyperfine field pattern, and the third a hyperfine field distribution. The experimental spectra often contained a curved background due to the variable source absorber distance when the source was moved to Doppler shift the gamma-ray energy. In the first type of fitting the background was fitted to a quadratic equation at the same time the Lorentzians were being fitted. For the second and third methods a background spectrum was obtained by tuning the single channel analyzer off the 14.4 keV gamma-ray to spoil the resonance. Before proceeding, the background was least squares fitted and the fitted curve subtracted from the original data to remove the background. The three fitting methods are outlined below. All three methods utilized an automatic plotter to plot the data and fitted curve.

1. Individual Lorentzians. In this method of fitting a sum of independent Lorentzians plus a curved background was least squares fitted to the data. The equation used was

$$y(v) = \sum_{i=1}^{N_L} \frac{A_i}{(2/\Gamma_i)^2 (v - c_i)^2 + 1} + a + bv + cv^2 \qquad \text{III-3}$$

where y(v) is the amount of absorption at velocity v, c_i the centroid of the i^{th} Lorentzian, N_L is the number of Lorentzians used, and Γ_i is the linewidth of the i^{th} Lorentzian. All fitting parameters were varied independently.

2. Six-Line Hyperfine Pattern. In this method the data, with the curved background removed, were fitted to an equation of the form

$$y(v,H) = \sum_{i=1}^{6} \frac{Ar_i}{(2/\Gamma)^2 (v^2 - Hg_i - Q\alpha_i - c)^2 + 1} \qquad \text{III-4}$$

where H represents the magnetic field, Q the quadrupole splitting, assumed small, and c the center of the spectrum. The six parameters r_i represent the relative strength of the six lines and were generally given the ratio 3:2:1:1:2:3. The six parameters g_i represent the relative splitting of the six lines and were given the values -0.01615, -0.00934, -0.00254, 0.00254, 0.00934 and 0.01615 mm(sec kG)$^{-1}$ respectively. The parameter α_i is +1 for lines 1 and 6 and -1 for lines 2, 3, 4 and 5. All parameters except r_i, g_i and α_i were allowed to vary independently.

3. Hyperfine Field Distribution. In this method the data, with the curved background removed, were fitted to an equation of the form

$$y(v) = \sum_{m=0}^{M_{max}} p(m\Delta H) \; y(v,m\Delta H) \qquad \text{III-5}$$

where $y(v,m\Delta H)$ is given by equation III-4, and $p(m\Delta H)$ is the field distribution function. The field increments, ΔH, are taken small enough to give a smooth y(v). The distribution is cut off at a field $M_{max}\ \Delta H$. The field distribution function was chosen to be a two

parameter function such as a Lorentzian. For this fitting procedure the parameters Γ, r_i, g_i and M_{max} were not varied and Q was set equal to zero.

CHAPTER IV

EXPERIMENTAL RESULTS

A. Preliminary. This chapter describes the Mössbauer effect results obtained from various Cu-Ni-Fe alloys studied as absorbers, for one source of $Cu_{0.67}Ni_{0.33}(^{57}Co)$, and for two Au-Fe alloys studied as absorbers. The Cu-Ni-Fe alloys will be designated by the formula

$$(Cu_{1-x}Ni_x)_{1-y}Fe_y,$$

where x and y are atomic fractions. The values of x ranged from 0 to 0.53. The values of y ranged from 0.005 to as high as 0.08 in one alloy which had x = 0.10. Sample preparation has been discussed in Section III-A which describes the heat treatments used in preparing the alloys. Here we refer to the alloys as being either furnace cooled, quenched, splat cooled or annealed.

The Mössbauer spectra observed for these alloys are complex and for purposes of discussion they are divided into components due to four types of Fe. Further justification for this division is given in Section V-A. The four types of Fe are:

(1) α-Fe: Fe in bcc precipitates. This iron normally yields a six-line pattern similar to that observed in pure Fe metal. The six-line pattern seen in the "wings" of Fig. IV-15(a) is an example of α-Fe. It arises from bcc Fe precipitating from a Cu matrix. The separation of the outer two absorption peaks is 10.7 mm/sec which is the same observed in pure Fe metal at room temperature.

(2) γ_0-Fe: Non-magnetic or paramagnetic Fe in solution. This

Fe is characterized by a single, relatively narrow, absorption line at room temperature. The large peak in Fig. IV-1(a) is an example of γ_0-Fe and is characteristic of Fe in solution in Cu. It has a linewidth of 0.22 mm/sec which is very close to the natural linewidth of 0.20 mm/sec based on the lifetime of the ^{57}Fe isomeric state.

(3) γ_1-Fe: Fe in fcc Fe-rich antiferromagnetic precipitates. This Fe is generally characterized by a single relatively narrow absorption line above liquid nitrogen temperature. Fig. IV-7 shows the spectrum of a sample of $Cu_{0.97}Fe_{0.03}$ annealed to precipitate the fcc γ_1-Fe which appears as the prominant single peak on the left. The smaller peak on the right is γ_0-Fe.

(4) γ_2-Fe: Fe in fcc regions generally characterized by an unresolved Mössbauer effect structure at room temperature having the appearance of a doublet. The doublet structure at the base of the central peak in Fig. IV-1(a) is an example of γ_2-Fe.

Spectra were obtained for a series of alloys with y = 0.005. These results are described in Section IV-B. One source with x = 0.33 was studied and the results are described in Section IV-C. Except for this source all alloys were studied as absorbers. The experiments performed on some alloys with x = 0 are described in Section IV-D. Results obtained in a magnetic field are described in Section IV-E. A series of other results for various compositions and heat treatments are described in Section IV-F.

B. Alloys Containing 0.5 Atomic Percent Fe. Spectra were obtained for a series of alloys with the formula

$$(Cu_{1-x}Ni_x)_{0.995}Fe_{0.005},$$

where x varied from 0 to 0.53. Each of these spectra were least squares fitted to a sum of individual Lorentzian lines whose position, height and width were allowed to vary independently. The spectra and the fits obtained by this technique are shown in Fig. IV-1(a) through (h). Table IV-1 lists the parameters obtained.

In the second fitting method a six-line hyperfine field pattern was least squares fitted to the spectra. The center of this six-line pattern, its intensity, the hyperfine field value and the linewidth varied independently. A 3:2:1:1:2:3 intensity ratio was used for the six lines. A small amount of quadrupole splitting was included in the six-line pattern and this is the source of the asymmetry in some of the fitted patterns such as seen in Fig. IV-2(c). For the two samples $(Cu_{0.99}Ni_{0.01})_{0.995}Fe_{0.005}$ and $(Cu_{0.95}Ni_{0.05})_{0.995}Fe_{0.005}$ two Lorentzian lines were also included in the fit. These lines were assumed to be in the same position as the γ_2 doublet of Fig. IV-1(a). Also, for these two samples only, the linewidth was not allowed to vary during the least squares fit and was held constant at 0.22 mm/sec. The spectra and the fits obtained are displayed in Fig. IV-2(a) through (g). The values of the parameters obtained by the fitting procedure are listed in Table IV-2.

The spectra, without any fits, are all displayed in Fig. IV-3. This figure illustrates the evolution of the Mössbauer effect absorption pattern as the Ni concentration is gradually increased.

C. Source Experiment. One source of $Cu_{0.67}Ni_{0.33}$ (^{57}Co) was prepared as described in Section III-A. The room temperature spectrum of this source, using the central two lines of metallic Fe as an absorber, is shown in Fig. IV-4. Each of the two absorption patterns in this spectrum have been least squares fitted either as two Lorentzians or as a hyperfine field. The theoretical line shown in Fig. IV-4 is for a hyperfine field. The averaged parameters obtained for these fits are listed in Tables IV-1 and IV-2 along with the results for the 0.5 atomic percent Fe absorbers.

D. Cu-Fe Alloys. Fig. IV-15(a) shows the room temperature spectrum of a furnace cooled sample of $Cu_{0.975}Fe_{0.025}$ (2.5 atomic percent Fe). Three types of Fe are evident in this spectrum. The most prominent central peak is γ_1-Fe. The smaller central peak is γ_0-Fe. The six-line pattern in the "wings" of the spectrum corresponds to α-Fe. The splitting of this six-line pattern corresponds to 330 ± 5 kG, the same field value found in metallic Fe at room temperature. This sample showed evidence of ferromagnetism, it was strongly attracted to a permanent magnet at room temperature.

Fig. IV-1(a) shows the room temperature spectrum of the first of two quenched samples of $Cu_{0.995}Fe_{0.005}$. The prominent central peak, comprising 73 percent of the absorption area, is γ_0-Fe. The two remaining peaks are the γ_2-Fe doublet. Fig. IV-5 shows the room temperature spectrum of the second of two quenched samples of $Cu_{0.995}Fe_{0.005}$. This spectrum appears identical to that for the first sample except that the central γ_0 peak contains slightly less of the total absorption area.

Fig. IV-6 shows the spectrum of the second sample of quenched

$Cu_{0.995}Fe_{0.005}$ at 4.2°K. There is no apparent increase in the γ_0 linewidth or in the splitting of the γ_2 doublet and no shift of the relative position of the γ_0 peak and γ_2 doublet. The centroid of the pattern has been shifted by 0.13 ± 0.03 mm/sec by the second order Doppler effect. This shift is, within experimental error, the same as reported by Preston et al.[101] for pure Fe metal.

Fig. IV-7 shows the room temperature spectrum of an annealed sample of $Cu_{0.97}Fe_{0.03}$. As described in Section III-A, the annealing procedure yielded Fe precipitates about 2μm in diameter. The prominent peak is due to these γ_1-Fe precipitates. The smaller peak is due to γ_0-Fe. The spectrum of this sample at 4.2°K, fitted to two Lorentzian lines is shown in Fig. IV-8(a).

Fig. IV-9 shows the room temperature spectrum of a splat cooled sample of $Cu_{0.975}Fe_{0.025}$. The central peak represents γ_0-Fe. The peak at higher velocity is one peak of the γ_2 doublet. The absorption peak at lower velocity is the sum of one peak of the γ_2 doublet and the γ_1 peak. The spectrum of Fig. IV-10 is for a quenched sample of $Cu_{0.97}Fe_{0.03}$ and, except for a slightly greater percentage of γ_1-Fe, is essentially the same spectrum as for the splat-cooled sample.

E. Magnetic Field Results. The absorption spectra for three Cu-Ni-Fe alloys and for two Au-Fe alloys were obtained in a field of approximately 50 kG at a temperature of 205°K. The spectra for the Cu-Ni-Fe alloys are displayed in Fig. IV-11 and those for the Au-Fe alloys in Fig. IV-12. Each sample was placed in the magnet, the absorber was brought to a temperature of 205°K and the source to 255°K, and a spectrum was obtained first for zero field and then for a field of 50 kG. As discussed below, one spectrum indicates that the applied

field, which was not precisely measured, may have been slightly less than 50 kG. However, the same magnet current was used for each spectrum labeled with H = 50 kG.

The spectrum of annealed $Cu_{0.97}Fe_{0.03}$ with H = 0 is shown least squares fitted to two Lorentzians in Fig. IV-13(a). The spectrum of this sample with the applied field is shown in Fig. IV-13(b) least squares fitted to two hyperfine field patterns with a 2:0:1:1:0:2 line ratio. Lines 2 and 5 are missing due to polarization effects. In the fitting procedure the linewidth, hyperfine field, and line ratios were assumed the same for each of the two patterns and lines 2 and 5 were assumed to be absent. All other parameters were allowed to vary independently. The lines for each of the two patterns are labelled in Fig. IV-13(a) and (b). The parameters obtained in the least squares fitting procedure for this sample are listed in Table IV-4. Although a field value slightly less than the applied field is expected, the field of 45.6 kG obtained indicates that the applied field may have been slightly less than 50 kG. The discrepancy between the γ_1 linewidth in zero field and in the applied field is due partly to the least squares fitting procedure which gave an equal linewidth to both the γ_0 and γ_1 linewidths while fitting the applied field spectrum.

The spectrum of quenched $(Cu_{0.90}Ni_{0.10})_{0.97}Fe_{0.03}$ at 205°K with no applied field is shown in Fig. IV-14(a) least squares fitted to two Lorentzians. The two lines were located at -0.07 ± 0.03 and $+0.29 \pm 0.03$ mm/sec and each had a linewidth of 0.39 ± 0.03 mm/sec. Fig. IV-14(b) shows the spectrum of this sample when a field of 50 kG was applied. The spectrum has been fitted to the field distribution shown

in the inset. This distribution has the shape of a cut-off Lorentzian. For this fit a line ratio of 2:0:1:1:0:2 was assumed. The amount of polarization and hence the proper line ratio to use is not certain. Since the field distribution obtained will change when the line ratio is changed, the field distribution obtained cannot be considered unique.

F. Other Results and Summary. Spectra obtained at room temperature and at liquid nitrogen temperature on several furnace cooled samples of $(Cu_{1-x}Ni_x)_{0.975}Fe_{0.025}$ are displayed in Fig. IV-15 and Fig. IV-16. The samples used to obtain the spectra of Fig. IV-15(c) and (d) were the same used to obtain Fig. IV-16(a) and (b) respectively.

Room temperature spectra for three quenched samples of $(Cu_{0.90}Ni_{0.10})_{1-y}Fe_y$ are shown in Figs. IV-17, IV-18, and IV-19. Part (a) of these figures shows each spectrum fitted to a six-line hyperfine field pattern with a 3:2:1:1:2:3 line ratio. Part (b) shows each spectrum fitted to two separate Lorentzians. The parameters obtained by the least squares fitting technique are listed in Table IV-5.

Table IV-6 gives a summary of the Mössbauer effect spectra obtained in this study. Where a resolved hyperfine field splitting was present its value has been estimated. All the six line hyperfine spectra observed were characteristic of a hyperfine field distribution with broad lines such as shown in Fig. IV-16(c) in contrast with Fig. IV-4.

All line positions have been measured with respect to a pure Fe absorber at room temperature. The isomer shifts for alloys containing 0.5 atomic percent Fe are plotted in Fig. IV-20. Also plotted are the results of Wertheim and Wernick[162] for Cu-Ni alloy sources at 4.2°K. Their results have been corrected to use pure Fe as a reference.

Considering the uncertainty in this correction, the results are in good agreement.

CHAPTER V

DISCUSSION OF RESULTS

A. Metallurgical Considerations. The study of copper rich Cu-Ni-Fe alloys with even small amounts of Fe presents severe metallurgical problems. Since the metallurgy and physics problems are intimately related a certain amount of effort has been devoted to gaining an understanding of the metallurgy. The work here, and elsewhere[131,163], has shown that the Mössbauer effect is quite sensitive to phase segregation in the Cu-Ni-Fe system. No attempt has been made here to carry out a systematic study of the phase boundaries and kinetics in this system, though it appears that the Mössbauer effect would be a powerful tool for such a study.

1. Cu-Fe. In a study of the Cu-Fe system Gonser et.al.[39,163] identified three types of Fe; that in solution, that precipitated in a fcc phase, and that precipitated in a bcc phase. The precipitated bcc iron, or α-Fe, has a six-line Mössbauer effect spectrum with the same hyperfine field splitting as pure iron. The precipitated fcc Fe, commonly termed γ-Fe, has a single narrow absorption line at room temperature with its centroid displaced by - 0.35 mm/sec from the single narrow line corresponding to Fe in solution in Cu. The fcc Fe precipitate line is easily recognized by its tendency to grow upon annealing a sample which contains Fe in excess of that soluble in Cu at the annealing temperature. These precipitates are Fe held in fcc form by the Cu matrix and thus can be called Guinier-Preston zones.

They transform to α-Fe upon reaching sufficient size or upon cold working.

The experimental results here are in agreement with those of Gonser et.al.[39,163] However we recognize another type of Fe in the fcc phase in Cu. This is Fe in solid solution that interacts with other Fe in solid solution in the Cu matrix. This interaction results in the formation of a doublet superimposed upon the central singlet, as seen in Fig. IV-5 for a quenched sample of 0.5% Fe in Cu. One peak of this doublet, that at lower velocity, is almost in the same location as the absorption peak for Fe in fcc γ-Fe precipitates. Thus the two are unresolved if both are present. The doublet seen in Fig. IV-5 is also evident in the well resolved spectrum of 0.6% Fe in Cu shown in Fig. 1(a) of Gonser et.al.[163] They interpreted one line of this doublet as precipitated fcc γ-Fe and reached the conclusion that complete solid solution had not been achieved in spite of severe quenching. Instead we believe that this line did not represent precipitated γ-Fe but rather one peak of a doublet, and hence complete solid solution had been achieved.

The doublet formation for Fe in Cu is analogous to that for Fe in Au as observed by Violet and Borg.[45] The increased solubility of Fe in Au over that for Fe in Cu allowed a study of this doublet over a wide range of iron concentration. In both Au-Fe and Cu-Fe the position and separation of the doublet appears relatively independent of Fe concentration. For both Au-Fe and Cu-Fe the doublet behaves in the same way when a magnetic field is applied. This helps confirm a common physical origin for the doublet structure in both.

We are thus led to distinguish three types of fcc Fe in Cu. Because all three are Fe in an fcc form the notation γ is appropriate in each case. The iron in solid solution which forms a single line at room temperature is denoted γ_0-Fe. The Fe which precipitates into fcc regions and forms a single line at room temperature is denoted γ_1-Fe. The Fe in solid solution which forms a doublet at room temperature due to interactions with other Fe in solid solution is denoted γ_2-Fe.

Thus we can picture what happens to the ^{57}Fe in Cu Mössbauer effect spectrum as the iron concentration is increased keeping the heat treatment constant. In the very dilute region only the single γ_0-Fe line will be observed. This is a narrow line with near natural linewidth and hence ^{57}Co in Cu is often used as a source in Mössbauer effect studies. As the Fe concentration is increased the γ_2-Fe doublet will appear. When solid solubility is exceeded the γ_1-Fe line will appear superimposed on one of the γ_2-Fe doublet peaks. Finally, at very high concentrations, some of the γ_1-Fe precipitates will grow large enough to transform into α-Fe and the six-line pattern of α-Fe will also be present in the Mössbauer effect spectrum.

The spectrum obtained for a splat cooled sample of Cu-Fe is shown in Fig. IV-9 and that for a quenched sample is shown in Fig. IV-10. The shapes of these two spectra are identical and hence can be regarded as characteristic of the Cu-Fe system and not of the particular heat treatment used. These spectra can then be interpreted as consisting of a central γ_0-Fe peak for isolated Fe in solution, a γ_2-Fe doublet which has two peaks of roughly equal intensity, and a γ_1-Fe peak which

is superimposed on the γ_2-Fe doublet peak at lower velocity. Referring to Table IV-6, for an iron concentration of 3 atomic percent Fe in Cu about 1/3 is precipitated as γ_1-Fe. The remaining 2/3 is present as γ_0- and γ_2-Fe. This compares with a solubility of about 3 percent at the quenching temperature of 1000°C indicated by the phase diagram in Hansen and Anderko[107]. Although both methods of rapid quenching used yielded roughly equivalent results it is still possible that more severe quenching, perhaps to liquid nitrogen temperatures, might reduce the amount of γ_1-Fe and give results closer to the phase diagram.

We have attributed the γ_2-Fe doublet as due to an Fe atom in solid solution interacting with other Fe atoms in solid solution. It is thus possible that the relative amount of γ_2-Fe present may result from a tendency for a clustering of Fe, i.e. the formation of small regions containing greater than the average amount of Fe but not yet identifiable as a γ_1-Fe precipitate. In this case the relative amount of γ_2-Fe present could be sensitive to the heat treatment of the sample.

2. Cu-Ni-Fe. A series of Mössbauer effect spectra for $(Cu_{1-x}Ni_x)_{0.995}Fe_{0.005}$ for x from 0 to 0.53 are shown in Fig. IV-3. As the Ni content is increased from zero the spectra are consistent with a disappearance of the γ_2-Fe doublet characteristic of Fe in Cu and an increase in a γ_2-Fe doublet characteristic of Fe in Cu-Ni. At x = 0.10 the Cu-Ni type of γ_2-Fe appears as the major component. For Fe in Cu-Ni the γ_2 doublet can be associated with Fe atoms in solid solution that interact with Ni atoms in solid solution.

When the solid solubility of Fe in Cu-Ni is exceeded fcc precipitates form that contain Ni as well as Fe. This is because Ni and

Fe have a complete range of solid solubility with a fcc form stable at room temperature for greater than 30 percent Ni. These precipitates, which will also contain some Cu, can be ferromagnetic at room temperature or below. Fig. IV-15(b) is an example of a Cu-Ni-Fe alloy containing these fcc precipitates ferromagnetic at room temperature. Fig. IV-15(c) and Fig. IV-16(a) show a Cu-Ni-Fe alloy with fcc precipitates ferromagnetic at 78°K but not at room temperature.

The results obtained here for Fe added to $Cu_{0.90}Ni_{0.10}$ are in agreement with the solubility diagram derived by Palmer and Wilson[126] if it is assumed that the furnace cooling treatment used here is roughly equivalent to quenching from a temperature of 650°C. The results on alloys with Ni fractions larger than 0.10 are consistent with an increasing Fe solubility as the Ni concentration is increased. Nagarajan and Flinn[131] found by use of the Mössbauer effect that an alloy of $Cu_{0.64}Ni_{0.25}Fe_{0.11}$ did not exhibit a two phase region after quenching from 1050°C but did develop two distinct phases when annealed at 600°C. The fraction of the spectrum in a six-line hyperfine pattern was found to be independent of temperature from 73°K to 143°K. The spectra obtained here for a furnace cooled sample of $(Cu_{0.79}Ni_{0.21})_{0.975}Fe_{0.025}$ and a quenched sample of $(Cu_{0.79}Ni_{0.21})_{0.97}Fe_{0.03}$ showed segregation in the former but not in the latter.

These results, along with the microprobe studies mentioned in Chapter III, indicate that all the quenched samples studied here, except the Cu with Fe concentration of 2.5 percent or more and the $(Cu_{0.90}Ni_{0.10})_{0.92}Fe_{0.08}$ sample, were solid solutions. However, the possibility of deviations from uniformity due to clustering remains.

This means that, for example, in a Cu-Ni-Fe alloy, an Fe atom may have a larger probability for having Ni neighbors than would be expected in a perfectly random solid solution. This form of non-randomness might not be observable by ordinary metallurgical techniques, including electron microscopy and X-rays, but could have a large influence on the Mössbauer effect spectrum and on the magnetic properties of the alloy.

B. Origin of the γ_2-Fe Doublet. In the previous section we have identified a "doublet" that is present in the Mössbauer effect spectra of Cu-Fe, Au-Fe, and Cu-Ni-Fe. This doublet has been termed γ_2-Fe. In this section we will consider the origin of this doublet. We are led to the conclusion, mostly by the behavior of the spectrum when an external magnetic field is applied, that the γ_2-Fe doublet is mainly magnetic in origin.

There are three possible origins for the observed doublet:

(1) The doublet is really two separate lines due to a separation of alloy phases giving Fe in two different environments with different isomer shifts.

(2) The doublet is really a quadrupole split line arising from the non-cubic environment of the Fe atoms. The non-cubic environment results from a given Fe atom having both Cu and Ni or Fe near neighbors.

(3) The doublet is really an unresolved six-line hyperfine pattern due to a weak magnetic field at the nucleus.

Possibility (1) is ruled out for several reasons including the metallurgical considerations presented in Section V-A. Further, the

γ_2-Fe doublet is present in Cu-Ni alloys down to very low Fe concentrations. Thus a $Cu_{0.67}Ni_{0.33}$ alloy containing 5 mCi of ^{57}Co used as a source gave a spectrum identical to the same alloy containing 0.5 atomic percent Fe and used as an absorber. These spectra are compared in Table IV-2. The presence of the γ_2-Fe doublet in Cu-Ni alloys at very low Fe concentrations shows that its origin must be in Fe-Ni interactions. In Cu-Fe and Au-Fe, where the relative amount of γ_2-Fe increases with increasing Fe concentration, the γ_2-Fe doublet must be due to Fe-Fe interactions.

Since a poorly resolved doublet, such as obtained for γ_2-Fe, has the appearance of a quadrupole splitting it might at first glance be assumed that this is the origin of the doublet. The small temperature dependence for the γ_2-Fe doublet separation seems to favor this interpretation. However a poorly resolved doublet can also be due to an unresolved six-line hyperfine field pattern. In the case of the γ_2-Fe doublet, which is poorly resolved in Au-Fe, Cu-Fe, and Cu-Ni-Fe, further examination is necessary to distinguish between the two possibilities.

A number of spectra have been least squares fitted assuming first that the quadrupole splitting (2) is dominant and then that the magnetic origin (3) is dominant. For Cu-Ni alloys containing 0.5 atomic percent Fe room temperature spectra are shown fitted to separate Lorentzians in Fig. IV-1. These same spectra are shown fitted to six-line patterns in Fig. IV -2. Both of these methods give reasonable fits. Hence it is not possible on the basis of these spectra alone to distinguish between a quadrupole or magnetic effect. There is a

slight asymmetry in the doublets, both in those observed here for Cu-Ni-Fe and those observed for Au-Fe.[45] In the case of a quadrupole origin the Goldanskii effect provides a mechanism to give the asymmetry. In the case of a magnetic origin a very small amount of added quadrupole effect will produce an asymmetric doublet. In either case the asymmetry could be due to a small amount of γ_0-Fe present but not resolved. Spectra for an alloy of $Cu_{0.9}Ni_{0.1}$ with 3, 6, and 8 atomic percent Fe are shown in Figs. IV-17, IV-18, and IV-19. Again it is impossible to distinguish whether two Lorentzian lines or a magnetic field interaction gives a better fit to the data.

It is interesting to compare the above with a doublet structure in a material which neutron diffraction has shown to be magnetic. From neutron diffraction data Abrahams et al.[164] concluded that γ_1-Fe, formed by annealing a Cu-Fe alloy, is antiferromagnetic at 4.2°K with a moment per iron atom of 0.7 μ_B. A spectrum of an annealed sample of $Cu_{0.97}Fe_{0.03}$ at 4.2°K is shown in Fig. IV-8 analyzed both as two Lorentzians and as a six-line magnetic hyperfine pattern. A room temperature spectrum showed this sample to be about 80% γ_1-Fe and 20% γ_0-Fe. Although it is known that a magnetic effect is being observed, it is difficult to tell by the shape of the spectrum alone whether the doublet structure is quadrupole or magnetic in origin. Also the γ_0-Fe, which is not resolved at 4.2°K, could be the source of the asymmetry in the spectrum.

To help determine the origin of the γ_2-Fe doublet several samples were observed in an externally applied longitudinal magnetic field of 50 kG. The spectra were all obtained at a temperature of 205°K. The

samples studied and their expected[39,44,164] transition temperature, T_c, are listed below:

Sample	T_c, °K
Annealed $Cu_{0.97}Fe_{0.03}$	< 77
Quenched $Cu_{0.97}Fe_{0.03}$	12
Quenched $(Cu_{0.90}Ni_{0.10})_{0.97}Fe_{0.03}$	< 77
Quenched $Au_{0.90}Fe_{0.10}$	35
Quenched $Au_{0.84}Fe_{0.16}$	180

Except for the latter sample the temperature used is considerably above the transition temperature.

The annealed sample of $Cu_{0.97}Fe_{0.03}$ contained about 80 percent γ_1-Fe and the rest γ_0-Fe. A spectrum at 205°K with H = 0 is shown in Fig. IV-13(a) and with H = 50 kG in Fig. IV-13(b). With the applied field the spectrum is the sum of two four-line patterns. These two four-line patterns have the proper centroids and area ratios (when corrected for finite thickness) to be identified as the γ_1 and γ_0-Fe observed at H= 0. This is further confirmation that these two spectral lines represent Fe in two distinct environments.

Consider next the sample of $(Cu_{0.90}Ni_{0.10})_{0.97}Fe_{0.03}$. A spectrum of this sample at 205°K with H = 0 is shown in Fig. IV-14(a). This spectrum is shown least squares fitted to two Lorentzians. Using the linewidth and line separation obtained in this fit, and assuming the doublet is of quadrupole origin, several theoretical spectra for the results expected when a magnetic field is applied are shown in Fig. V-1(a) through (d). These spectra have been calculated using the method of Gabriel and Ruby.[89]

The spectrum obtained when a 50 kG longitudinal field is applied

to the $(Cu_{0.90}Ni_{0.10})_{0.97}Fe_{0.03}$ sample is shown in Fig. IV-14(b). This spectrum more closely resembles a magnetic hyperfine field distribution than the spectrum expected from a combined magnetic field and electric field gradient.

The quenched sample of $Cu_{0.97}Fe_{0.03}$ has been shown to consist of three types of Fe, roughly 14% γ_2-Fe, 33% γ_1-Fe, and 52% γ_0-Fe. Spectra for this sample with and without an applied field are shown in Fig. IV-11(c) and (d). Subtracting out of the spectrum obtained with a magnetic field those four-line spectra expected for the γ_0-Fe and γ_1-Fe must result in a spectrum that closely resembles Fig. IV-11(f). This is evident since such a subtraction will remove less from the central region of the spectrum, leaving an enhanced central region. Again this is not the spectrum expected from the γ_2-Fe doublet in Cu if it were due to a quadrupole interaction.

The spectrum for the $Au_{0.90}Fe_{0.10}$ sample with no applied field, shown in Fig. IV-12(a) consists of about 1/3 γ_0-Fe singlet and 2/3 γ_2-Fe doublet. Using the approximate linewidth and line separation of the doublet, theoretically generated spectra for the appearance of an equivalent quadrupole doublet are shown in Fig. V-1(e) and (f). If a four-line pattern expected from the γ_0-Fe is subtracted from the magnetic field spectrum, Fig. IV-12(b), a spectrum with a shape similar to Fig. IV-11(f) would be obtained. This is a spectrum with the central region much enhanced over that expected from a combined magnetic field and electric field gradient.

Spectra obtained for the sample of $Au_{0.84}Fe_{0.16}$ with and without an applied field are shown in Fig. IV-12(c) and (d). The temperature

205°K, was very close to the transition temperature of 180°K expected[39,45] for this alloy. The spectrum observed in a magnetic field is characteristic of a broad hyperfine field distribution with a maximum much greater than the applied field. The large fields indicate a large internal field and hence a considerable alignment of Fe moments by the external field. This is to be expected in a high field for a material near a magnetic transition temperature. Although poorly resolved, the spectrum appears symmetric which would not be expected if a quadrupole interaction were present.

C. Discussion of the γ_2-Fe Doublet. When Fe in dilute quantities is dissolved in Au, Cu, or copper-rich Cu-Ni the ^{57}Fe Mössbauer effect reveals a similar behavior in each. At room temperature the spectrum consists of a central γ_0-Fe singlet and a poorly resolved γ_2-Fe doublet. In Cu-Ni, with more than about 10 atomic percent Ni, only the γ_2-Fe doublet appears to be present. At low temperature all three systems have a relatively broad transition temperature, T_c, below which a large magnetic splitting develops in the Mössbauer spectrum. This transition temperature is a different function of Fe concentration in each matrix. For a given Fe concentration the transition temperature appears to be slightly lower in Cu than in Au. For example Gonser et al.[39] found $T_c = 13 \pm 2$ °K for 1.6 percent Fe in Cu, whereas 2 percent Fe in Au was required for the same transition temperature. Although the evidence is scanty, it appears that as Ni is added to Cu, keeping the relative Fe concentration constant, T_c first decreases, and then increases again as the critical composition of 40 percent Ni is approached.

Below T_c the hyperfine spectrum indicates a distribution of hyperfine fields. This distribution is much broader in Cu-Fe alloys than in Au-Fe or Cu-Ni-Fe alloys. If any difference exists for the spectrum of γ_0-Fe and γ_2-Fe below T_c, it cannot be resolved in the observed Mössbauer spectra. Above T_c the separation of the γ_2-Fe doublet has a very small dependence on both temperature and Fe concentration. In Au-Fe Violet and Borg[45] measured a γ_2-Fe doublet separation of 0.77 $\pm$ 0.02 mm/sec at 77°K and 0.69 $\pm$ 0.02 mm/sec at 294°K. In Cu-Fe the γ_2-Fe doublet separation was 0.57 $\pm$ 0.02 mm/sec at 4.2°K and 0.58 $\pm$ 0.02 mm/sec at 298°K. In $Cu_{0.67}Ni_{0.33}$ the γ_2-Fe doublet separation was 0.28 $\pm$ 0.02 mm/sec at 4.2°K and 0.23 $\pm$ 0.02 mm/sec at 298°K.

One of the objections to a magnetic origin for the γ_2-Fe doublet is the above mentioned temperature region over which the magnetic splitting remains small and relatively constant. Though not expected to be the exact physical picture here, one model which illustrates that this behavior is possible in principle has been given by Brout.[165] This model is based on a dilute ferromagnet with a strong first neighbor interaction and a weak second neighbor interaction. The magnetization versus temperature curve given by Brout is shown below.

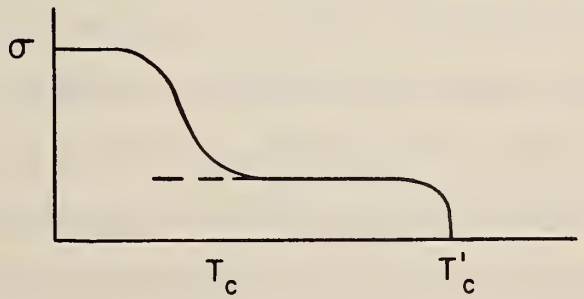

Fig. V-2. Magnetization vs. temperature for model with strong first neighbor and weak second neighbor interaction.

The plateau above T_c represents a region where a portion of the sample is aligned due to the strong first neighbor interaction. Below T_c the second neighbor interactions become important and a standard magnetization curve results.

1. Ferromagnetic-Antiferromagnetic Model. Of interest in considering possible models to explain the Mössbauer effect results is the ferromagnetic-antiferromagnetic model proposed by Kouvel[25,166,167] for Cu-Mn, Ag-Mn and related alloys. Mn appears to form a local moment in Cu of about 4 μ_B. For concentrations greater than about 1 atomic percent Mn in Cu, Ag and Mg, Owen et al.[21,22] found, on the basis of electron-spin resonance and susceptibility measurements, that the magnetic properties were dominated by short range Mn-Mn interactions such as direct and super exchange. Kouvel found that the magnetization of dilute Mn in Cu or Ag displayed a displaced hysteresis loop at low temperature when cooled in a magnetic field. When cooled in zero field a hysteresis loop centered about the origin with a relatively small remanence was observed. The displaced hysteresis loops have a thermoremanance which decreases with increasing temperature. The phenomenological model proposed by Kouvel to explain this behavior was that of very small ferromagnetic regions (or domains) coupled antiferromagnetically through nearest-neighbor Mn atom pairs. This sort of model requires the sign of the magnetic interaction between Mn atoms to depend critically on their distance of separation. The type of interaction proposed was strong short-range magnetic forces such as direct exchange or superexchange involving intervening Cu atoms. It is tempting to apply a modified model of this type to the Au-Fe, Cu-Fe, and Cu-Ni-Fe Mössbauer results. The existence of the γ_2-Fe

could perhaps be correlated to magnetic clusters which are coupled together below T_c and uncoupled above T_c. Further Mössbauer and magnetic measurements would be necessary to verify any such model.

2. Invar Effect Model. Another interesting model that deserves mention here is that proposed by Weiss[168,169] as an explanation for the "invar" effect in Fe-Ni alloys. The so-called invar region in fcc Fe-Ni alloys occurs around 30 percent Ni. In this region the thermal expansion coefficient changes rapidly with composition and undergoes a minimum with a near zero coefficient. The presence of small amounts of Cu or other elements can shift the position of this minimum. This phenomenon has proven useful, for example, for making low expansion alloys for absolute standards of length, watch balance wheels, etc. The model proposed by Weiss appears to explain this coefficient expansion minimum and a number of other anomalous properties of Fe-Ni alloys in the invar region. These include magnetization and pressure dependence of the Curie temperature.

Weiss proposes that Fe in a face centered cubic structure (γ-Fe) has two electronic structures γ_1 and γ_2. We retain this notation although it is by no means certain that these can be identified with the γ_1-Fe and γ_2-Fe described earlier. However, the analogy is suggestive. The proposed γ_1 electronic structure is antiferromagnetic with a moment of about 0.5 μ_B and a transition temperature around 80°K. The γ_2 electronic structure is ferromagnetic with a moment of about 2.8 μ_B and a transition temperature around 1800°K. It is further proposed that the energy separation of these two structures is a function of alloy composition. A small volume change of about 8% is proposed, with γ_2 having the larger volume. Mott[170] has speculated that according

to the model of Friedel et al.[171] the low moment structure of Fe with about 0.5 μ_B could be stabilized if there were a minimum in the density of states situated at a valence electron-to-atom ratio of about 7. That Fe can actually be antiferromagnetic in fcc structure is supported for example, by the neutron diffraction evidence of Abrahams et al.[164] on γ_1-Fe precipitated in Cu, by the susceptibility measurements of stainless steels by Kondorsky and Sedov,[172] and by the neutron diffraction studies on fcc Fe-Mn alloys by Ishikawa and Endoh.[173]

The application of this model to explain the spectra observed here would be a complex task. However, if it is admitted that the model is actually operative in Fe-Ni alloys, then it is likely that it plays a role in some of the observed Cu-Ni-Fe spectra, especially if a tendency existed for Fe and Ni to cluster together and form small regions with compositions close to $Fe_{0.7}Ni_{0.3}$. Around this composition one could have ferromagnetic regions with very small hyperfine fields, as has been observed in Fe-Ni alloys by Johnson et al.[174] and by Nakamura et al.[175] This might, for example, be the explanation for the quenched alloy of 8% Fe in $Cu_{0.9}Ni_{0.1}$. This sample had indications of ferromagnetism at room temperature, but its spectrum did not show a resolved six-line pattern (Fig. IV-19) at that temperature.

D. Isomer Shifts. The isomer shifts bear no obvious relation to the observed magnetic properties of Cu-Ni-Fe alloys. However, for completeness, they are considered briefly here. Using the data presented by Walker et al.[176] the 0.20 mm/sec isomer shift decrease on going from Fe in Cu to Fe in Ni (Fig. V-20) corresponds to a 3.8% increase in s-electron density at the Fe nucleus. This increase is the

sum of a number of contributions, some of which may be of opposite sign and tend to cancel. A decrease in 3d-electron density around the ^{57}Fe impurity would give in increase in s-electron density at the nucleus. A decrease in 4s-electron density would have the opposite effect.[176] Also, the 2.6% decrease in lattice parameter from pure Cu to pure Ni, corresponding to a 7.4% decrease in atomic volume, could have a considerable effect.

Isomer shift data are also available[177-179] for both ^{119}Sn and ^{197}Au as impurities in Cu-Ni alloys. The results are consistent with a net decrease in d-character around an Fe or Au atom, and a net decrease in s-character around a Sn atom, as the Ni concentration is increased. On the basis of a simple rigid band model, the addition of Fe, which has fewer atomic electrons than Ni, should have a larger effect on the isomer shift than the same amount of Ni. However, the addition of 6% Fe to $Cu_{0.9}Ni_{0.1}$ reduced the ^{57}Fe isomer shift only 0.01 mm/sec, compared to a reduction of 0.025 mm/sec expected for the addition of 6% Ni. This tendency of the isomer shift to be relatively independent of Fe concentration has also been observed[44] in gold-rich Au-Fe alloys.

Further work appears necessary to obtain an understanding of the various contributions to the isomer shifts in these alloys.

E. Conclusions. The major result presented here has been the discovery of a doublet structure in the high temperature Mössbauer effect spectra of Cu-Fe and Cu-Ni-Fe alloys. This doublet is responsible for the line broadening observed by Wertheim and Wernick[162] in their study of Cu-Ni(^{57}Co) sources, and one peak of the doublet is the

unidentified line in the Cu-Fe spectra previously presented by Gonser et al.[39,163] This doublet is similar to the one observed in gold-rich Au-Fe by Violet and Borg,[45] who proposed a quadrupole interaction as the origin of the doublet. We have shown here, by observation of the spectra in an externally applied magnetic field, that in both Au-Fe and Cu-Ni-Fe the doublet is of magnetic origin. This implies that some form of magnetic order persists above what has usually been considered the magnetic transition temperature in these alloys.

Two phenomenological models for the magnetic behavior of these alloys appear worthy of further consideration. They are the ferromagnetic - antiferromagnetic model of Kouvel[25,166,167] and the invar effect model of Weiss.[168,169] Further experimental work, especially magnetic susceptibility measurements, would be helpful in this regard. Also, it would be interesting to extend the Mössbauer effect measurements above room temperature since a second ordering temperature should exist.

Using the identification presented here for the types of Mössbauer effect spectra present in Cu-Ni-Fe alloys, it appears that the Mössbauer effect could be a very useful tool for further study of the metallurgy of this system. For example, a study of the relative amounts of γ_0, γ_1 and γ_2-Fe in Cu-Fe as a function of heat treatment could provide information about the kinetics of precipitation in Cu-Fe.

ACKNOWLEDGEMENTS

The author wishes to thank, first of all, his adviser Dr. L. H. Bennett, who provided essential ingredients of knowledge, enthusiasm, and intuition. Dr. R. E. Watson provided several profitable and interesting discussions. Useful advice was contributed by Drs. I. D. Weisman, B. Mozer, M. Kuriyama, B. W. Christ, J. C. Travis, J. J. Spijkerman, A. W. Ruff, H. Yakowitz, J. A. Manning, J. R. Cuthill, R. W. Mebs, A. J. McAlister, N. M. Wolcott, R. A. Falge, T. A. Kitchens and R. M. Housley.

I also wish to thank D. P. Fickle and G. O. Queen for their aid in sample preparation, F. C. Reugg for advice on instrumentation, R. L. Parke, R. D. Robbins, and G. P. Spurlock for technical assistance, and Katie Walder for typing the manuscript.

Thanks are also due to the many staff members of the University of Maryland and the National Bureau of Standards who provided encouragement and assistance. The research was performed at the National Bureau of Standards and received support from the Office of Saline Water, Department of the Interior. Relevance of this work to desalination is discussed elsewhere.

REFERENCES

1. R. L. Mössbauer, Z. Physik 151, 124 (1958).

2. R. L. Mössbauer, Z. Naturforsch. 149, 211 (1958).

3. R. L. Mössbauer and M. J. Clauser, Hyperfine Interactions, eds. A. J. Freeman and R. B. Frankel, (Academic Press, New York, 1967) p. 497.

4. P. A. Flinn, Experimental Methods of Materials Research, ed. H. Herman, (J. Wiley and Sons, New York, 1967) p. 163.

5. U. Gonser, Zeits. fur Metallkunde 57, 85 (1966).

6. A. H. Muir, Jr., K. J. Ando, and H. M. Coogan, Mössbauer Effect Data Index 1958-1965, (Interscience, New York, 1966).

7. K. G. Malinfors and R. L. Mössbauer, Alpha, Beta, and Gamma Ray Spectroscopy, ed. K. Siegbahn, (North Holland Publishing Co., Amsterdam, 1965) p. 1281.

8. A. J. Freeman and R. E. Watson, Magnetism Vol. IIA, eds. G. T. Rado and H. Suhl, (Academic Press, New York, 1965) p. 168.

9. G. K. Wertheim, Mössbauer Effect: Principles and Applications, (Academic Press, New York, 1964).

10. A. Abragam, L'Effect Mössbauer, (Gordon and Breach, New York, 1964).

11. R. L. Mössbauer and D. H. Sharp, Rev. Mod. Phys. 36, 410 (1964).

12. G. K. Wertheim, Am. J. Phys. 31, 1 (1963).

13. H. Fraunfelder, The Mössbauer Effect, (Benjamin, New York, 1962).

14. A. J. F. Boyle and H. E. Hall, Repts. Progr. Phys. 25, 441 (1962).

15. R. L. Mössbauer, Ann. Rev. Nuclear Sci. 12, 123 (1962).

16. H. Lustig, Am. J. Phys. 29, 1 (1961).

17. H. J. Lipkin, Ann. Phys. (N.Y.) 9, 332 (1960).

18. T. A. Kitchens, W. A. Steyert, and R. D. Taylor, Phys. Rev. 138, A467 (1965).

19. A. M. Clogston, B. T. Matthias, M. Peter, H. J. Williams, E. Corenzwit, and R. C. Sherwood, Phys. Rev. 125, 541 (1962).

20. C. Zener, Phys. Rev. 81, 440 (1951).

21. J. Owen, M. Browne, W. D. Knight, and C. Kittel, Phys. Rev. 102, 1501 (1956).

22. J. Owen, M. Browne, V. Arp, and A. F. Kip, J. Phys. Chem. Solids 2, 85 (1957).

23. I. S. Jacobs and R. W. Schmidt, Phys. Rev. 113, 459 (1959).

24. R. W. Schmidt and I. S. Jacobs, J. Phys. Chem. Solids 3, 324 (1957).

25. J. S. Kouvel, J. Phys. Chem. Solids 24, 795 (1963).

26. K. Yosida, Phys. Rev. 106, 893 (1957).

27. H. Sato, A. Arott, and R. Kikuchi, J. Phys. Chem. Solids 10, 19 (1959).

28. M. W. Klein and R. Brout, Phys. Rev. 132, 2412 (1963).

29. M. W. Klein, Phys. Rev. 136, A1156 (1964).

30. A. W. Overhauser, J. Phys. Chem. Solids 13, 71 (1960).

31. R. J. Borg, R. Booth, and C. E. Violet, Phys. Rev. Letters 11, 464 (1963).

32. A. R. Kaufmann, S. T. Pan, and J. R. Clark, Rev. Mod. Phys. 17, 87 (1945).

33. S. T. Pan, A. R. Kaufmann, and F. Bitter, J. Chem. Phys. 10, 318 (1942).

34. A. Arrott, Phys. Rev. 108, 1394 (1957).

35. O. S. Lutes and J. L. Schmidt, Phys. Rev. 134, A676 (1964).

36. W. E. Henry, Phys. Rev. Letters 11, 468 (1963).

37. T. A. Kitchens, W. A. Steyert, and R. D. Taylor, Phys. Rev. 138, A467 (1965).

38. T. A. Kitchens and P. P. Craig, J. Appl. Phys. 37, 1187 (1966).

39. U. Gonser, R. W. Grant, C. J. Meechan, A. H. Muir, Jr., and H. Wiedersich, J. Appl. Phys. 36, 2124 (1965).

40. M. S. Ridout, T. E. Cranshaw, and C. E. Johnson, Proceedings of the International Conference on Magnetism, (Nottingham, 1964) p. 214.

41. R. M. Housley, J. Appl. Phys. 39, 1107 (1968).

42. S. H. Liu, Phys. Rev. 157, 411 (1967).

43. M. W. Klein, J. Appl. Phys. 35, 944 (1964).

44. C. E. Violet and R. J. Borg, Phys. Rev. 149, 540 (1966).

45. C. E. Violet and R. J. Borg, Phys. Rev. 162, 608 (1967).

46. E. C. Stoner, Phil. Mag. 15, 1018 (1933).

47. W. H. Keesom and B. Kurrelmeyer, Physica 7, 1003 (1940).

48. J. Smit, Physica 16, 612 (1951).

49. J. E. Goldman, Phys. Rev. 82, 339 (1951).

50. J. E. Goldman, Rev. Mod. Phys. 25, 108 (1953).

51. A. I. Schindler and E. M. Pugh, Phys. Rev. 89, 295 (1953).

52. J. Friedel, Can. J. Phys. 34, 1190 (1956).

53. T. Sagawara, J. Phys. Soc. Japan 12, 309 (1957).

54. E. M. Pugh and F. M. Ryan, Phys. Rev. 111, 1038 (1958).

55. A. C. Chapman and E. F. W. Seymour, Proc. Phys. Soc. 72, 797 (1958).

56. S. A. Ahern, M. J. C. Martin, and W. Sucksmith, Proc. Roy. Soc. 284A, 145 (1958).

57. G. L. Guthrie, S. A. Friedberg, and J. E. Goldman, Phys. Rev. 113, 45 (1959).

58. M. D. Blue, J. Phys. Chem. Solids 11, 31 (1959).

59. A. Blandin and E. Daniel, J. Phys. Chem. Solids 10, 126 (1959).

60. D. L. Weinberg and N. Bloembergen, J. Phys. Chem. Solids, 15, 240 (1960).

61. D. L. Weinberg, J. Phys. Chem. Solids 15, 249 (1960).

62. O. S. Galkina and L. A. Chernikova, Sov. Phys.-JETP 11, 1 (1960).

63. T. J. Rowland, Phys. Rev. 119, 900 (1960).

64. D. M. S. Bagguley and M. Heath, Proc. Phys. Soc. 77, 913 (1961).

65. H. Nose, J. Phys. Soc. Japan 16, 2475 (1961).

66. K. Schröder, J. Appl. Phys. 32, 880 (1961).

67. J. Clift, C. Curry and B. J. Thompson, Phil. Mag. 8, 593 (1963).

68. K. Asayama, J. Phys. Soc. Japan 18, 1727 (1963).

69. K. Asayama, S. Kobayashi, and J. Itoh, J. Phys. Soc. Japan 18, 458 (1963).

70. L. F. Mattheis, Phys. Rev. 134, A970 (1964).

71. N. Mori, J. Phys. Soc. Japan 20, 1383 (1965).

72. H. Nagasawa, S. K. Togawa, and Y. Tomono, J. Phys. Soc. Japan 21, 588 (1966).

73. J. A. Gardner and C. P. Flynn, Phys. Rev. Letters 17, 579 (1966).

74. R. L. Odle and C. P. Flynn, Phil. Mag. 13, 699 (1966).

75. J. A. Gardner and C. P. Flynn, Phil. Mag. 15, 1233 (1967).

76. K. Bennemann , Phys. Rev. 167, 564 (1968).

77. K. Schröder and D. Önegüt, Phys. Rev. 162, 628 (1968).

78. K. Schröder and K. Mamola, Phys. Rev. 167, 658 (1968).

79. N. D. Lang and H. Ehrenreich, Phys. Rev. 168, 605 (1968).

80. N. F. Mott and H. Jones, The Theory of the Properties of Metals and Alloys (Clarendon Press, Oxford, England, 1936) p. 196.

81. H. Frauenfelder, D. E. Nagle, R. D. Taylor, D. R. F. Cochran and W. M. Visscher, Phys. Rev. 126, 1065 (1962).

82. D. A. Shirley, Rev. Mod. Phys. 36, 339 (1962).

83. R. E. Watson and A. J. Freeman, Phys. Rev. 123, 2027 (1961).

84. W. Marshall and C. E. Johnson, Metallic Solid Solutions, eds. J. Friedel and A. Guinier, (W. A. Benjamin Inc., New York, 1963) Ch. 29.

85. V. I. Goldanskii, E. F. Markarov, and V. V. Khrapov, Soviet Phys.-JETP 17, 508 (1963).

86. R. E. Watson, A. C. Gossard, and Y. Yafet, Phys. Rev. 140, A375 (1965).

87. R. E. Watson and A. J. Freeman, Phys. Rev. 131, 250 (1963).

88. R. M. Sternheimer, Phys. Rev. 132, 1637 (1963); 130, 1423 (1963); 105, 158 (1957); 96, 951 (1954); 95, 736 (1954); 86, 316 (1954); 84, 244 (1952); 80, 102 (1950).

89. J. R. Gabriel and S. L. Ruby, Nucl. Instr. Meth. 36, 23 (1965).

90. R. L. Collins and J. C. Travis, Mössbauer Effect Methodology Vol. 3, ed. I. J. Gruverman, (Plenum Press, New York, 1967) p. 123.

91. F. van der Woude and A. J. Dekkar, Phys. Stat. Sol. 9, 775 (1965).

92. M. Blume, Phys. Rev. Letters 14, 96 (1965).

93. M. Blume and J. A. Tjon, Phys. Rev. 165, 446 (1968).

94. J. A. Tjon and M. Blume, Phys. Rev. 165, 456 (1968).

95. B. C. van Zorge, W. J. Caspers, and A. J. Dekkar, Phys. Stat. Sol. 18, 761 (1966).

96. M. V. Kazarnovskii and A. V. Stepanov, Soviet Phys.-JETP 20, 362 (1965).

97. F. van der Woude and A. J. Dekkar, Solid State Comm. 3, 319 (1965).

98. E. Bradford and W. Marshall, Proc. Phys. Soc. 87, 731 (1966).

99. A. J. F. Boyle and J. R. Gabriel, Phys. Letters 19, 451 (1965).

100. H. Wegener, Z. Physik 186, 498 (1965).

101. S. M. Harris, Phys. Rev. 163, 280 (1967).

102. R. S. Preston, S. S. Hanna, and J. Heberle, Phys. Rev. 128, 2207 (1962).

103. R. Segnan, Phys. Rev. 160, 404 (1967).

104. W. Kundig, H. Bommel, G. Constabaris, and R. H. Lindquist, Phys. Rev. 142, 327 (1966).

105. G. Constabaris, R. H. Lindquist, and W. Kundig, Appl. Phys. Letters 7, 59 (1965).

106. S. M. Quaim, Proc. Phys. Soc. 90, 1065 (1967).

107. M. Hansen and K. Anderko, Constitution of Binary Alloys, (McGraw-Hill, New York, 1958).

108. K. Schröder, J. Appl. Phys. 32, 880 (1961).

109. J. L. Meijering, Acta Met. 5, 257 (1957).

110. R. A. Oriani and W. K. Murphy, Acta Met. 8, 23 (1960).

111. R. A. Rapp and F. Maab, Acta. Met. 10, 63 (1962).

112. W. Koster and W. Schule, Z. Metallkde. 48, 592 (1957).

113. F. Ryan, E. Pugh, and R. Smoluchowski, Phys. Rev. 116, 1106 (1959).

114. W. Schule and H. P. Kehrer, Z. Metallkde. 52, 168 (1961).

115. B. Mozer, D. T. Keating, and C. S. Moss, Phys. Rev. (to be published)

116. A. Kirdon, Phys. Letters 26A, 593 (1968).

117. R. V. Wakelin and E. L. Yates, Proc. Phys. Soc. (London) B66, 221 (1953).

118. F. Bitter and A. Kaufmann, Phys. Rev. 56, 1044 (1939).

119. F. Bitter, A. R. Kaufmann, C. Starr and S. T. Pan, Phys. Rev. 60, 134 (1941).

120. C. S. Smith, Phys. Rev. 57, 186 and 337 (1940).

121. J. M. Denney, Phys. Rev. 92, 531 (1953).

122. J. M. Denney, Acta. Met. 4, 586 (1956).

123. J. B. Newkirk, Trans. AIME 9, 1214 (1957).

124. K. E. Easterling and H. M. Meikk-Oja, Acta. Met. 15, 1133 (1967).

125. A. J. Bradley, W. F. Cox and H. J. Goldschmidt, J. Inst. Metals 67, 189 (1941).

126. E. W. Palmer and F. H. Wilson, Trans. AIME 4, 55 (1952).

127. E. Kneller, Proceedings of the International Conference on Magnetism, (Nottingham, 1964) p. 174.

128. E. Kneller, M. Wolff, and E. Egger, J. Appl. Phys. 37, 1838 (1966).

129. R. K. Ham, J. S. Kirkaldy, and J. T. Plewes, Acta. Met. 15, 861 (1952).

130. M. Hillert, M. Cohen, and B. L. Auerbach, Acta. Met. 9, 536 (1961).

131. A. Nagarajan and P. A. Flinn, Appl. Phys. Letters 11, 120 (1967).

132. The Cu-Ni alloy foils were prepared by Materials Research Corporation, Orangeburg, New York.

133. I thank E. R. Deardorf and E. J. Marenthal of the National Bureau of Standards, Gaithersburg, Maryland, for performing the chemical analysis.

134. I thank E. K. Hubbard of the National Bureau of Standards, Gaithersburg, Maryland, for performing the spectrochemical analysis.

135. The Au foil was obtained from Leico Industries Inc., New York.

136. The enriched Fe_2O_3 was obtained from Oak Ridge National Laboratory, Oak Ridge, Tennessee. The spectrochemical analysis on this Fe_2O_3 was performed at Oak Ridge.

137. I thank V. A. Lamb and C. L. Burton for suggesting the plating technique which is adapted from one of the methods given by Smith, Electroanalysis, (Blakiston, 1918).

138. J. G. Mullen, Phys. Rev. 121, 1649 (1959).

139. J. I. Goldstein, F. J. Majeske, and H. Yakowitz, Advances in X-ray Analysis, Vol. 10, ed. W. M. Mueller, (Plenum Press, New York, 1967) p. 431. I thank Dr. H. Yakowitz for the loan of a splat cooling apparatus.

140. P. Duwez and R. H. Willens, Trans. AIME 227, 362 (1963).

141. I thank D. L. Vieth for performing the electron-probe micro-analysis.

142. Sources were prepared by New England Nuclear Corporation, Boston, Massachusetts.

143. D. Rubin, Rev. Sci. Instr. 33, 1358 (1962).

144. P. A. Flinn, Rev. Sci. Instr. 34, 1422 (1963).

145. R. L. Cohen, P. G. McMullin, and G. K. Wertheim, Rev. Sci. Instr. 34, 671 (1963).

146. T. E. Cranshaw, Nucl. Instr. and Meth. 30, 101 (1964).

147. E. Kankeleit, Rev. Sci. Instr. 35, 194 (1964).

148. J. Lipkin, B. Schecter, S. Shtrikman and D. Treves, Rev. Sci. Instr. 35, 1336 (1964).

149. V. Voli and T. W. Nybakken, Rev. Sci. Instr. 35, 1085 (1964).

150. E. Kankeleit, Mossbauer Effect Methodology Vol. 1, ed. I. J. Gruverman, (Plenum Press, New York, 1965) p. 47.

151. L. Lovborg, Nuc. Instr. and Meth. 34, 307 (1965).

152. F. C. Ruegg, J. J. Spijkerman and J. R. Devoe, Rev. Sci. Instr. 36, 356 (1965).

153. F. C. Ruegg, Nat. Bur. Stds. Tech. Note 276, ed. J. R. Devoe, (U.S. Govt. Printing Office, 1966) p. 89.

154. University Loudspeaker, Oaklahoma City, Oaklahoma, model UL6114. This and further references to commercial components are for identification purposes and in no sense constitute an endorsement of the components or their manufacturers.

155. L. V. Syn Model 6LV2, Sanborn Electronics, Waltham, Massachusetts.

156. G. K. Wertheim, Phys. Today 20, 31 (1967).

157. S. S. Hanna and R. S. Preston, Phys. Rev. 139, A722 (1965); ibid 142, 286 (1966).

158. H. M. Hersch, Phys. Rev. 105, 1158 (1957).

159. The dewar with superconducting magnet was supplied by Andonian Associates, Waltham, Massachusetts.

160. A. Polinger, J. J. Spijkerman, and B. W. Christ, Parlors MF Computer Program (Nat. Bur. of Stds. unpublished report).

161. B. L. Chrisman and T. A. Tumolillo, Non-Linear Least Squares Analysis of Mössbauer Transmission Spectra, (Dept. of Physics, Univ. of Illinois, Urbana, Illinois, unpublished report).

162. G. K. Wertheim and J. H. Wernick, Phys. Rev. 123, 755 (1961).

163. U. Gonser, R. W. Grant, Jr., and H. Wiedersich, Acta Met. 14, 259 (1966).

164. S. C. Abrahams, L. Guttman, and J. S. Kasper, Phys. Rev. 127, 2052 (1961).

165. R. Brout, Magnetism Vol. IIA, eds. G. T. Rado and H. Suhl, (Academic Press, New York, 1965) p. 43.

166. J. S. Kouvel, J. Appl. Phys. 31, 142 S (1960).

167. J. S. Kouvel, J. Phys. Chem. Solids 21, 57 (1961).

168. R. J. Weiss, Proc. Phys. Soc. 82, 281 (1963).

169. R. J. Weiss, Phil. Mag. 9, 361 (1964).

170. N. F. Mott, Adv. Phys. 13, 325 (1964).

171. J. Friedel, G. Lehman, and S. Olszewski, J. Appl. Phys. 32, 325 S (1961).

172. E. I. Kondorsky and V. L. Sedov, J. Appl. Phys. 31, 331 S (1960).

173. Y. Ishikawa and Y. Endoh, J. Phys. Soc. Japan 23, 205 (1967).

174. C. E. Johnson, M. S. Ridout, and T. E. Cranshaw, Proc. Phys. Soc. 81, 1079 (1963).

175. Y. Nakamura, M. Shiga, N. Shikazona, J. Phys. Soc. Japan 19, 1177 (1964).

176. L. R. Walker, G. K. Wertheim, and V. Jaccarino, Phys. Rev. Letters 6, 98 (1961).

177. A. E. Balabanov and N. N. Delyagin, Soviet Phys.-Solid State 9, 1498 (1968).

178. J. P. Bacquet, Y. Y. Chu, O. C. Kistner, M. L. Perlam, and G. T. Emery, Phys. Rev. Letters 17, 809 (1966).

179. L. D. Roberts, R. L. Becker, F. E. Obenshain and J. O. Thomson, Phys. Rev. 137, A895 (1965).

Table III-1

Impurities detected by spectrochemical analysis of starting Cu-Ni alloy foils. Metallic impurities not listed were not detected to a sensitivity of better than 0.001%.

Element	Amount at.%	Element	Amount at.%
Ag	< 0.001	Mg	0.001 - 0.01
Al	0.001 - 0.01	Mn	< 0.001
Ca	< 0.001	Si	0.001 - 0.01
Cr	< 0.001	W	0.001 - 0.01
Fe	0.001 - 0.01	V	0.001 - 0.01

Table III-2

Impurities detected by spectrochemical analysis of ^{57}Fe enriched Fe_2O_3.

Element	Amount at.%	Element	Amount at.%
Ag	<0.01	Mo	<0.02
Al	<0.05	Na	<0.01
B	<0.01	Nb	<0.05
Ba	<0.01	Ni	<0.05
Be	<0.001	Pb	<0.02
Bi	<0.02	Pt	<0.05
Ca	0.01	Rb	<0.02
Cd	<0.05	Sb	<0.05
Co	<0.05	Si	0.02
Cr	<0.05	Sn	<0.02
Cu	0.05	Sr	<0.01
Ge	<0.05	Ta	<0.05
Hg	<0.01	Ti	0.02
K	<0.01	V	0.02
Li	0.005	W	<0.05
Mg	<0.01	Zn	<0.2
Mn	<0.02	Zr	<0.05

Table III-3

Absorption spectrum of Fe calibration sample.

Absorption Line	Measured[a] Position mm/sec ± 0.005	Expected[b] Position mm/sec ± 0.012	Measured[a] Linewidth mm/sec ± 0.014	Theoretical Linewidth mm/sec	Measured[a] Area fraction ± 0.01	Theoretical Area fraction (unpolarized sample)
1	-5.322	-5.328	0.245	0.226	0.24	0.250
2	-3.077	-3.083	0.230	0.216	0.17	0.167
3	-0.844	-0.838	0.212	0.205	0.09	0.083
4	0.838	0.838	0.217	0.205	0.10	0.083
5	3.075	3.083	0.230	0.216	0.17	0.167
6	5.331	5.328	0.246	0.226	0.24	0.250

[a]Uncertainty listed is statistical error of the least squares fit.

[b]From the data of Preston et al.[101]

Table IV-1

Parameters for quenched $(Cu_{1-x}Ni_x)_{0.995}Fe_{0.005}$ alloy spectra analyzed as a sum of separate Lorentzian lines.

x	T °K	Sample Thickness μm	Line Position[a] mm/sec (± 0.02)[e]			Γ mm/sec (± 0.02)			Relative Area (± 0.05)		
			$\gamma_2(-)$	γ_0	$\gamma_2(+)$	$\gamma_2(-)$	γ_0	$\gamma_2(+)$	$\gamma_2(-)$	γ_0	$\gamma_2(+)$
0	298	25	-0.10	0.24	0.48	0.29	0.22	0.28	0.13	0.73	0.14
0[b]	298	25	-0.09	0.23	0.49	0.24	0.24	0.28	0.17	0.66	0.17
0[b]	4.2	25	0.04	0.36	0.61	0.42	0.25	0.26	0.24	0.64	0.12
0.01	298	25	-0.10	0.22	0.49	0.22	0.30	0.19	0.18	0.71	0.11
0.05[c]	298	25		0.15			0.40			1.0	
0.10	298	25	0.01		0.20	0.30		0.25	0.52		0.48
0.21	298	25	-0.06		0.19	0.26		0.26	0.50		0.50
0.33[d]	298	25	-0.09		0.16	0.24		0.27	0.50		0.50
0.33	298	25	-0.08		0.15	0.24		0.24	0.50		0.50
0.33	4.2	25	0.04		0.32	0.32		0.33	0.50		0.50
0.47	298	25	-0.08		0.13	0.24		0.29	0.46		0.54
0.53	298	25	-0.07		0.13	0.27		0.26	0.57		0.43

a. $\gamma_2(-)$ refers to the peak of the γ_2 doublet at lower velocity, $\gamma_2(+)$ to the peak at higher velocity.
b. Second of two samples prepared identically.
c. This spectrum was analyzed only as a single line although the γ_2 doublet appears to be present.
d. This sample was a 5 mCi source of $Cu_{0.67}Ni_{0.33}(^{57}Co)$.
e. Unless otherwise stated error limits refer to estimated uncertainties.

Table IV-2

Parameters for quenched $(Cu_{1-x}Ni_x)_{0.995}Fe_{0.005}$ alloy spectra analyzed as a six-line hyperfine pattern (plus two separate Lorentzian lines at low Ni concentration).

x	T °K	Sample Thickness μm	Field kG	Position mm/sec (± 0.02)			Γ mm/sec (± 0.02)			Relative Area (± 0.05)			$(eQ V_{zz}/4)$ mm/sec[c] (± 0.01)
				$\gamma_2(-)$[a]	γ_2[a]	$\gamma_2(+)$	$\gamma_2(-)$	γ_2	$\gamma_2(+)$	$\gamma_2(-)$	γ_2	$\gamma_2(+)$	
0.01	298	25	< 8	-0.10	0.22	0.49	0.22	0.22	0.22	0.23	0.61	0.16	0.001
0.05	298	25	< 8	-0.10	0.16	0.49	0.22	0.22	0.22	0.13	0.80	0.07	-0.011
0.10	298	25	8.4 ± 2.0		0.10			0.24			1.0		-0.017
0.21	298	25	10.5 ± 2.0		0.06			0.22			1.0		-0.002
0.33	298	25	10.6 ± 2.0		0.03			0.21			1.0		0.008
0.33[b]	298	25	10.9 ± 2.0		0.00			0.21			1.0		0.000
0.47	298	25	9.4 ± 2.0		0.03			0.22			1.0		0.009
0.53	298	25	8.7 ± 2.0		0.02			0.24			1.0		0.009

a. $\gamma_2(-)$ and $\gamma_2(+)$ refer to the γ_2 doublet in the same location as those found in CuFe, while γ_2 refers to the central line being analyzed as a 6-line pattern. The position and Γ of the $\gamma_2(-)$ and $\gamma_2(+)$ lines were held constant in the least squares fitting. The γ_2 doublet in CuFe corresponds to 18 ± 2 kG.

b. This sample was a 5 mCi source of $Cu_{0.67}Ni_{0.33}(Co^{57})$.

c. Values listed assume $(3\cos^2\theta-1)/2 = 1$.

Table IV-3

Parameters for $Cu_{1-y}Fe_y$ alloy spectra analyzed as a sum of separate Lorentzian lines.

y	Heat Treatment[a]	Sample Thickness μm	T °K	Line Position mm/sec (± 0.02)			Γ mm/sec (± 0.02)			Relative Area (± 0.05)		
				$\gamma_2(-)+\gamma_1$[b]	γ_0	$\gamma_2(+)$	$\gamma_2(-)+\gamma_1$	γ_0	$\gamma_2(+)$	$\gamma_2(-)+\gamma_1$	γ_0	$\gamma_2(+)$
0.005	Q	25	298	-0.10	0.24	0.48	0.29	0.22	0.28	0.13	0.73	0.14
0.005[c]	Q	25	298	-0.09	0.23	0.49	0.24	0.24	0.28	0.17	0.66	0.17
0.005[c]	Q	25	4.2	0.04	0.36	0.61	0.42	0.25	0.26	0.24	0.64	0.12
0.025	SC	30	298	-0.09	0.23	0.48	0.30	0.38	0.25	0.37	0.54	0.09
0.03	Q	13	298	-0.09	0.23	0.47	0.28	0.37	0.24	0.40	0.52	0.07
0.03	A	13	298	-0.08	0.21	(d)	0.40	0.29	(d)	0.69	0.31	(d)
0.03	A	13	4.2[e]	(1) -0.12 (2) 0.31			(1) 0.69 (2) 0.55			(1) 0.55 (2) 0.45		
0.03	A	13	4.2[f]	(1) 0.07 (2)18.5 ± 2			0.31					

a. Q refers to quenched, SC to splat cooled, and A to annealed.
b. $\gamma_2(-)$ refers to the peak of the γ_2 doublet at lower velocity, $\gamma_2(+)$ to the peak at higher velocity. The $\gamma_2(-)$ and γ_1 peaks lie very close together and cannot be resolved.
c. Second of two samples prepared identically.
d. Appears to be present, but too weak to resolve.
e. Analyzed as two lines referred to as (1) and (2). The γ_0 and γ_1 contributions are superimposed.
f. Analyzed as a six-line hyperfine field pattern. (1) is center of spectrum, (2) is field in kG.

Table IV-4

Parameters for annealed $Cu_{0.97}Fe_{0.03}$ spectra at 205°K with and without an applied field (source at 255°K).

Field Splitting kG	Position mm/sec (± 0.03)		Γ mm/sec (± 0.03)		Relative Area	
	γ_0	γ_1	γ_0	γ_1	γ_0	γ_1
0	0.25	-0.07	0.31	0.41	0.29	0.71
45.6 ± 1.0	0.25	-0.06	0.30	0.30	0.22	0.78

Table IV-5

Parameters obtained for 298°K spectra from three quenched samples of $(Cu_{0.90}Ni_{0.10})_{1-y}Fe_y$.

y	Thickness μm	Fitted by separate Lorentzians				Fitted by hyperfine field splitting			
		Line Position mm/sec (± 0.02)		Linewidth mm/sec (± 0.02)		Center mm/sec (± 0.02)	FWHM mm/sec (±0.04)	Field kG ± 2	$eQV_{zz}/4$ mm/sec[a] (±0.01)
		$\gamma_2(-)$	$\gamma_2(+)$	$\gamma_2(-)$	$\gamma_2(+)$				
0.03	12	-0.09	0.24	0.36	0.43	0.10	0.31	13.9	-0.010
0.06	12	-0.11	0.26	0.37	0.45	0.09	0.31	15.4	-0.005
0.08	12	-0.12	0.27	0.49	0.52	0.08	0.39	16.6	0.000

a. Values listed assume $(3\cos^2\theta-1)/2 = 1$.

Table IV-6

Summary of Mossbauer Effect Spectra for $(Cu_{1-x}Ni_x)_{1-y}Fe_y$ Alloys.

Sample Composition[a]		Heat Treatment[b]	T °K	Estimated Fractions of Spectral Compositions				H for 6-line pattern kG	Remarks
x	y			γ_0	γ_1	γ_2 doublet	resolved 6-line pattern		
0	0.005	Q	298	0.7	0.3				
0	0.005	Q	4.2	0.6	0.4				
0	0.005	FC	298	0.4	0.6				γ_2 barely resolved
0	0.015	FC	298	0.3	0.7				γ_2 barely resolved
0	0.025	FC	298	0.2	0.4		0.4	330 ± 5	6-line pattern is α-Fe
0	0.025	SC	298	0.5	0.3	0.2			
0	0.025	SC	4.2				unresolved splitting	150 ± 20	very broad unresolved structure
0	0.03	Q	298	0.5	0.3	0.2			
0	0.03	Q	4.2				unresolved splitting	170 ± 20	very broad unresolved structure
0	0.03	A	298	0.3	0.7				γ_2 barely resolved
0	0.03	A	4.2				unresolved splitting	18 ± 5	γ_0 and γ_1 spectra superimposed

Table IV-6 (continued)

x	y	Heat Treatment	T	γ_0	γ_1	γ_2 doublet	resolved 6-line pattern	<H>	Remarks
0	0.06	Q	298	0.3	0.6	0.1			
0	0.06	Q	78	0.3	0.6	0.1			
0.10	0.005	Q	298			1.0			
0.10	0.007	FC	298			1.0			
0.10	0.007	FC	4.2			1.0			
0.10	0.008	FC	298			1.0			
0.10	0.015	FC	298						
0.10	0.015	FC	78			.3	.7	304 $\pm$ 8	
0.10	0.025	FC	298			.3	.7	292 $\pm$ 8	
0.10	0.03	Q	298			1.0			
0.10	0.03	Q	78			1.0			
0.10	0.03	Q	4.2				1.0	194 $\pm$ 8	
0.10	0.06	Q	298			1.0			

Table IV-6 (continued)

x	y	Heat Treatment	T	γ_0	γ_1	γ_2 doublet	resolved 6-line pattern	<H>	Remarks
0.10	0.08	A	298			0.2	0.8	288 ± 8	Ferromagnetic at 298°K
0.10	0.08	Q	298			1.0			Ferromagnetic at 298°K
0.10	0.08	Q	78			0.5	0.5	318 ± 8	
0.10	0.08	Q	4.2				1.0	315 ± 8	
0.21	0.005	FC	298			1.0			
0.21	0.005	Q	298			1.0			
0.21	0.015	FC	298			1.0			
0.21	0.025	FC	298			1.0			
0.21	0.025	FC	78			0.4	0.6	292 ± 8	
0.21	0.025	SC	298			1.0			
0.21	0.025	SC	78			1.0			
0.21	0.03	FC	298			1.0			
0.21	0.03	Q	298			1.0			

Table IV-6 (continued)

x	y	Heat Treatment	T	γ_0	γ_1	γ_2 doublet	resolved 6-line pattern	H	Remarks
0.21	0.03	Q	78			1.0			
0.21	0.03	Q	4.2				1.0	185 $\pm$ 8	
0.21	0.05	FC	298			1.0			
0.21	0.05	Q	298			1.0			
0.33	0.005	Q	298			1.0			
0.33	0.005	Q	4.2			1.0			
0.33	0.015	FC	298			1.0			
0.33	0.015	FC	78			1.0			
0.33	0.025	FC	78			1.0			
0.47	0.005	Q	298			1.0			
0.47	0.005	Q	4.2				1.0	235 $\pm$ 8	
0.47	0.015	FC	298			1.0			

Table IV-6 (continued)

x	y	Heat Treatment	T	γ_0	γ_1	γ_2 doublet	resolved 6-line pattern	<H>	Remarks
0.47	0.015	FC	78			1.0			
0.47	0.025	FC	298			1.0			
0.47	0.025	FC	78				1.0	217 $\pm$ 8	
0.53	0.005	FC	298			1.0			
0.53	0.015	FC	298			1.0			
0.53	0.015	FC	78				1.0	210 $\pm$ 8	
0.53	0.025	FC	298			1.0			
0.53	0.025	FC	78				1.0	222 $\pm$ 8	

[a] Composition formula is $(Cu_{1-x}Ni_x)_{1-y}Fe_y$ with x and y atomic fractions.

[b] Q = quenched, FC = furnace cooled, SC = splat cooled, and A = annealed.

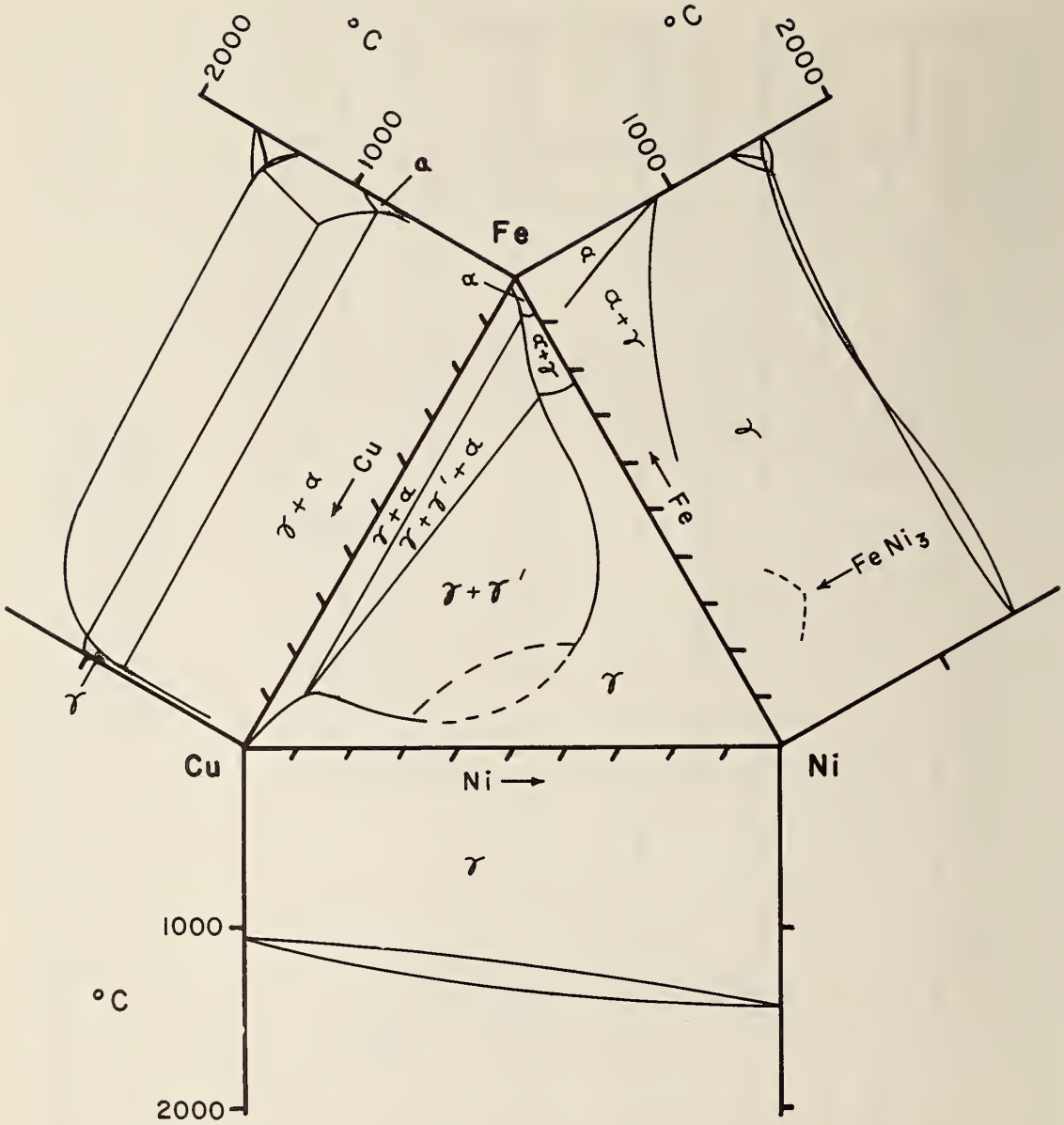

Figure II-1. Ternary and binary diagrams for Cu-Ni-Fe alloys. The ternary diagram is as given by Bradley et al.[125] for slow cooling. The notation of Bradley et al. has been changed so that α refers to bcc structures and γ to fcc structures.

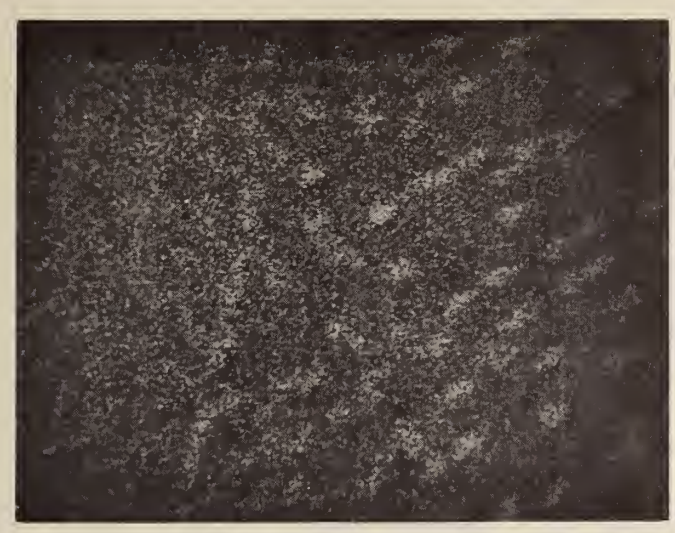

10μm

Figure III-1(a). Electron-probe scan of annealed $Cu_{0.97}Fe_{0.03}$ using FeKα X-ray.

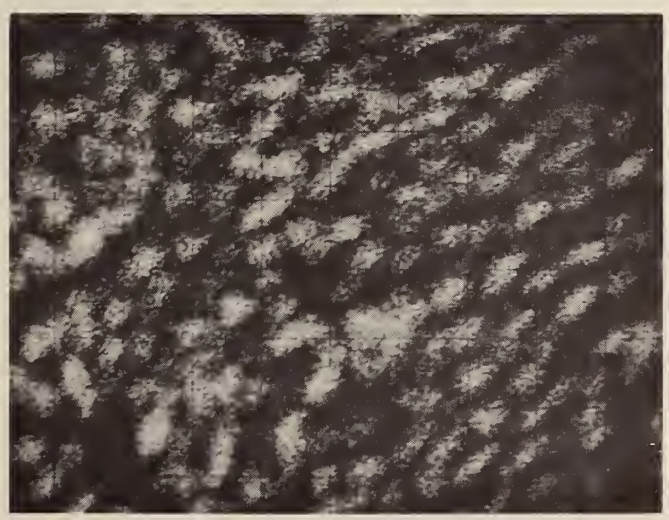

Figure III-1(b). Electron-probe scan of annealed $Cu_{0.94}Fe_{0.06}$ using FeKα X-ray.

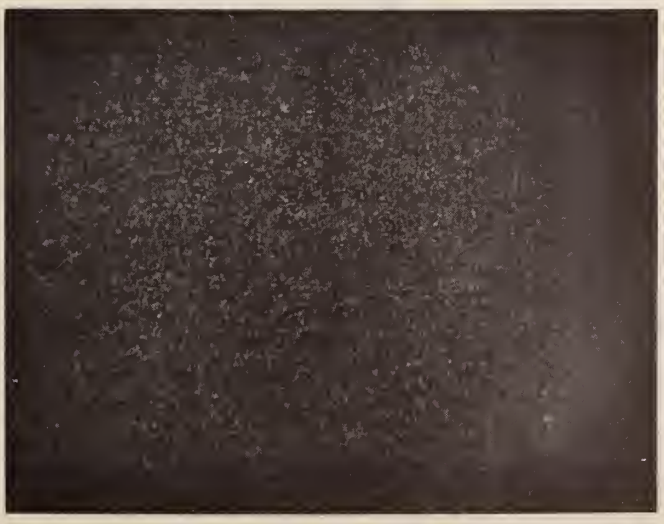

Figure III-1(c). Electron-probe scan of annealed $(Cu_{0.90}Ni_{0.10})_{0.92}Fe_{0.08}$ using FeKα X-ray.

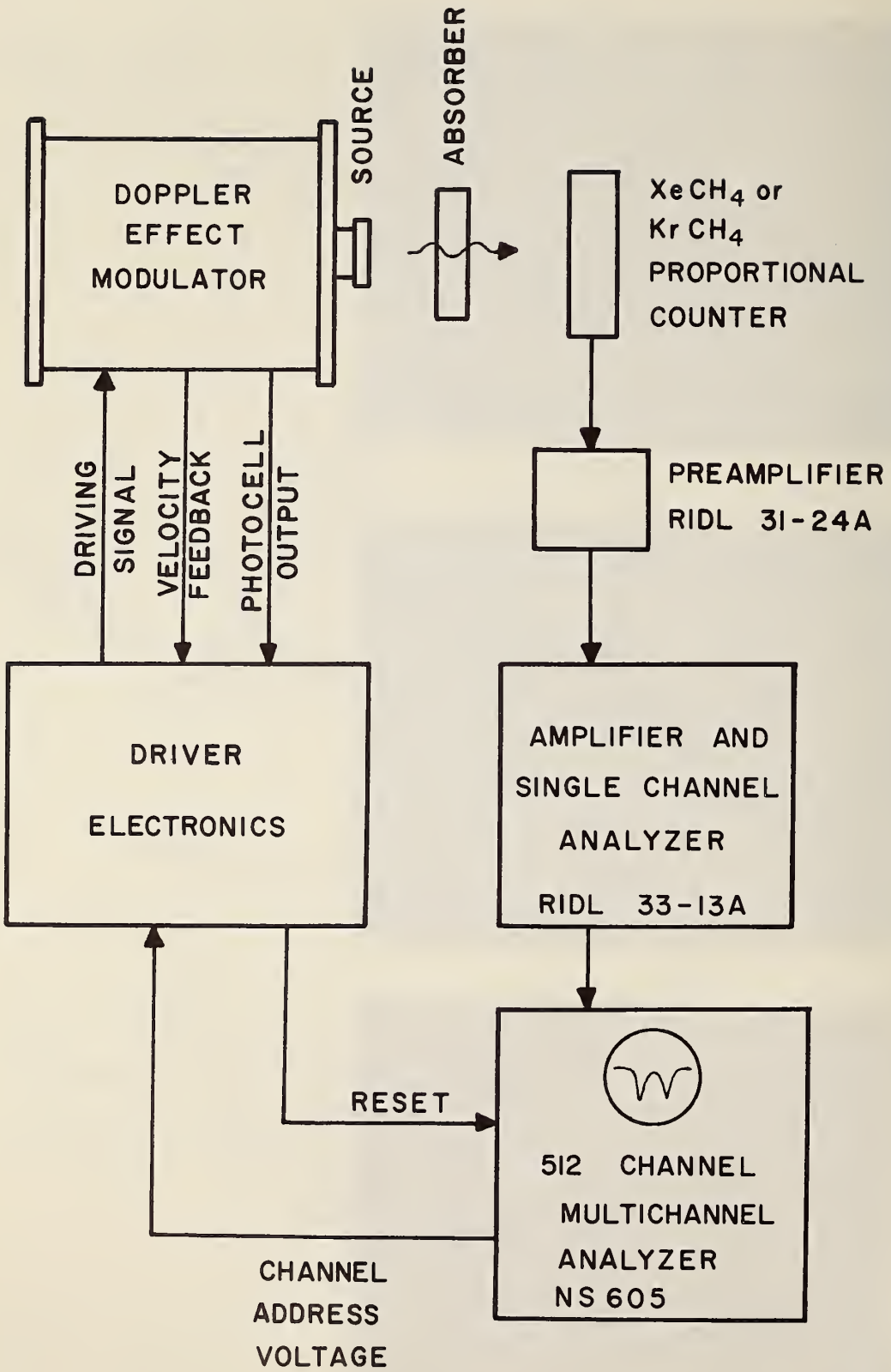

Figure III-2. Block diagram of Mössbauer effect spectrometer.

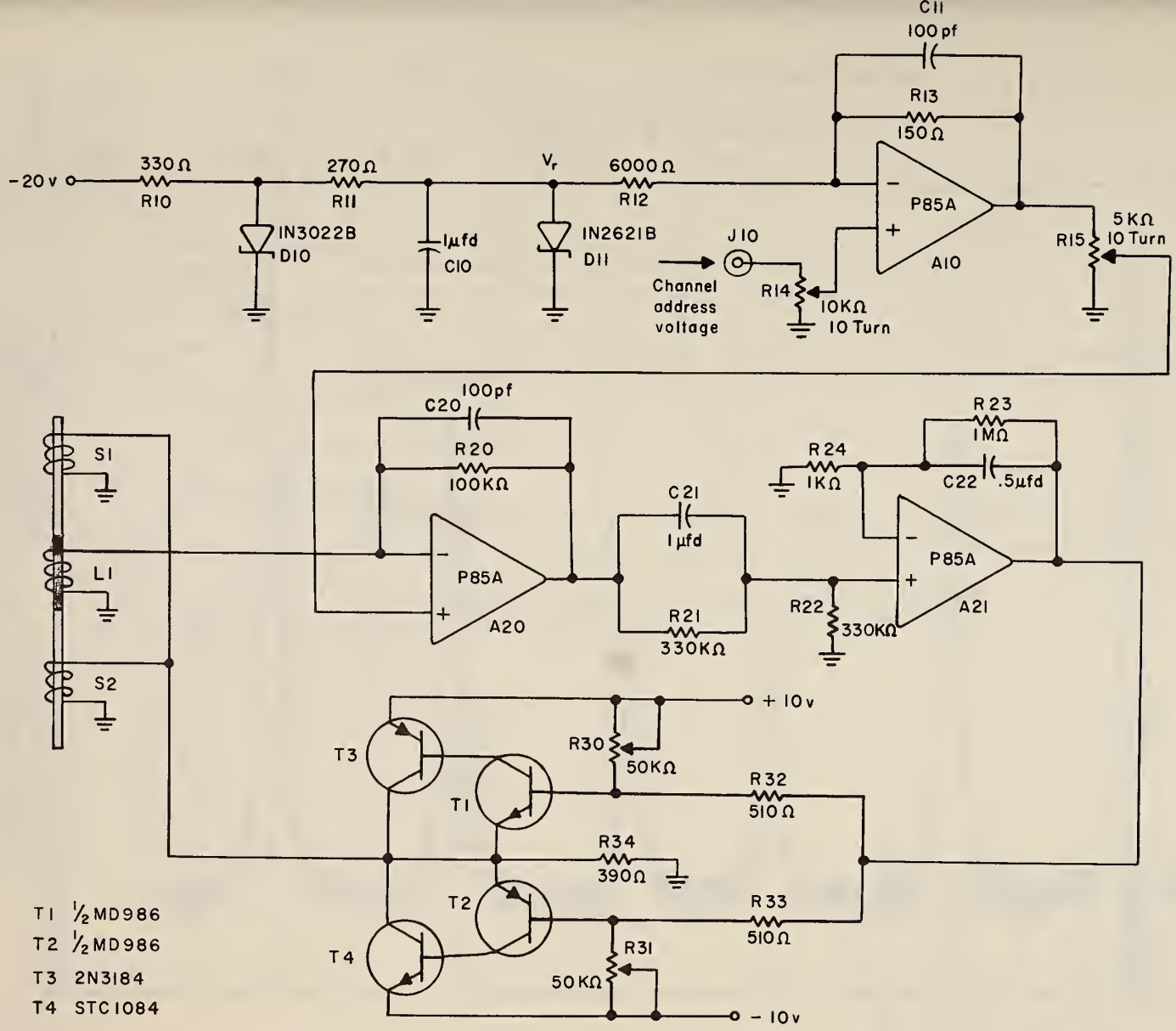

Figure III-3. Schematic of driver electronics.

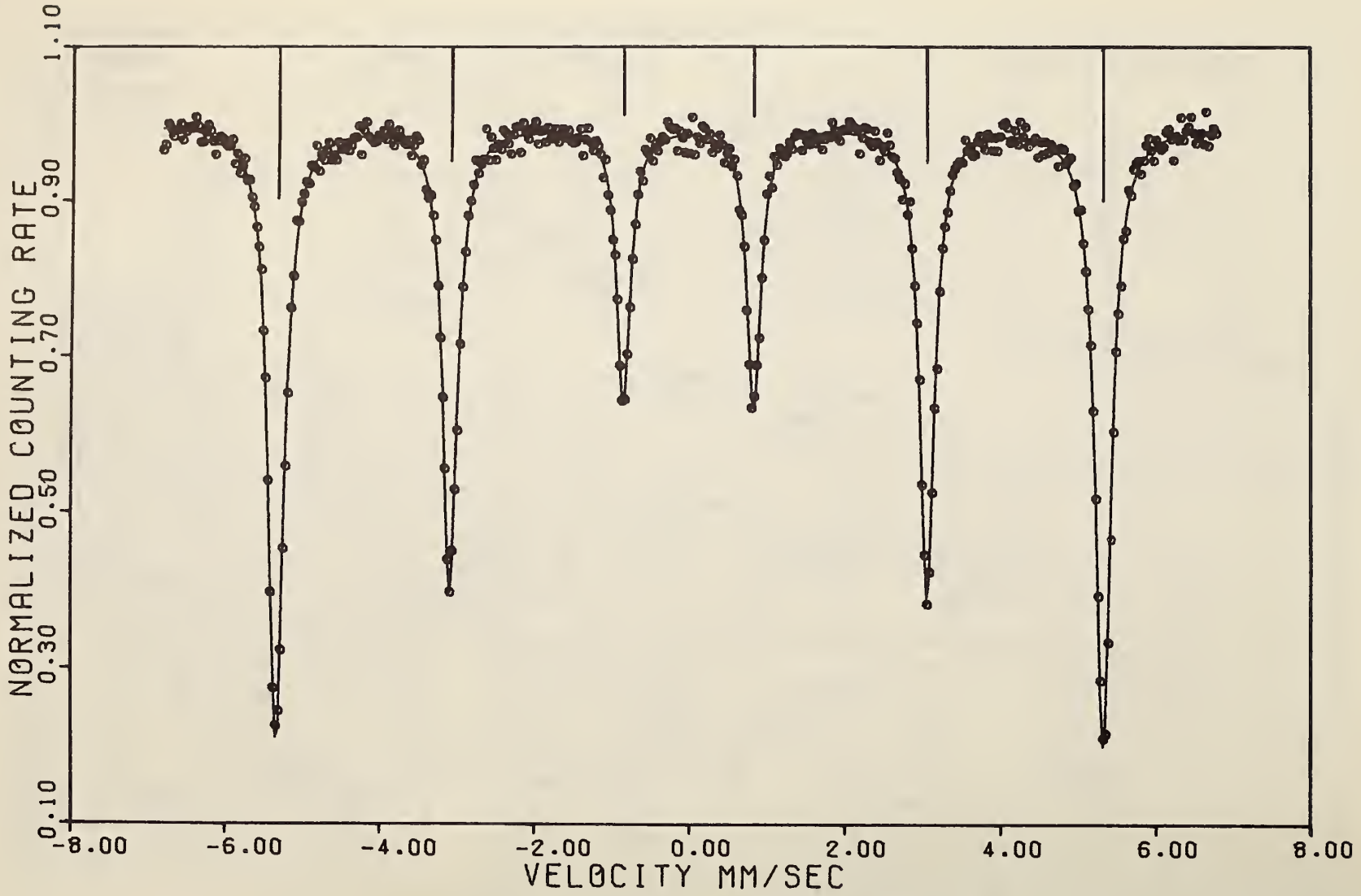

Figure III-4. Iron calibration spectrum.

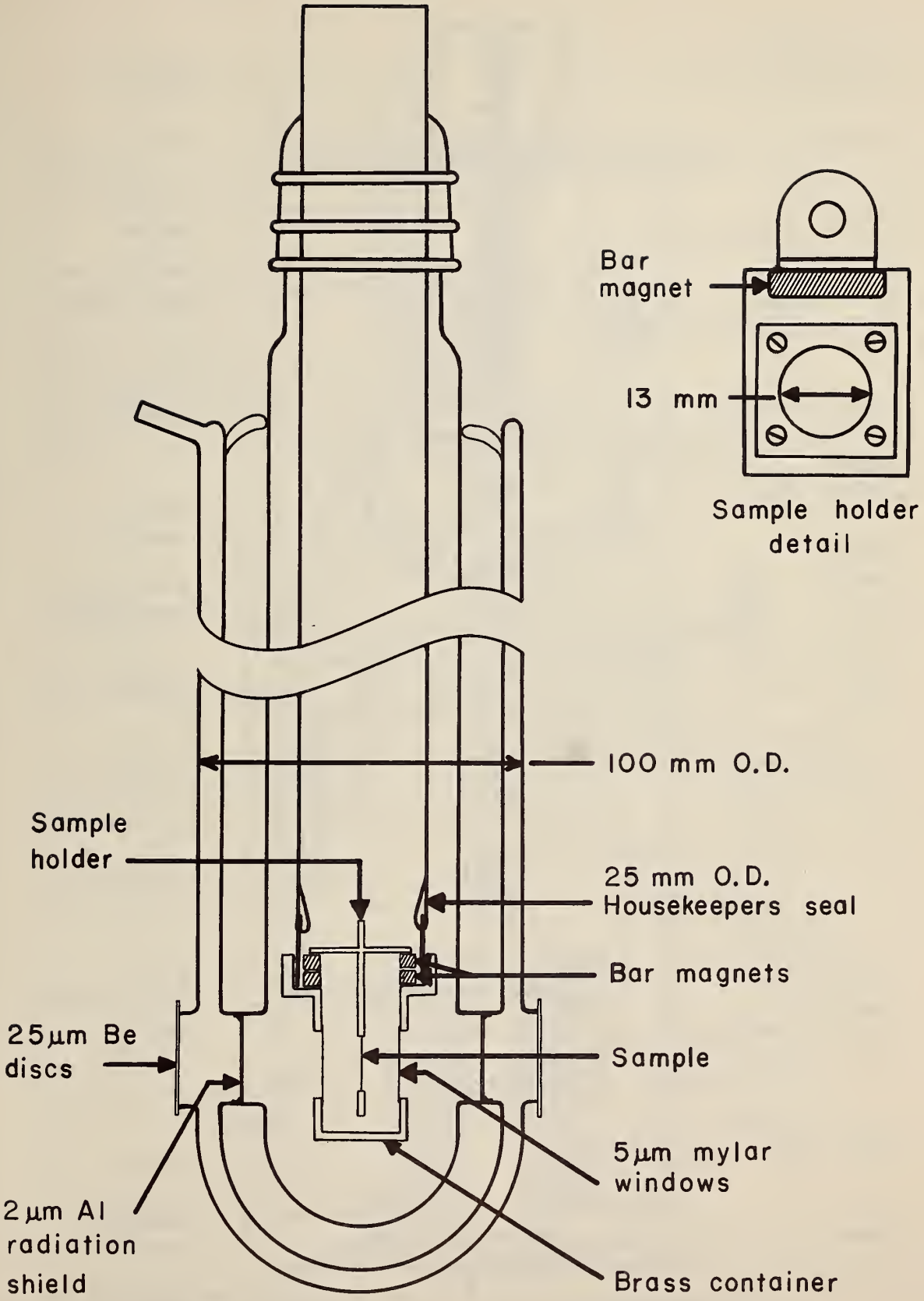

Figure III-5. Fixed temperature dewar.

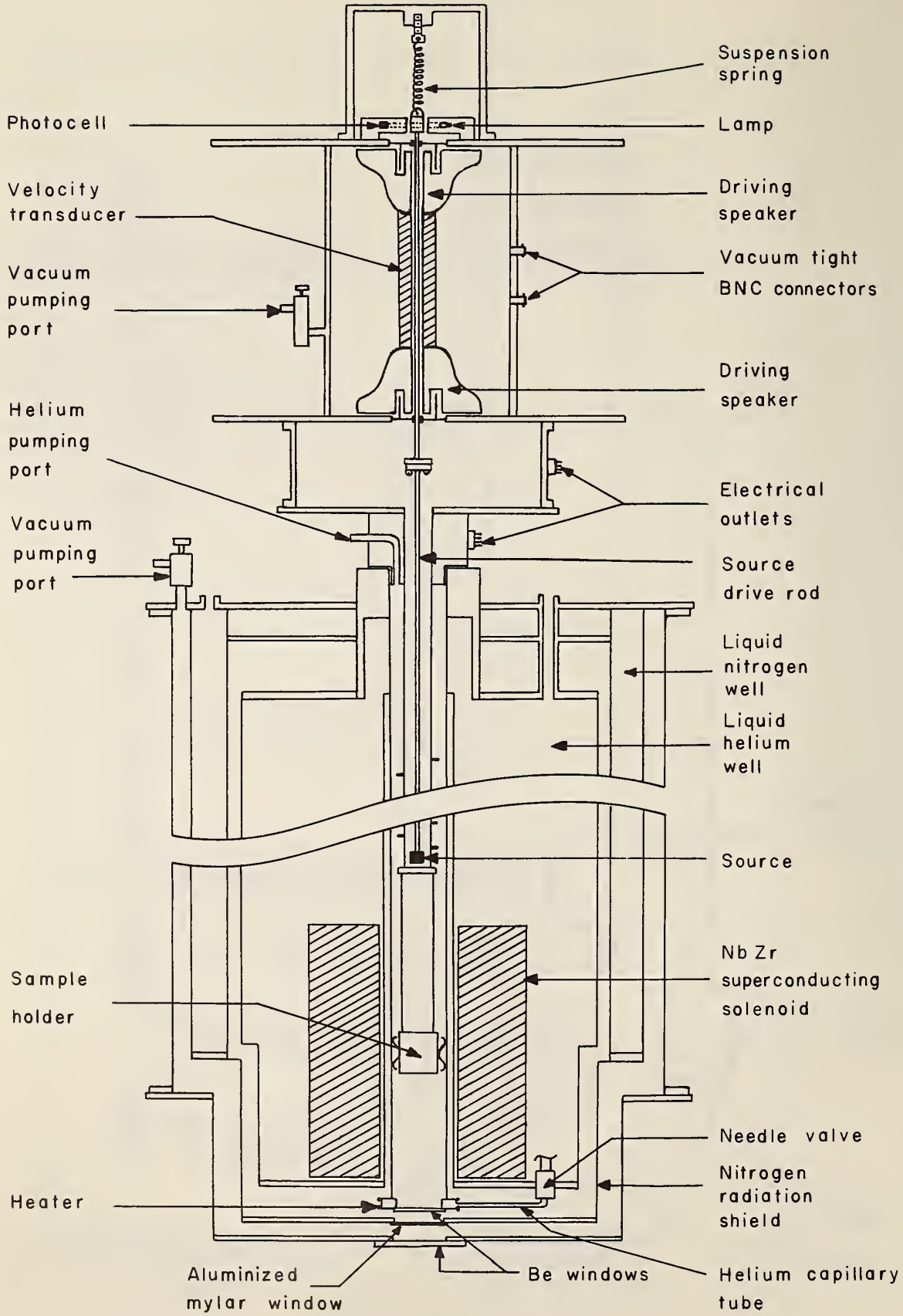

Figure III-6. Superconducting magnet and dewar system.

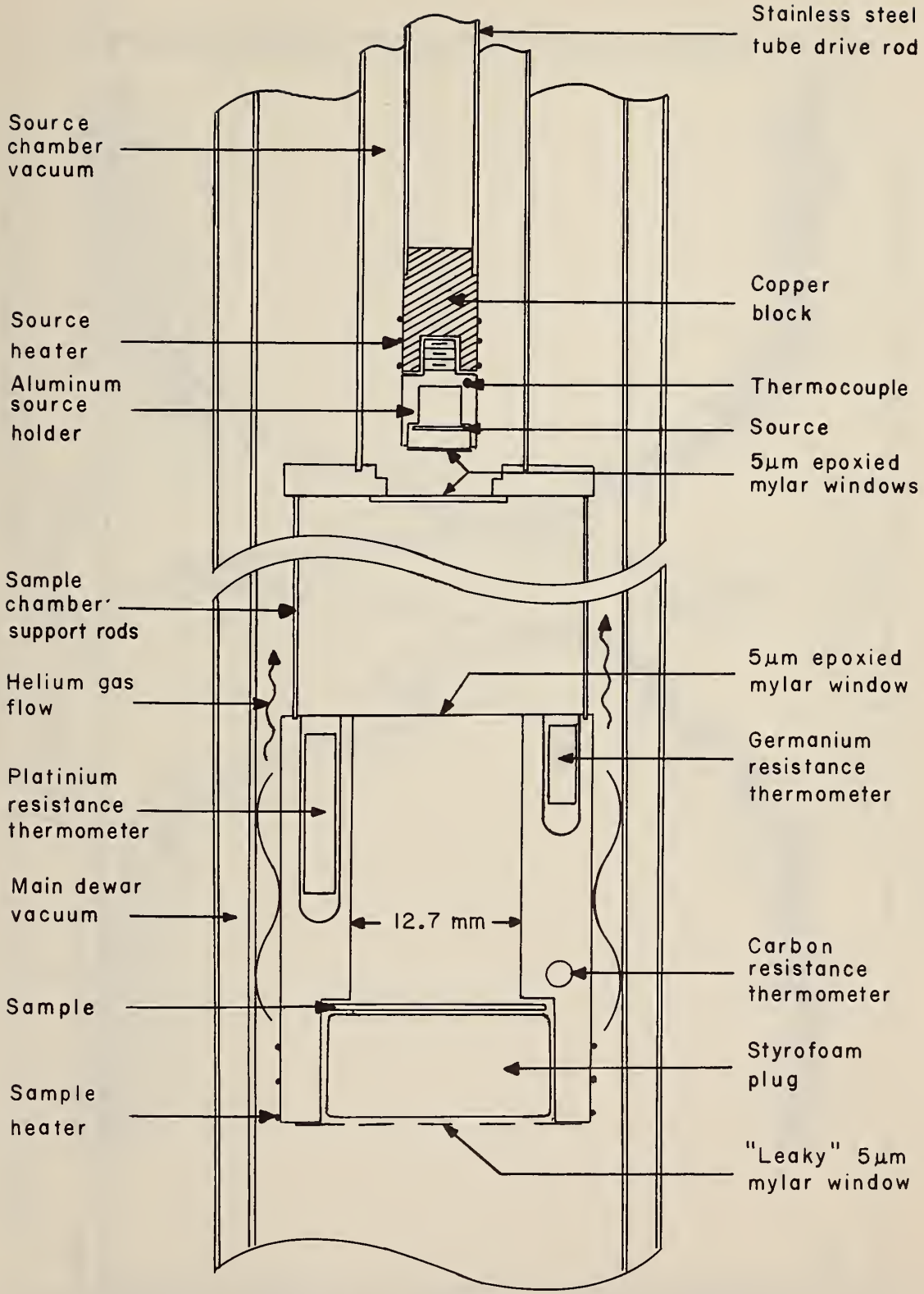

Figure III-7. Detail of sample holder and source chamber.

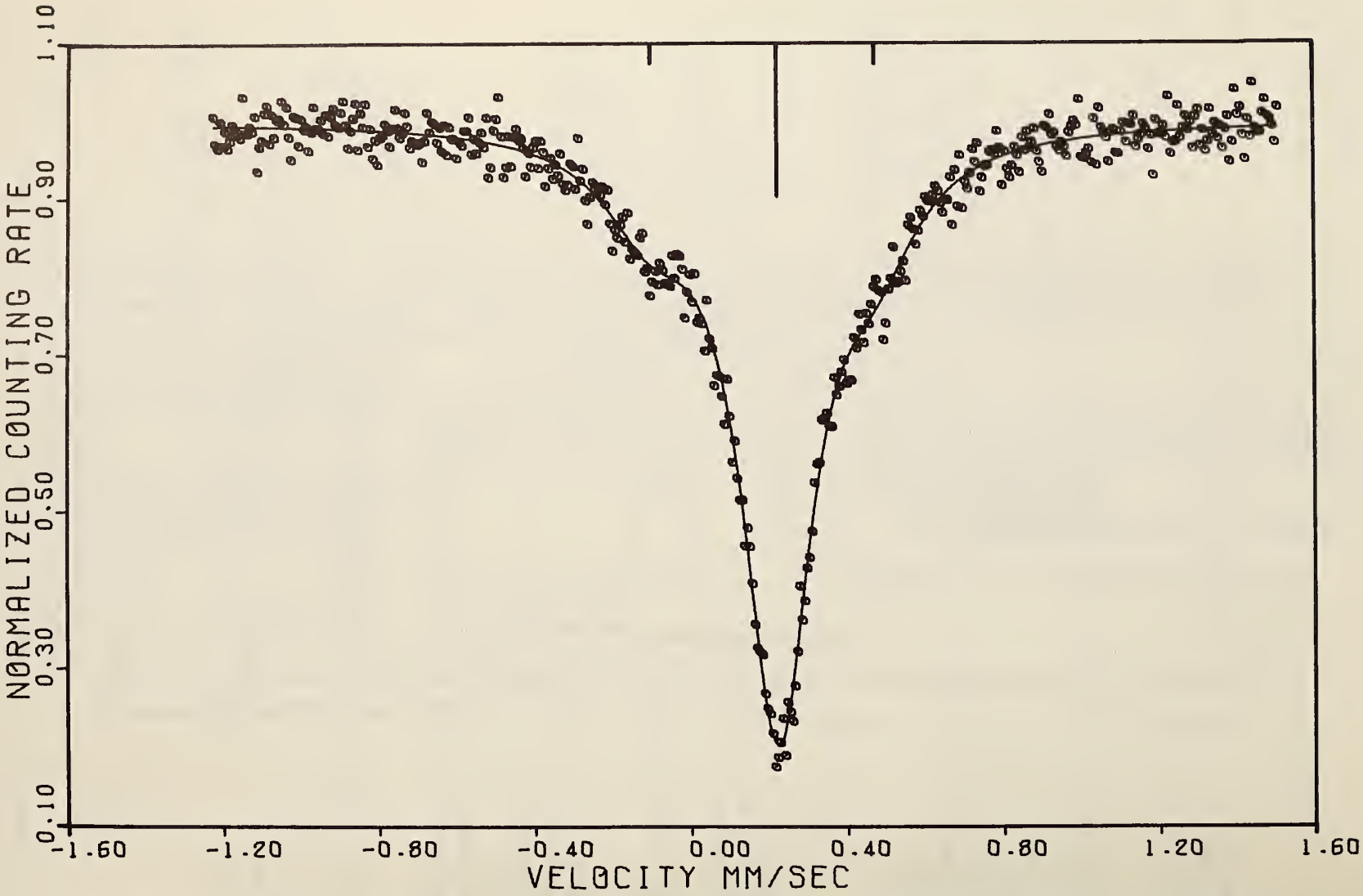

Figure IV-1(a). Sample no. 1 of $Cu_{0.995}Fe_{0.005}$ at 298°K fitted to three Lorentzians.

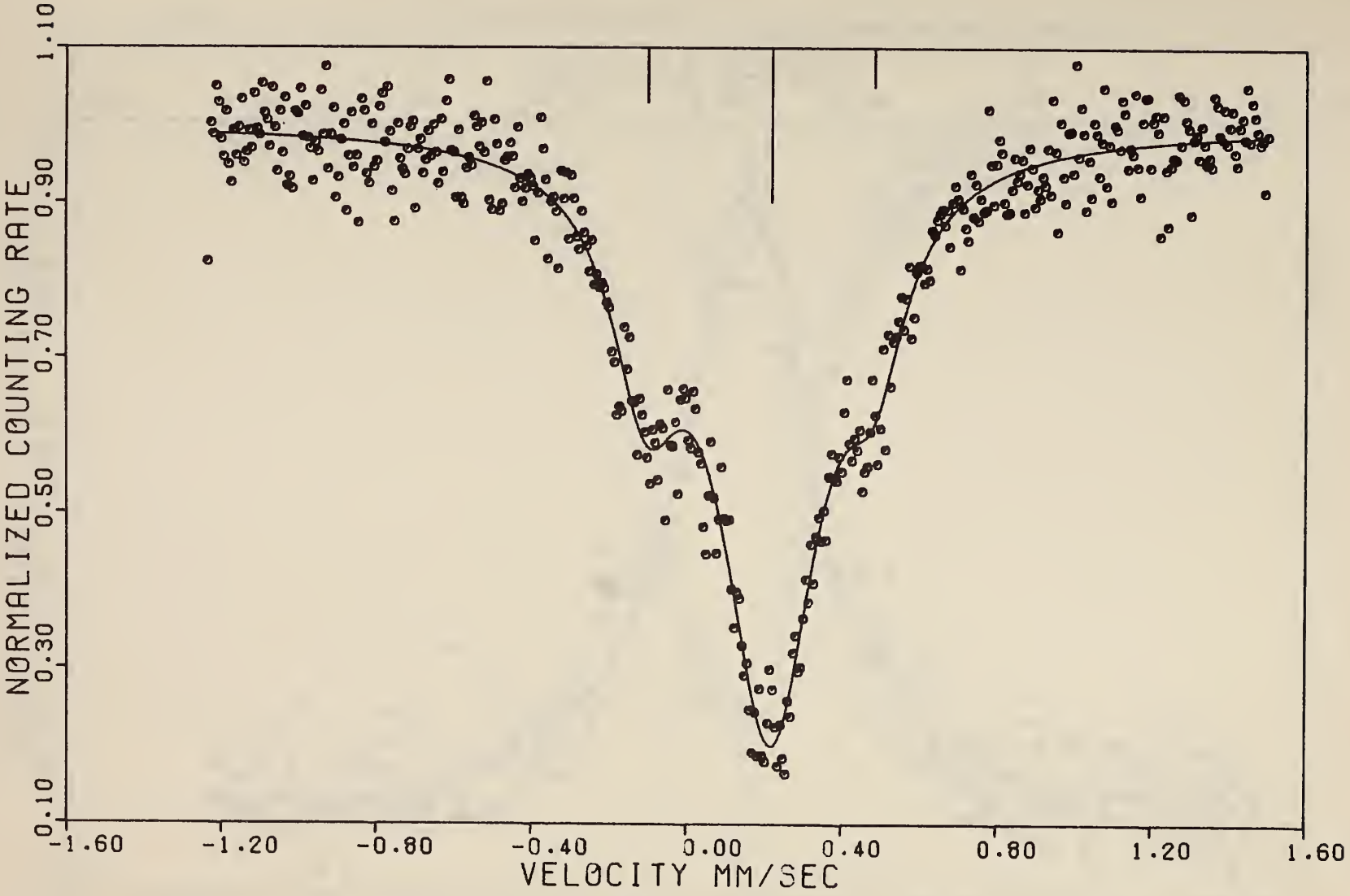

Figure IV-1(b). $(Cu_{0.99}Ni_{0.01})_{0.995}Fe_{0.005}$ at 298°K fitted to three Lorentzians.

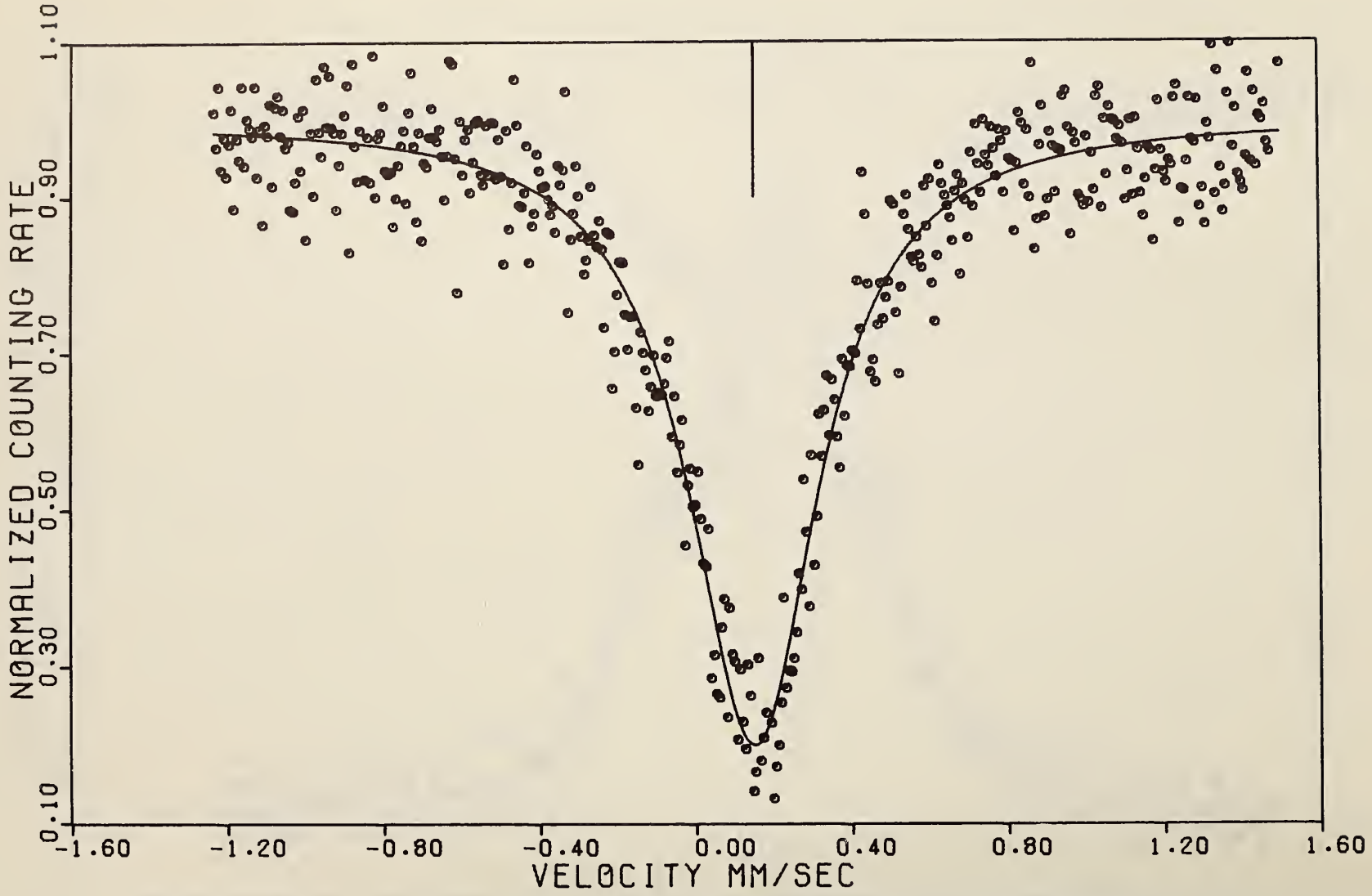

Figure IV-1(c). $(Cu_{0.95}Ni_{0.05})_{0.995}Fe_{0.005}$ at 298°K fitted to one Lorentzian.

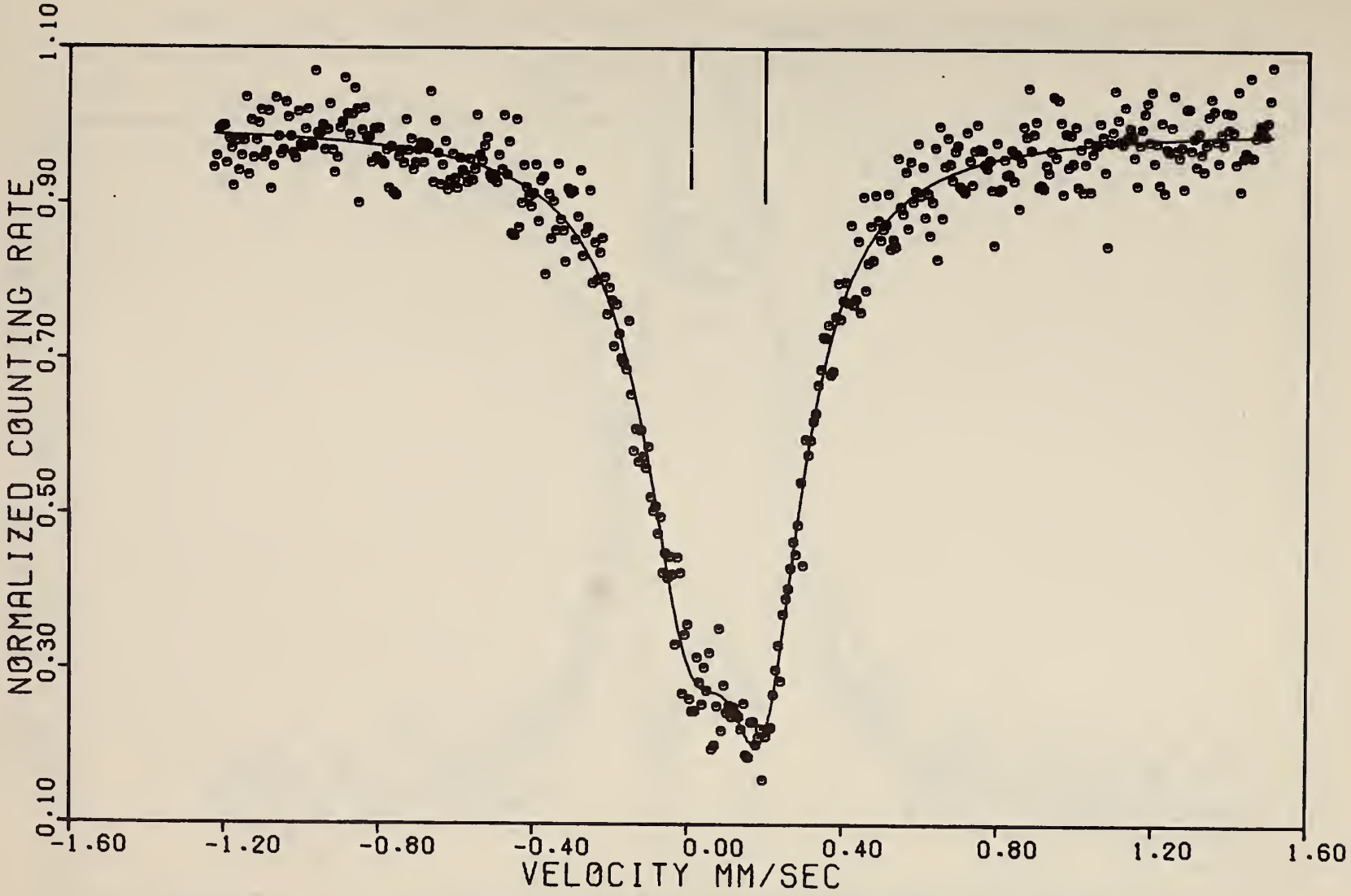

Figure IV-1(d). $(Cu_{0.90}Ni_{0.10})_{0.995}Fe_{0.005}$ at 298°K fitted to two Lorentzians.

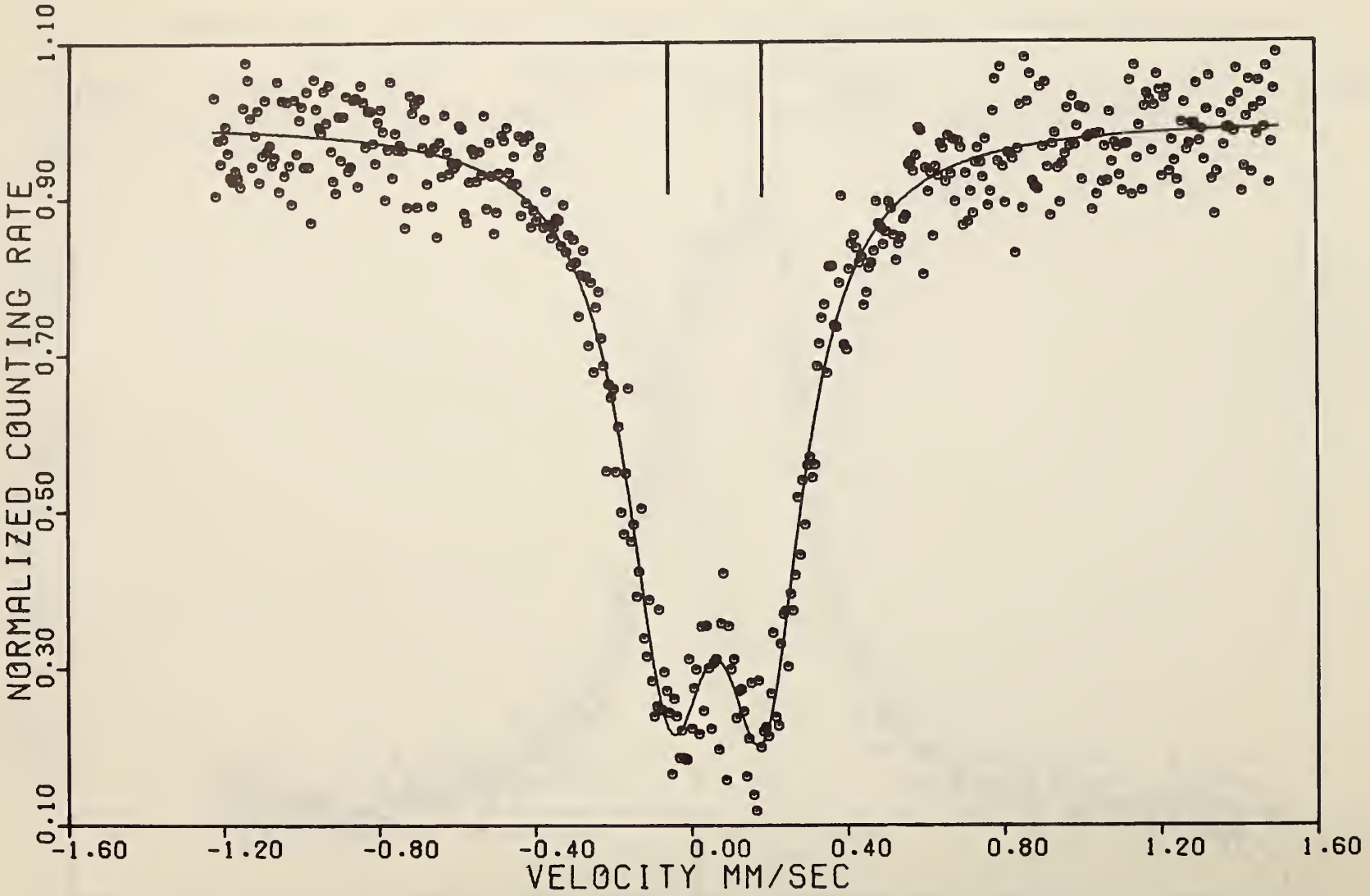

Figure IV-1(e). $(Cu_{0.79}Ni_{0.21})_{0.995}Fe_{0.005}$ at 298°K fitted to two Lorentzians.

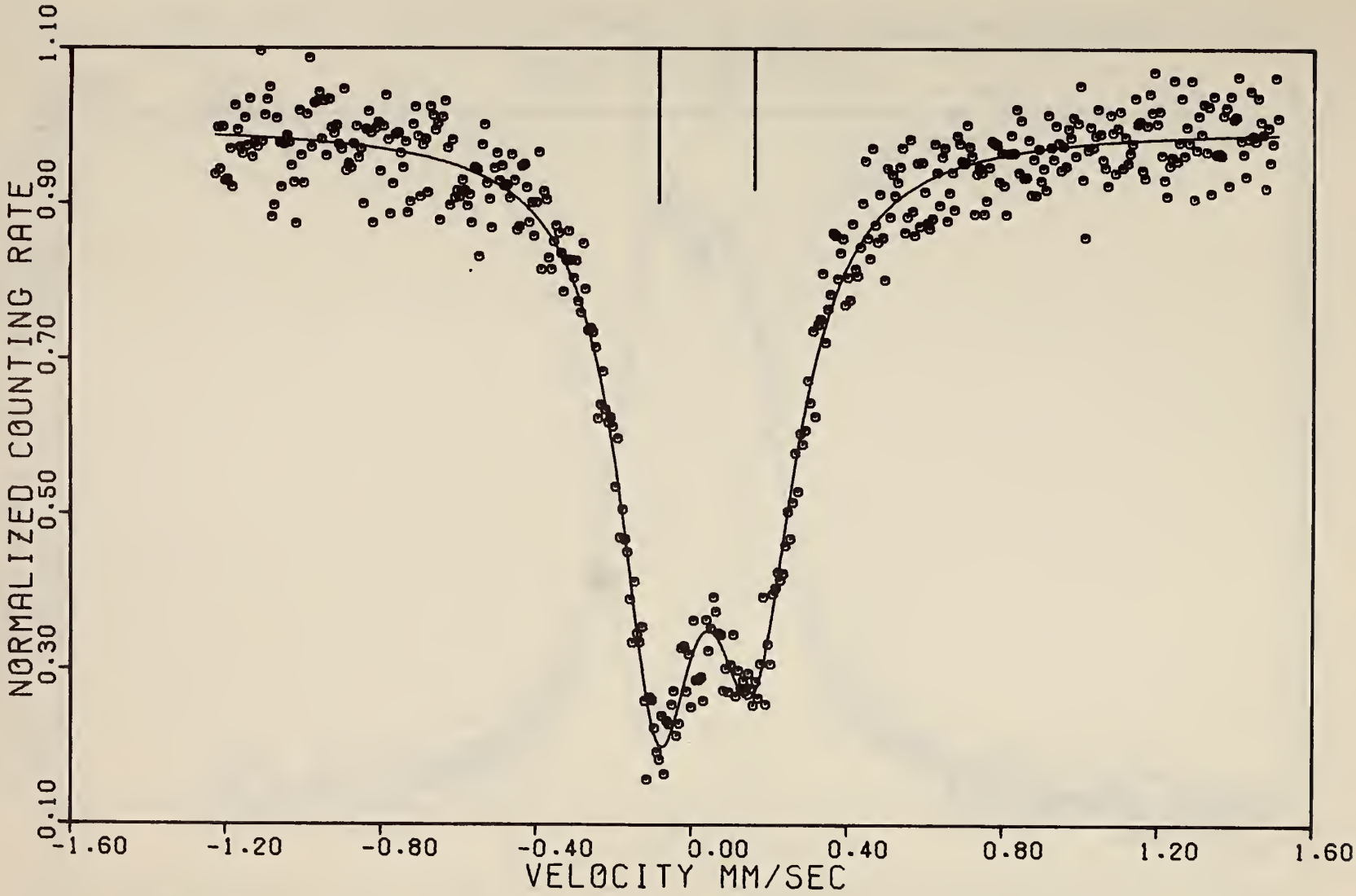

Figure IV-1(f). $(Cu_{0.67}Ni_{0.33})_{0.995}Fe_{0.005}$ at 298°K fitted to two Lorentzians.

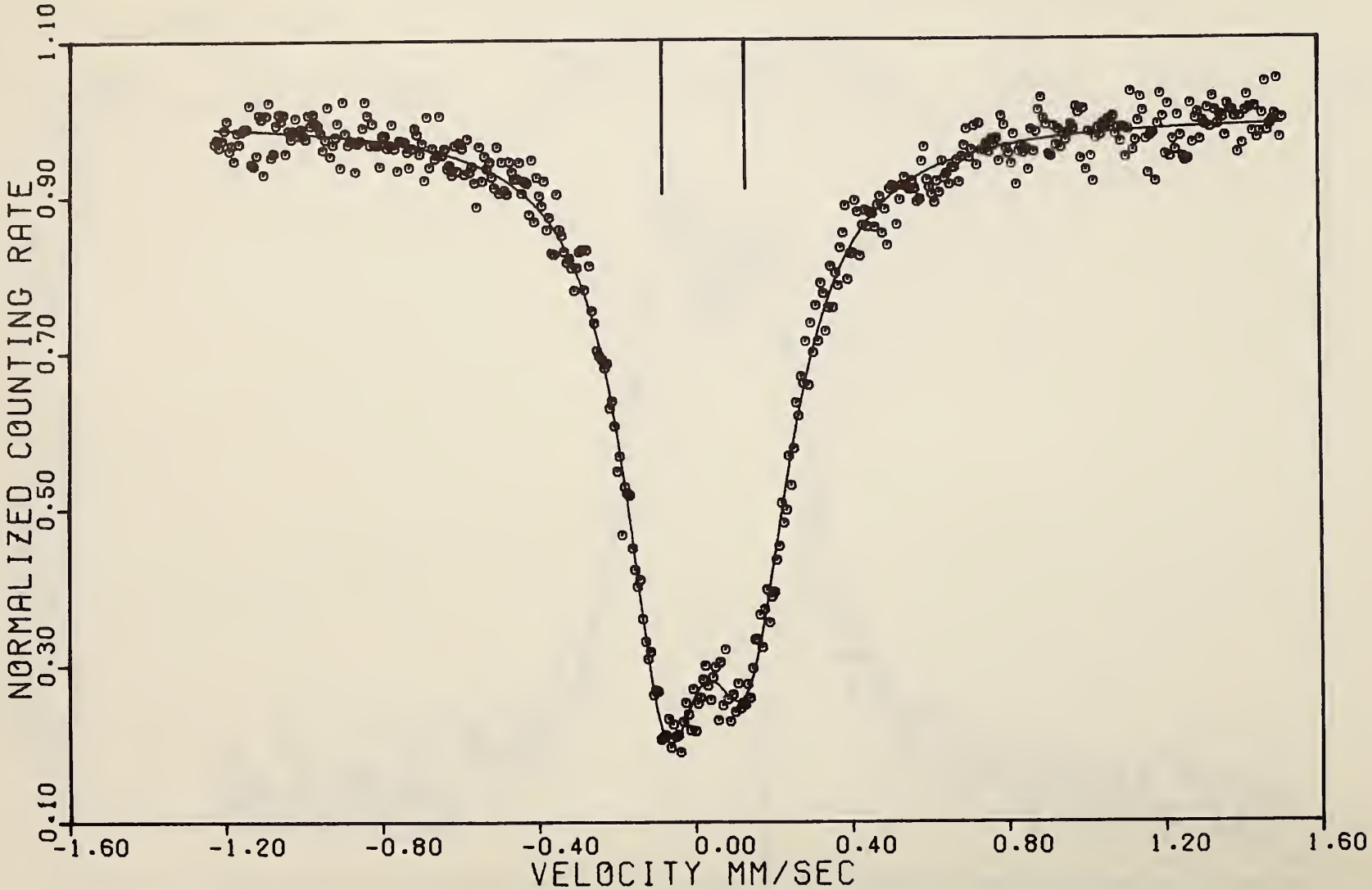

Figure IV-1(g). $(Cu_{0.53}Ni_{0.47})_{0.995}Fe_{0.005}$ at 298°K fitted to two Lorentzians.

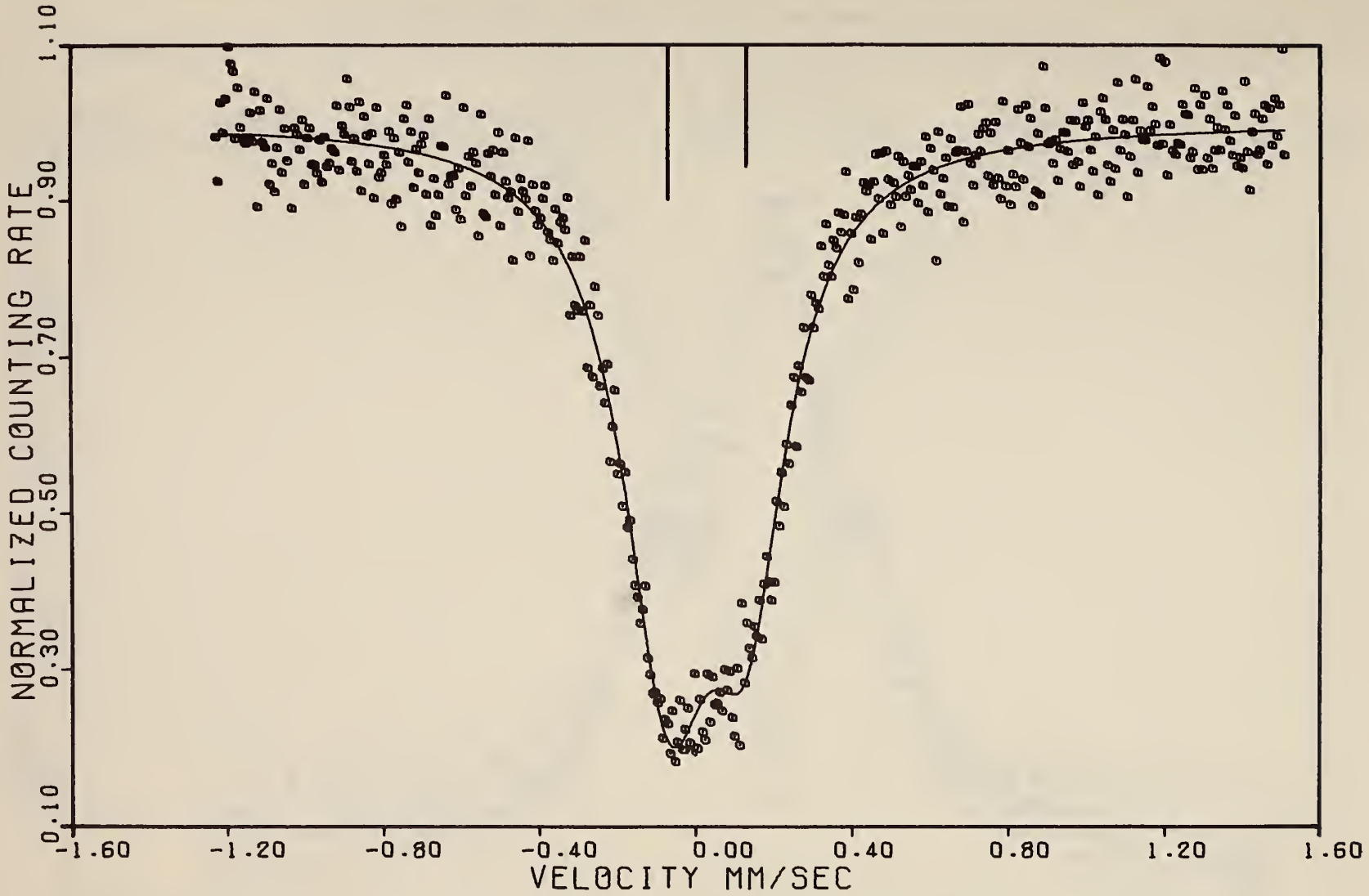

Figure IV-1(h). $(Cu_{0.47}Ni_{0.53})_{0.995}Fe_{0.005}$ at 298°K fitted to two Lorentzians.

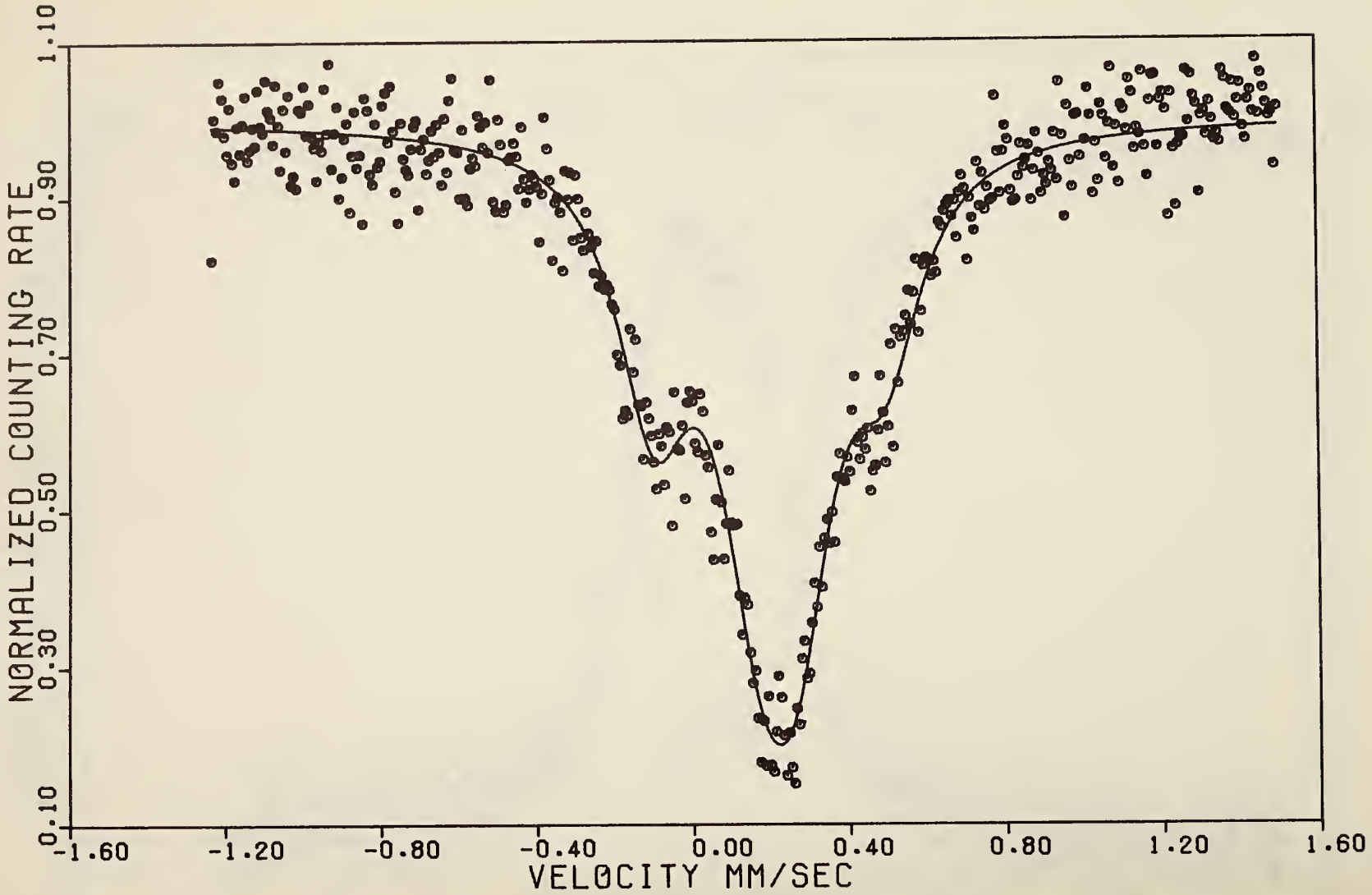

Figure IV-2(a). $(Cu_{0.99}Ni_{0.01})_{0.995}Fe_{0.005}$ at 298°K fitted to two Lorentzians plus a central unresolved six-line hyperfine field pattern.

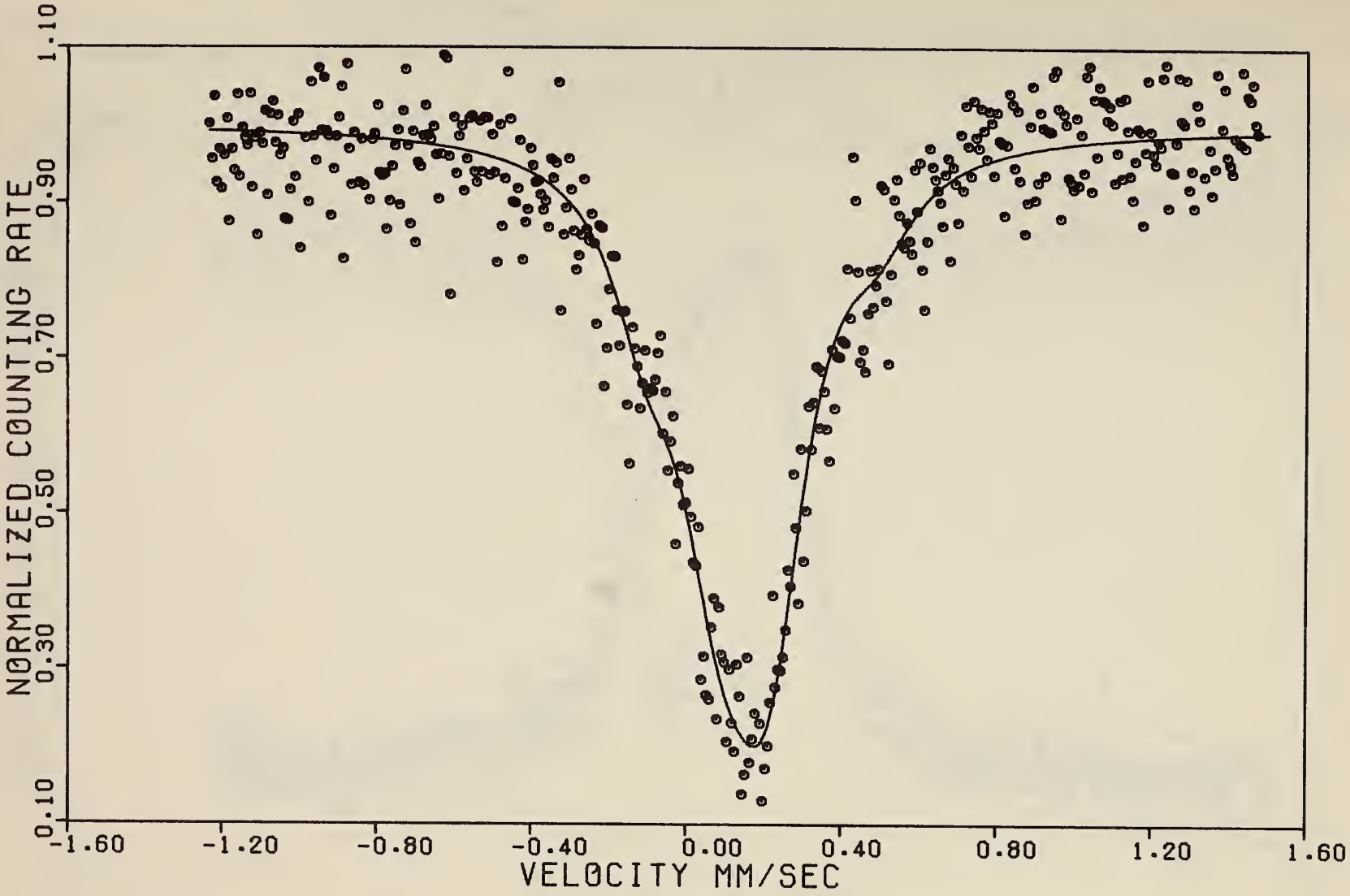

Figure IV-2(b). $(Cu_{0.95}Ni_{0.05})_{0.995}Fe_{0.005}$ at 298°K fitted to two Lorentzians plus a central unresolved six-line hyperfine field pattern.

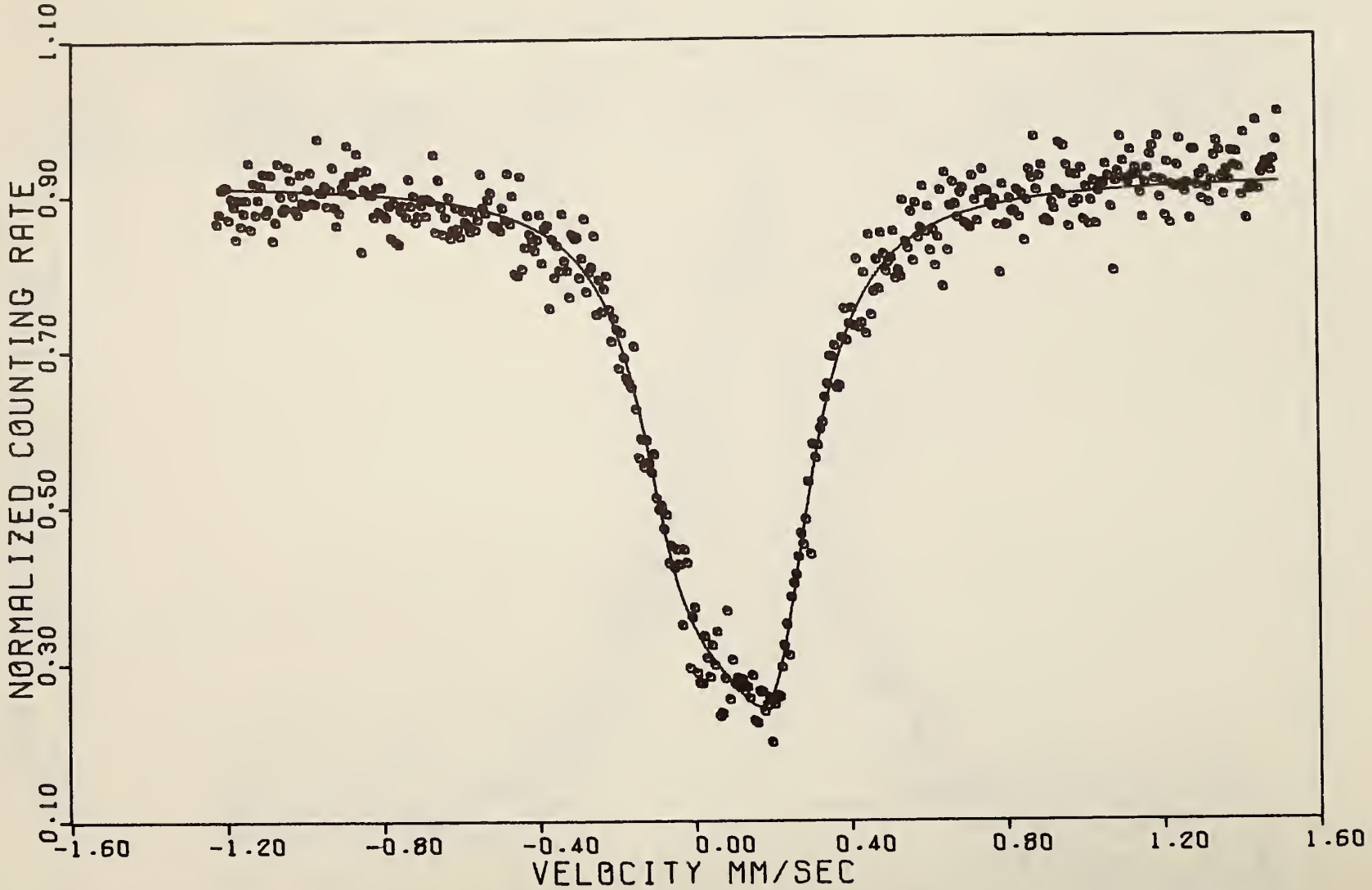

Figure IV-2(c). $(Cu_{0.90}Ni_{0.10})_{0.995}Fe_{0.005}$ at 298°K fitted to an unresolved six-line hyperfine field pattern.

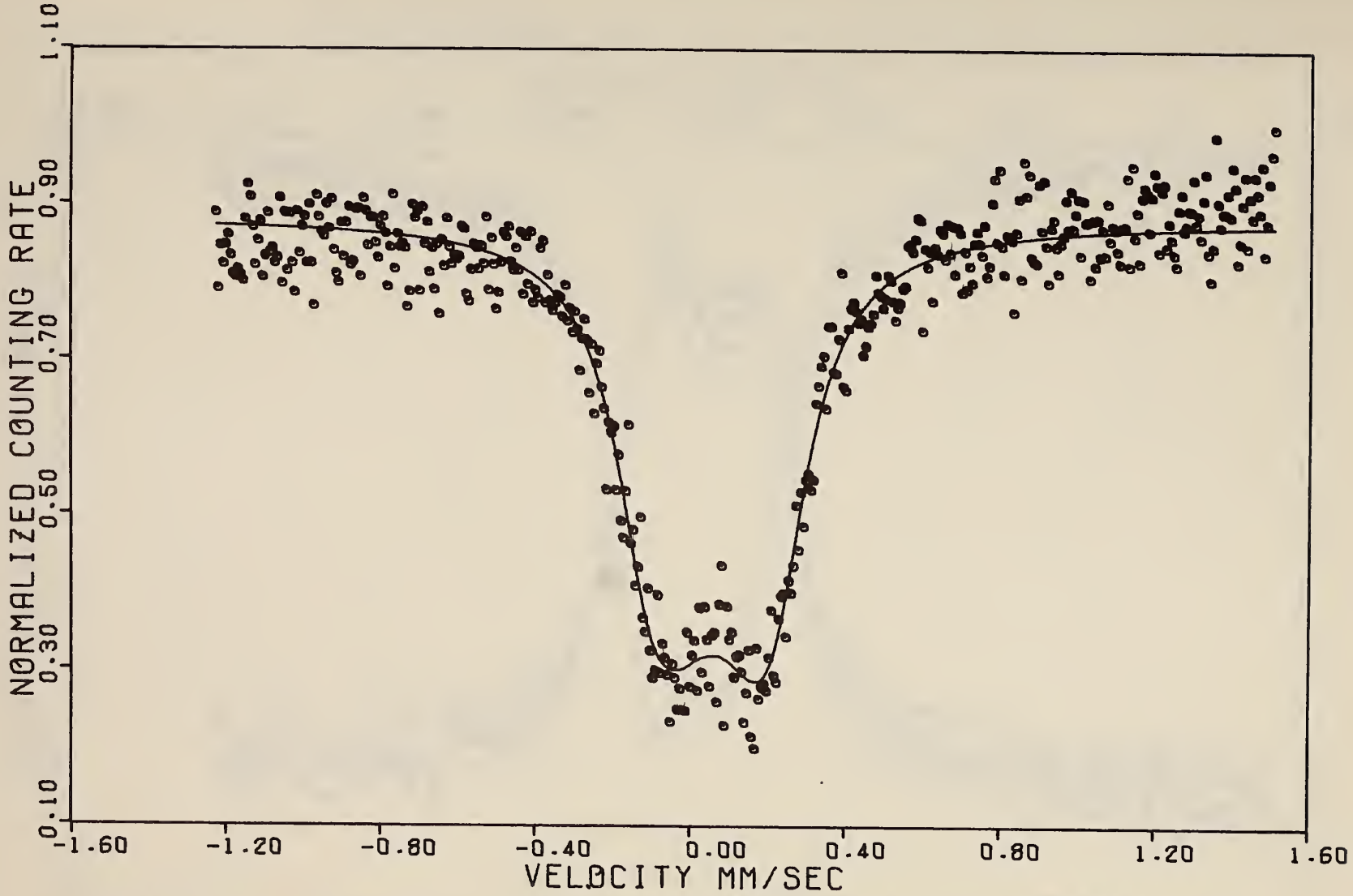

Figure IV-2(d). $(Cu_{0.79}Ni_{0.21})_{0.995}Fe_{0.005}$ at 298°K fitted to an unresolved six-line hyperfine field pattern.

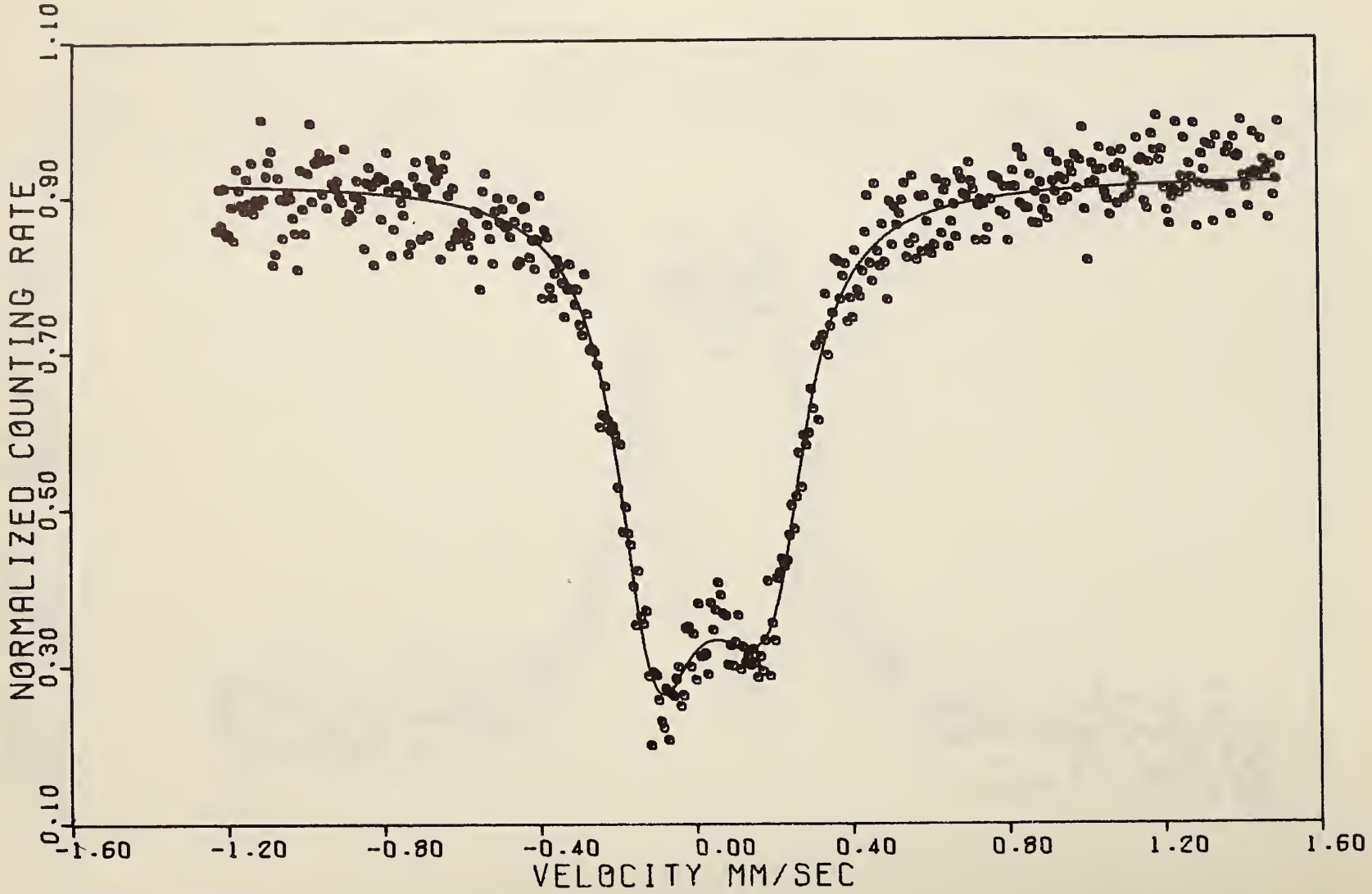

Figure IV-2(e). $(Cu_{0.67}Ni_{0.33})_{0.995}Fe_{0.005}$ at 298°K fitted to an unresolved six-line hyperfine field pattern.

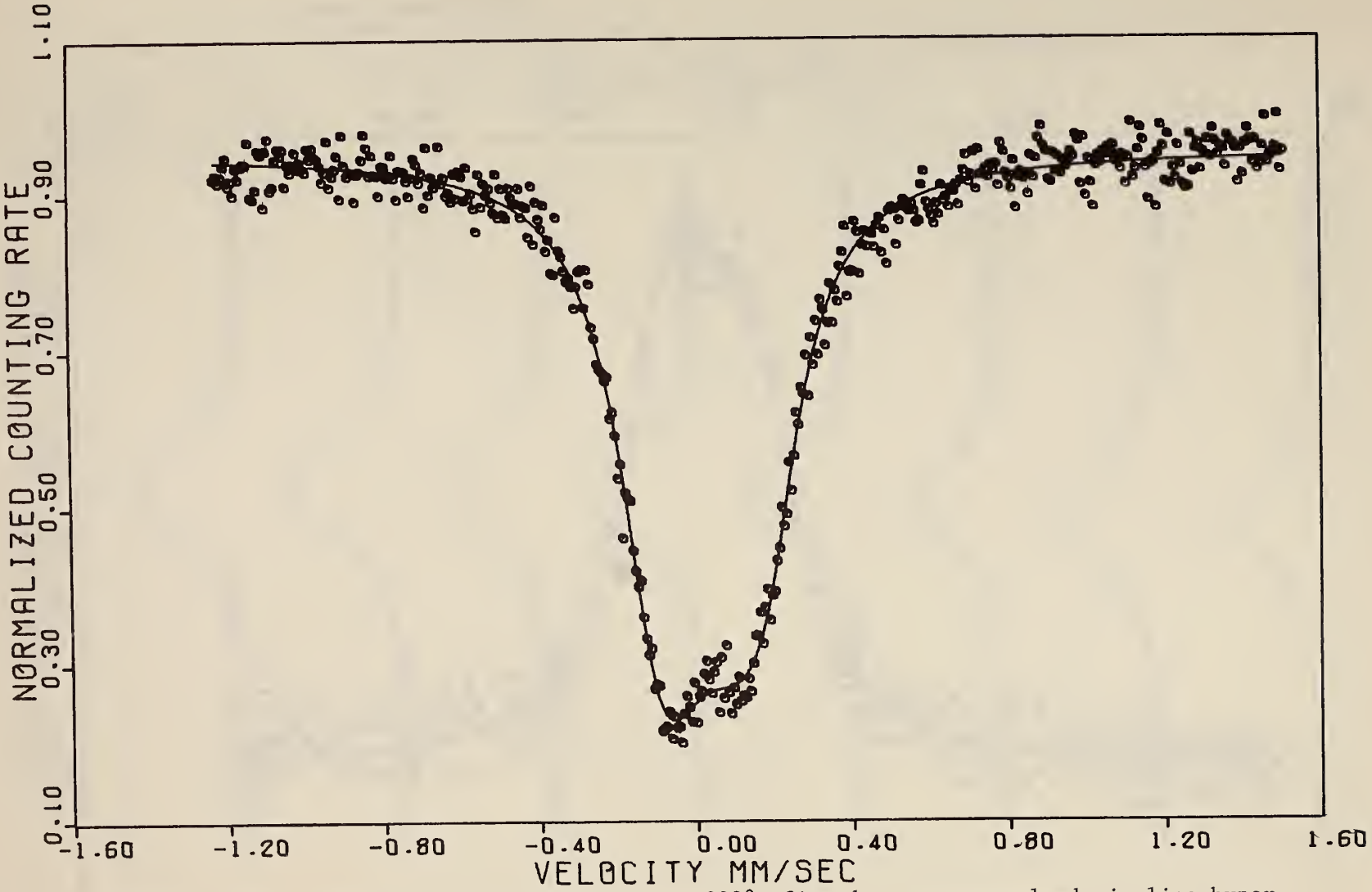

Figure IV-2(f). $(Cu_{0.53}Ni_{0.47})_{0.995}Fe_{0.005}$ at 298°K fitted to an unresolved six-line hyperfine field pattern.

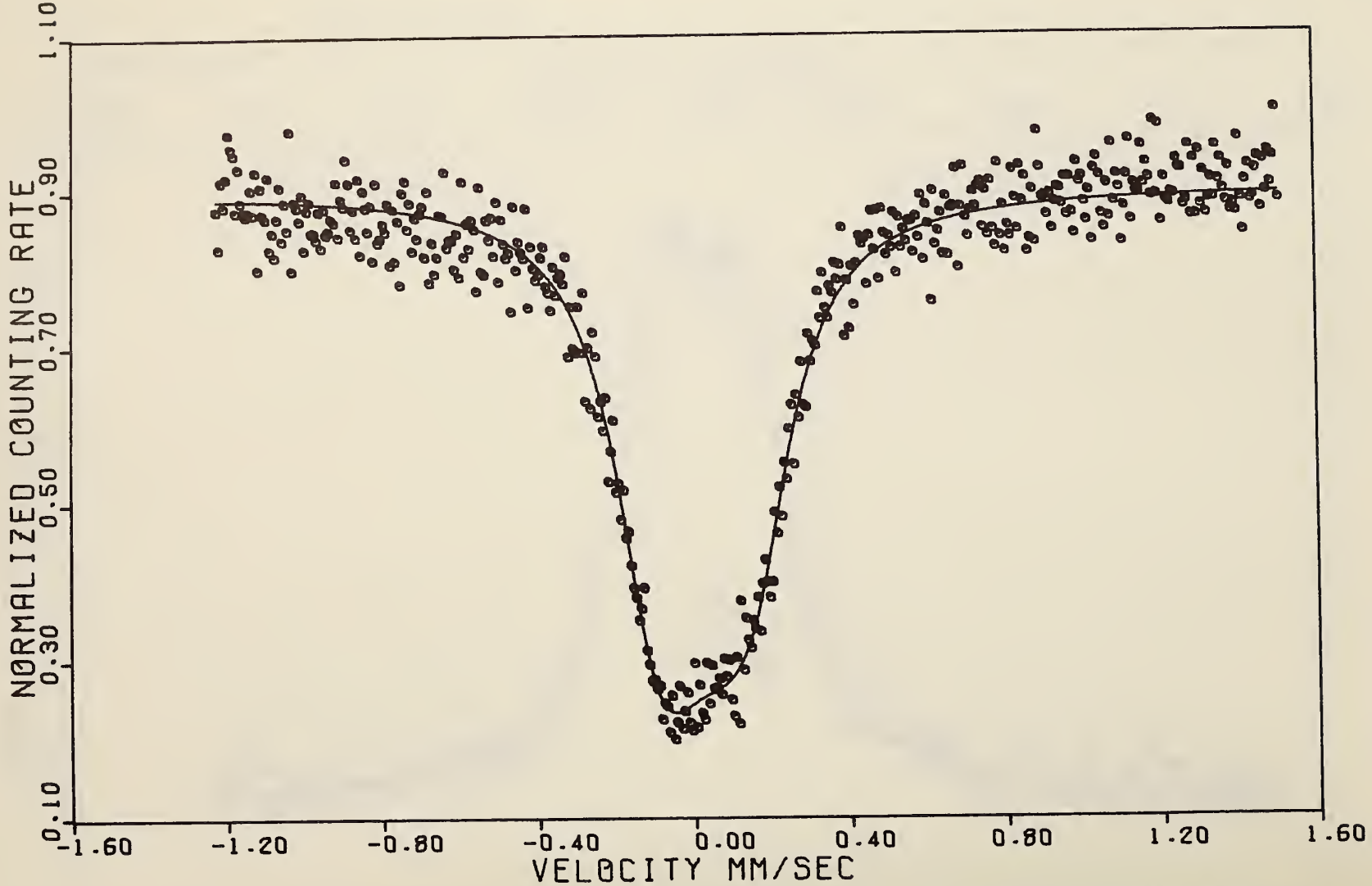

Figure IV-2(g). $(Cu_{0.47}Ni_{0.53})_{0.995}Fe_{0.005}$ at 298°K fitted to an unresolved six-line hyperfine field pattern.

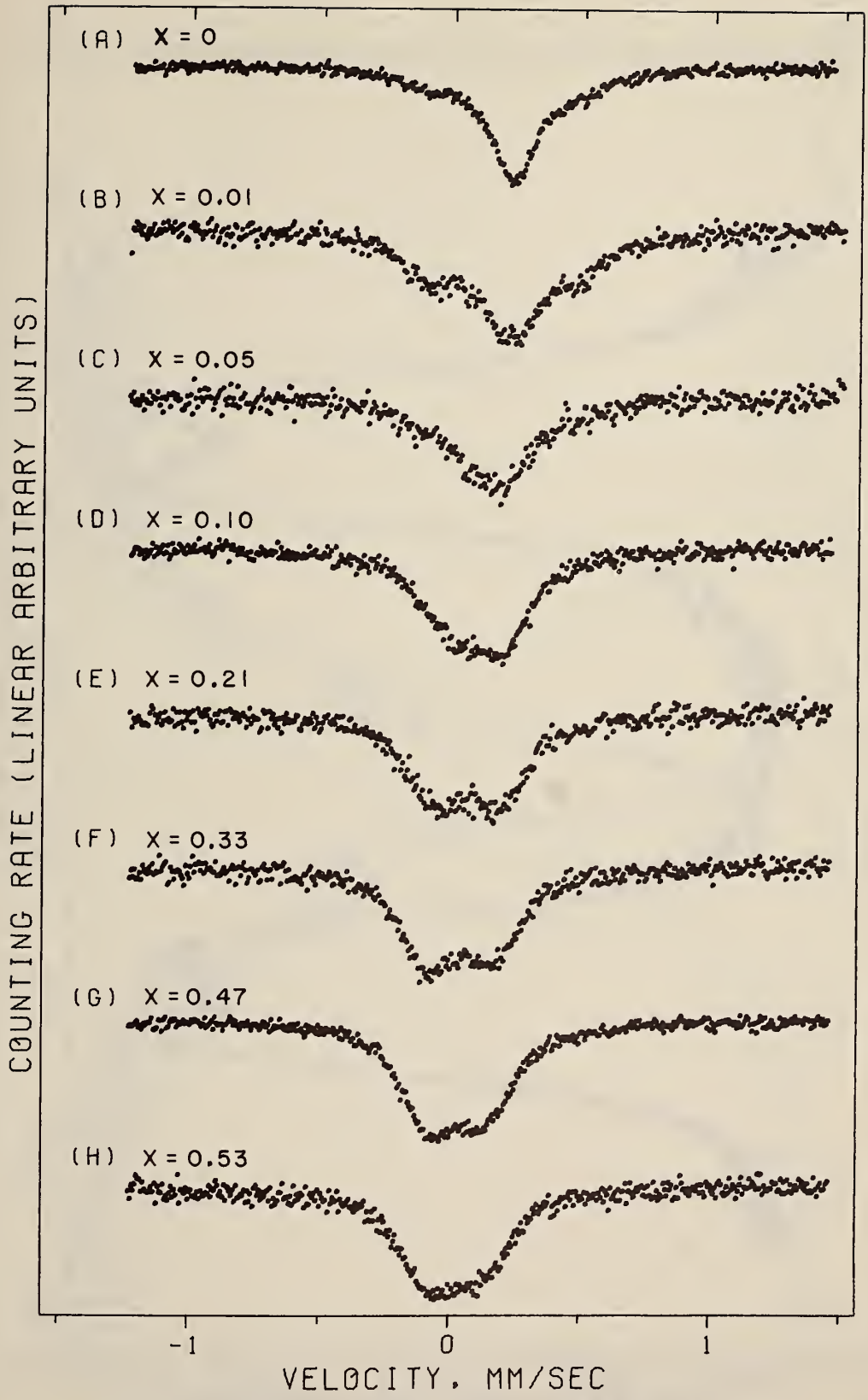

Figure IV-3. Spectra of $(Cu_{1-x}Ni_x)_{0.995}Fe_{0.05}$ alloys at 298°K.

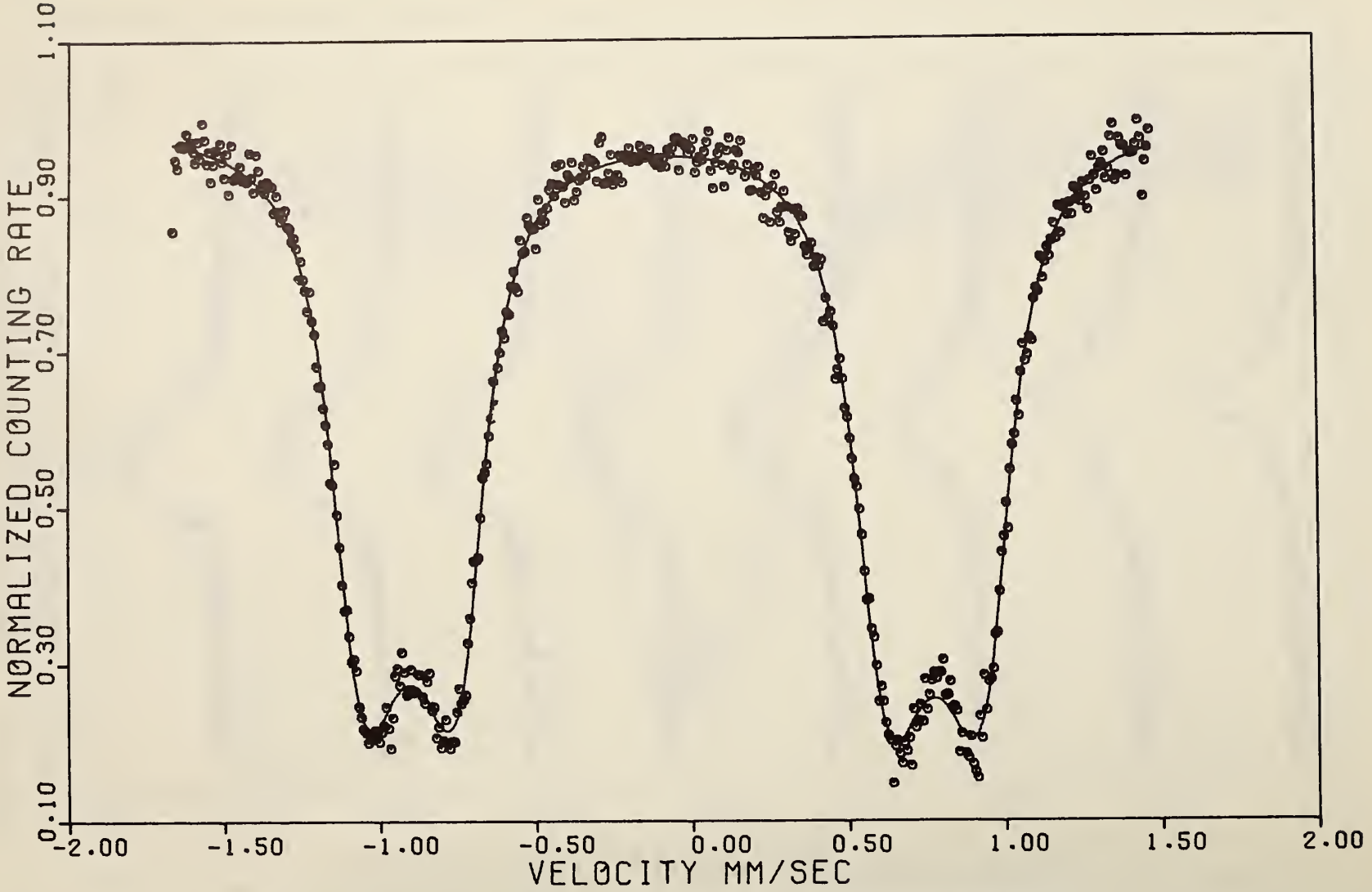

Figure IV-4. $Cu_{0.67}Ni_{0.33}$ (^{57}Co) source, metallic Fe absorber.

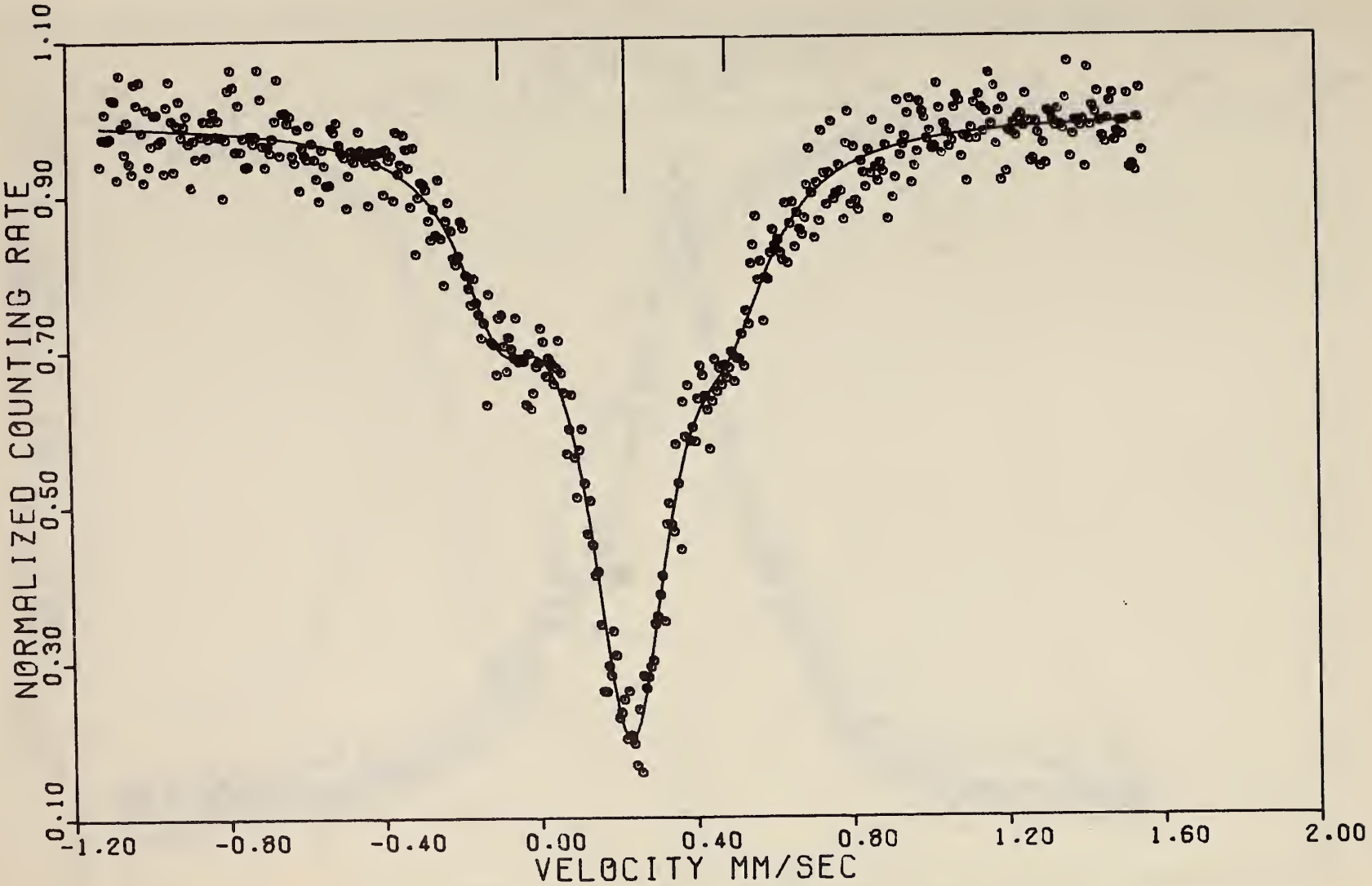

Figure IV-5. Sample no. 2 of $Cu_{0.995}Fe_{0.005}$ at 298°K fitted to three Lorentzian lines.

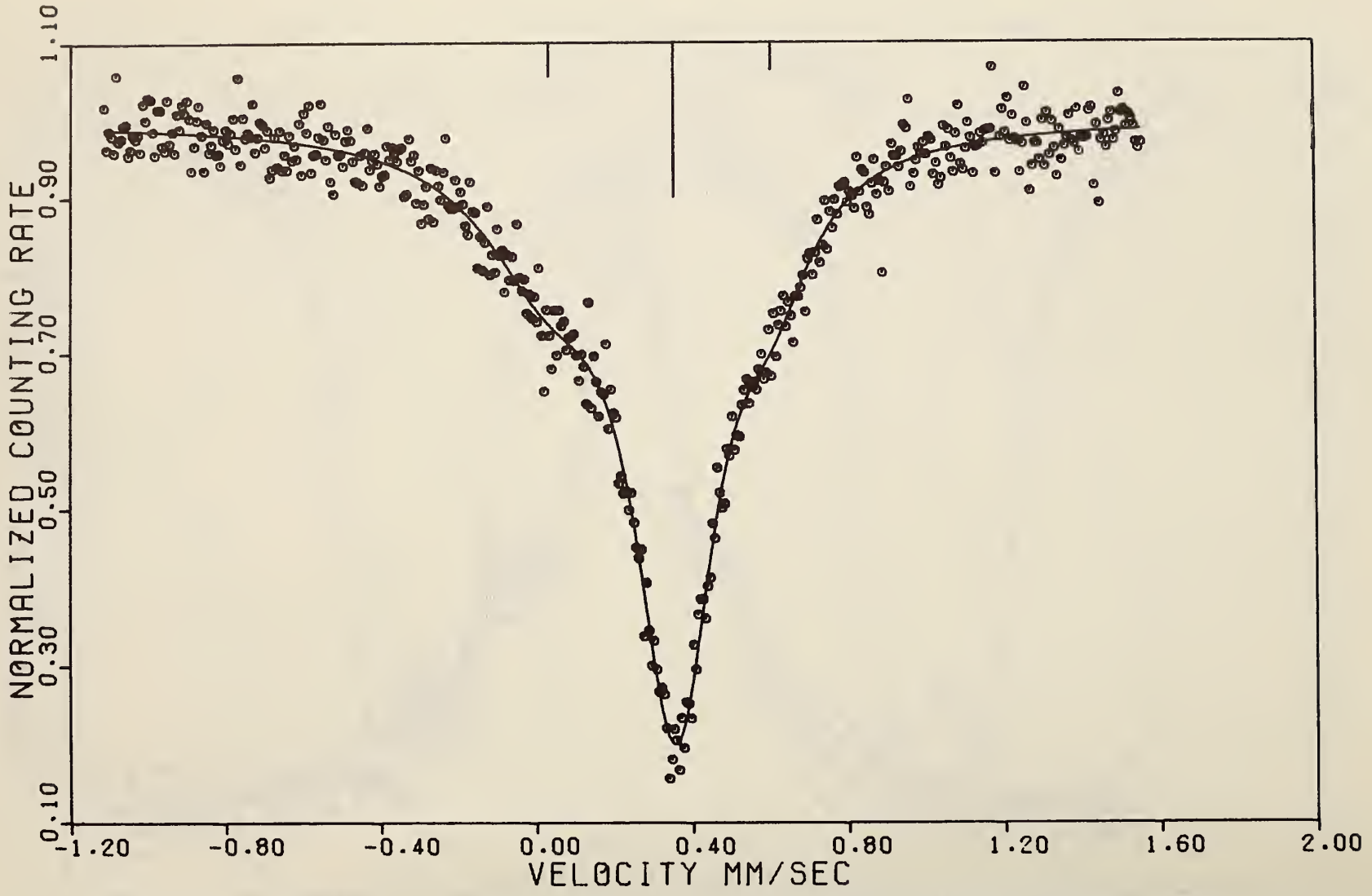

Figure IV-6. Sample no. 2 of $Cu_{0.995}Fe_{0.005}$ at 4.2°K fitted to three Lorentzian lines.

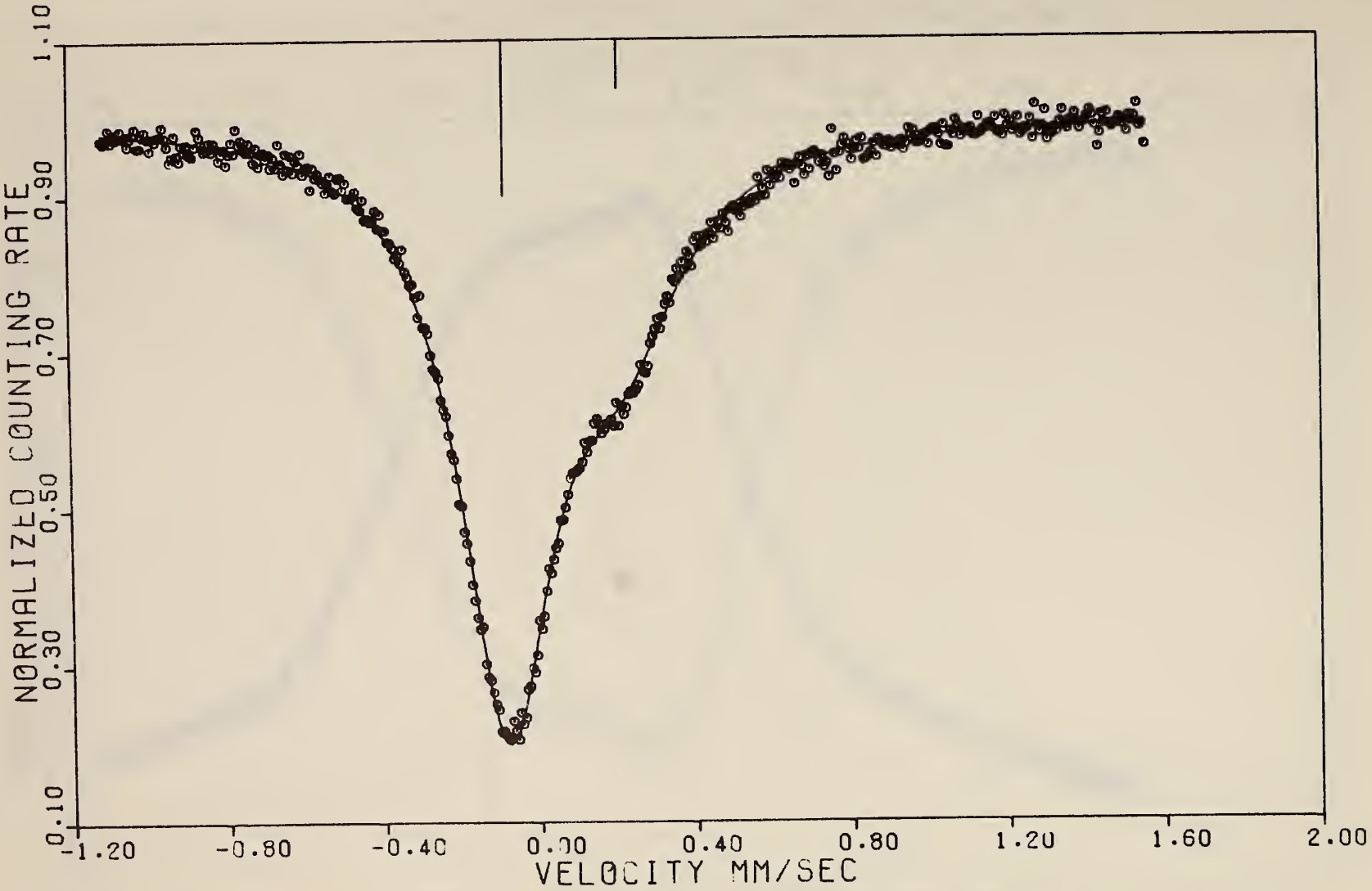

Figure IV-7. Annealed $Cu_{0.97}Fe_{0.03}$ at 298°K. Fit is to two Lorentzian lines.

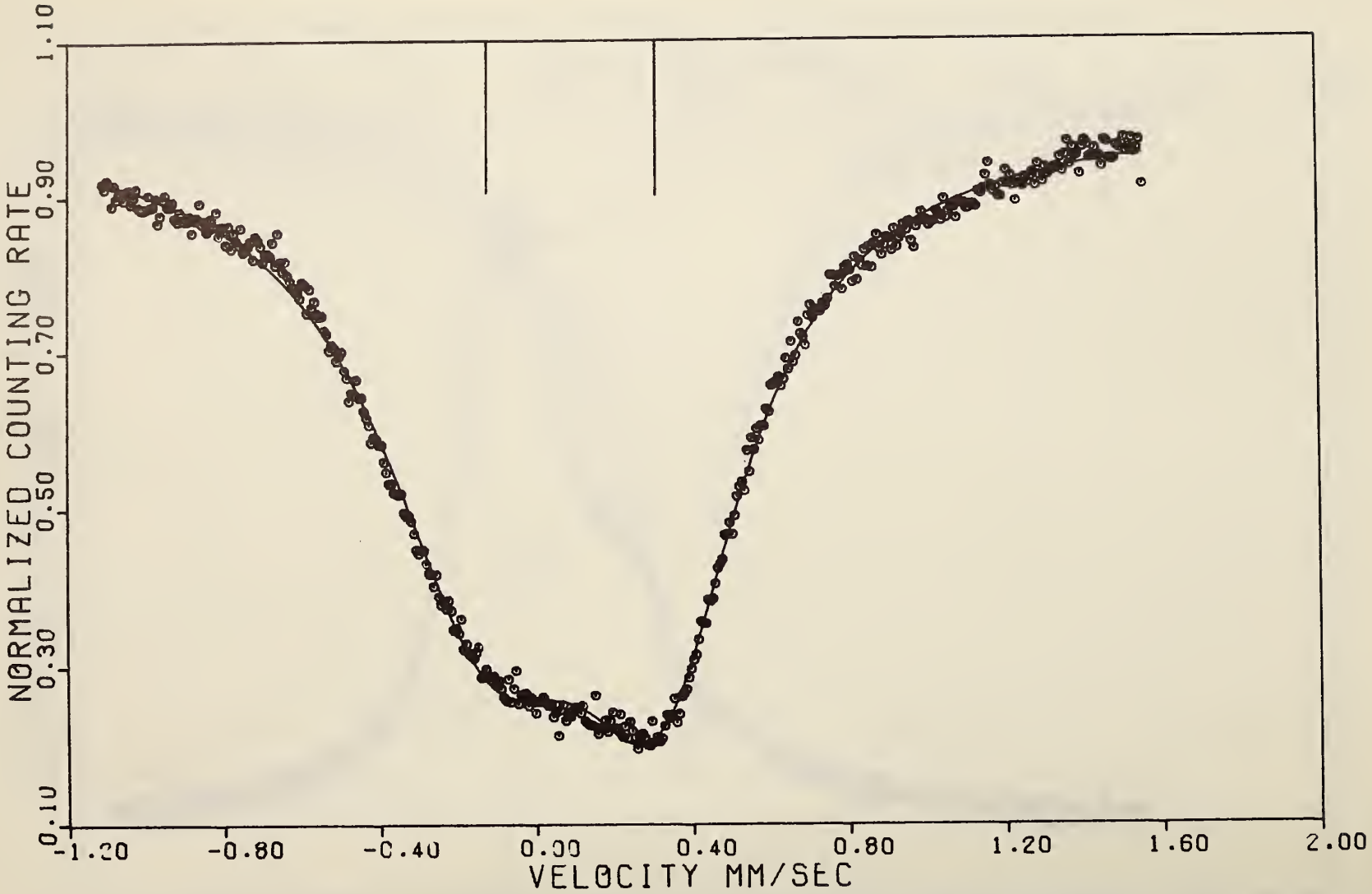

Figure IV-8(a). Annealed $Cu_{0.97}Fe_{0.03}$ at 4.2°K fitted to two Lorentzians.

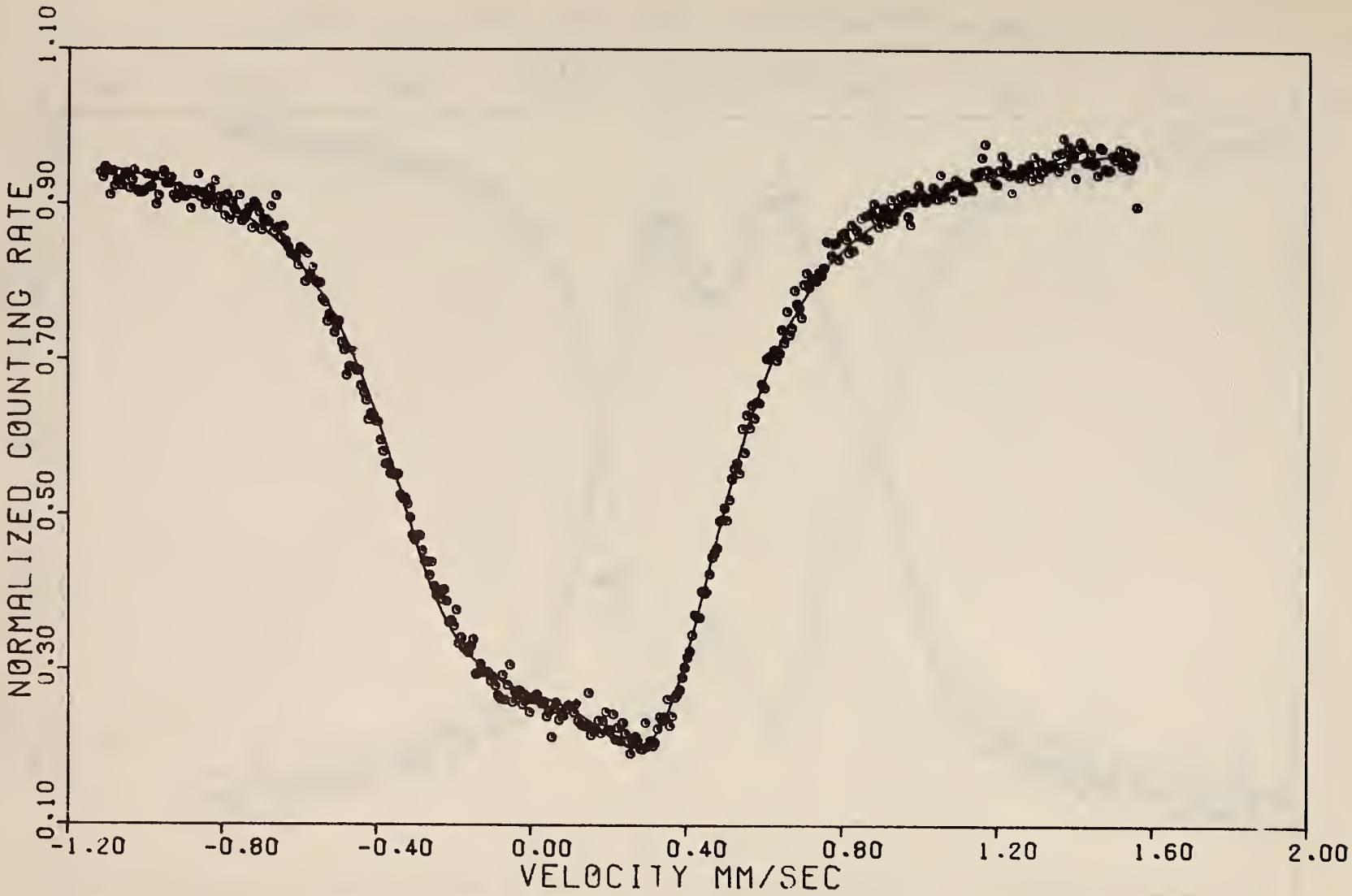

Figure IV-8(b). Annealed $Cu_{0.97}Fe_{0.03}$ at 4.2°K fitted to a six-line hyperfine field pattern.

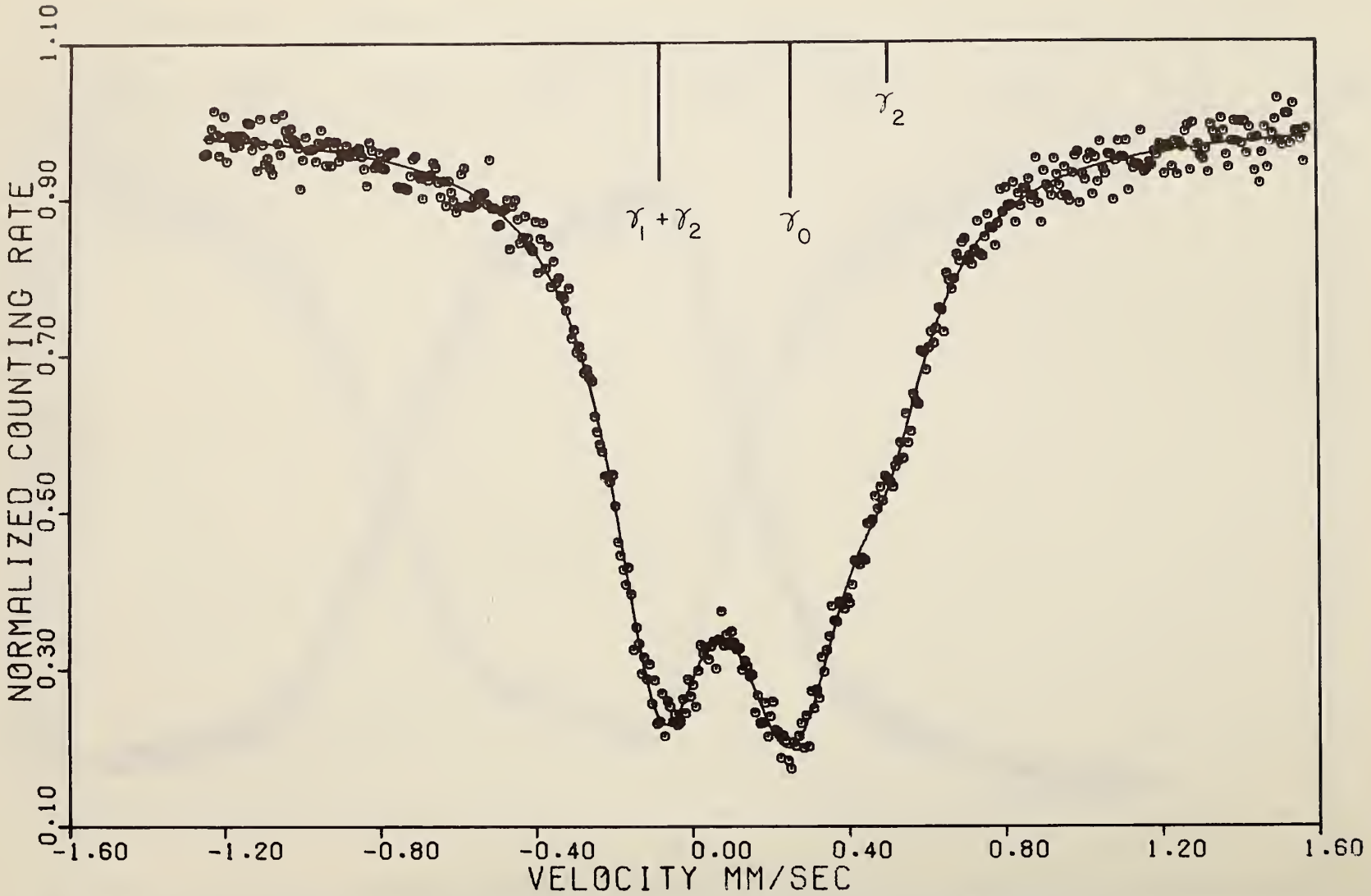

Figure IV-9. Splat cooled sample of $Cu_{0.975}Fe_{0.025}$ at 298°K.

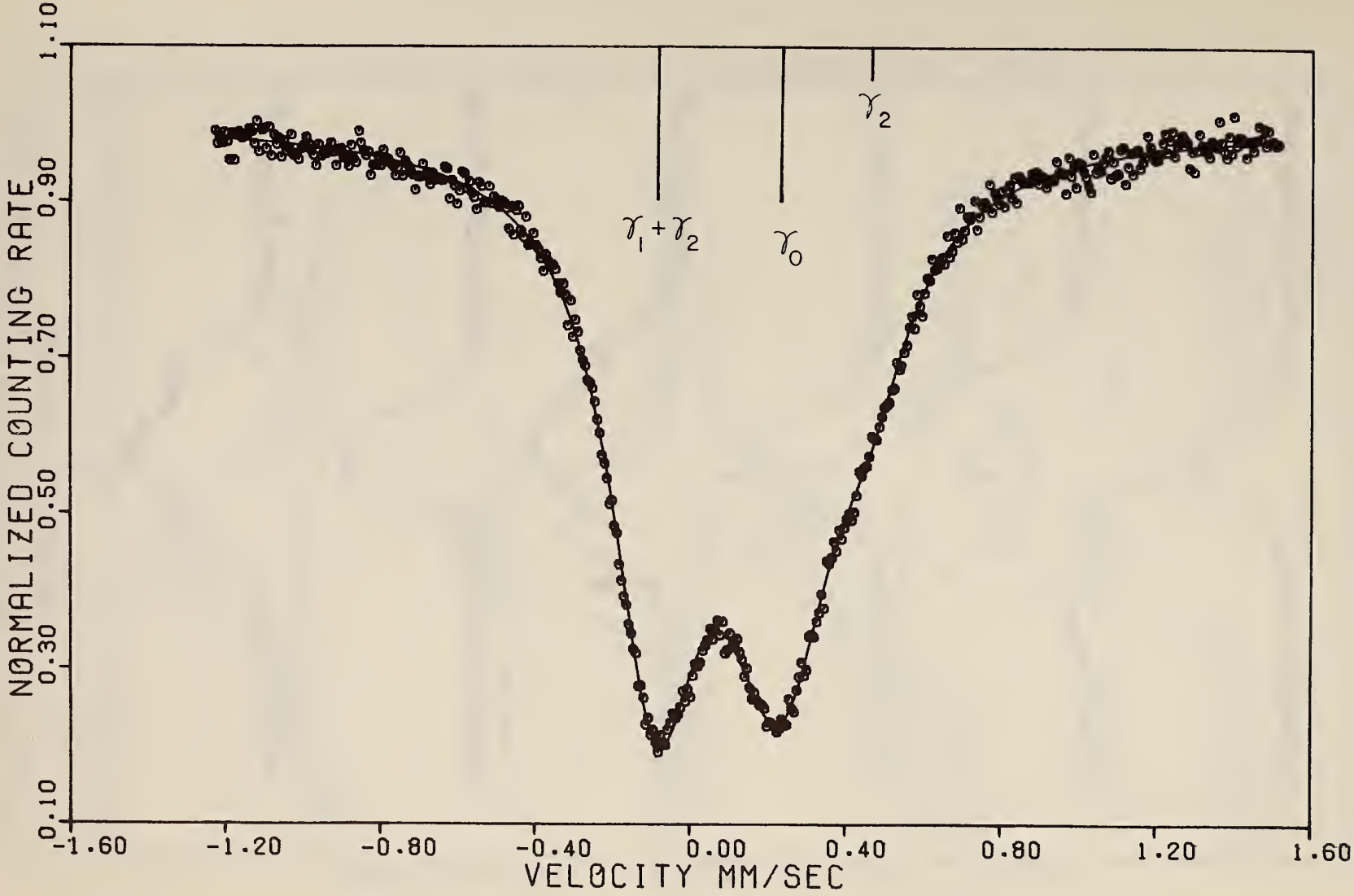

Figure IV-10. Quenched sample of $Cu_{0.97}Fe_{0.03}$ at 298°K.

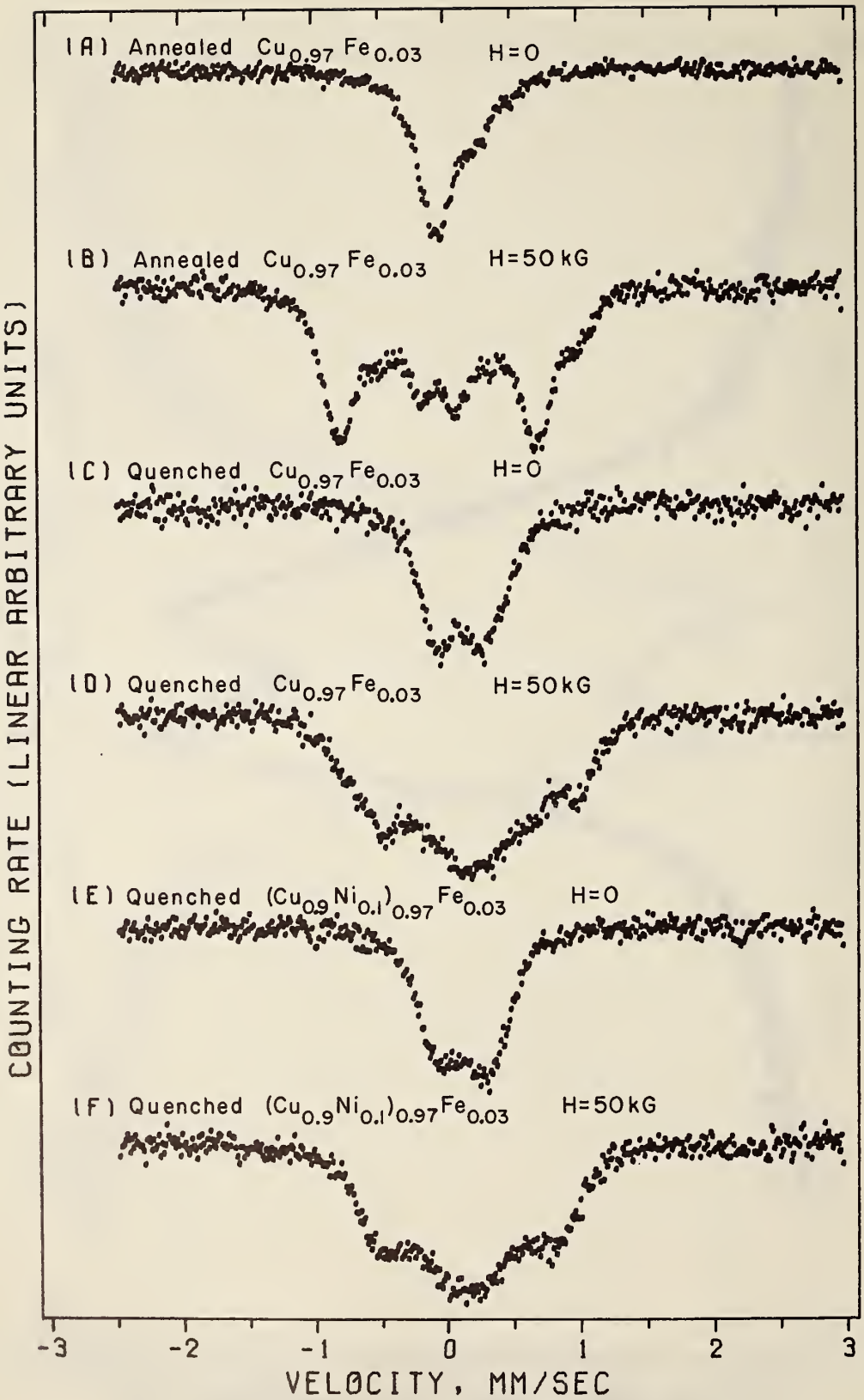

Figure IV-11. Cu-Ni-Fe alloy spectra at 205°K with zero field and an applied field of 50 kG.

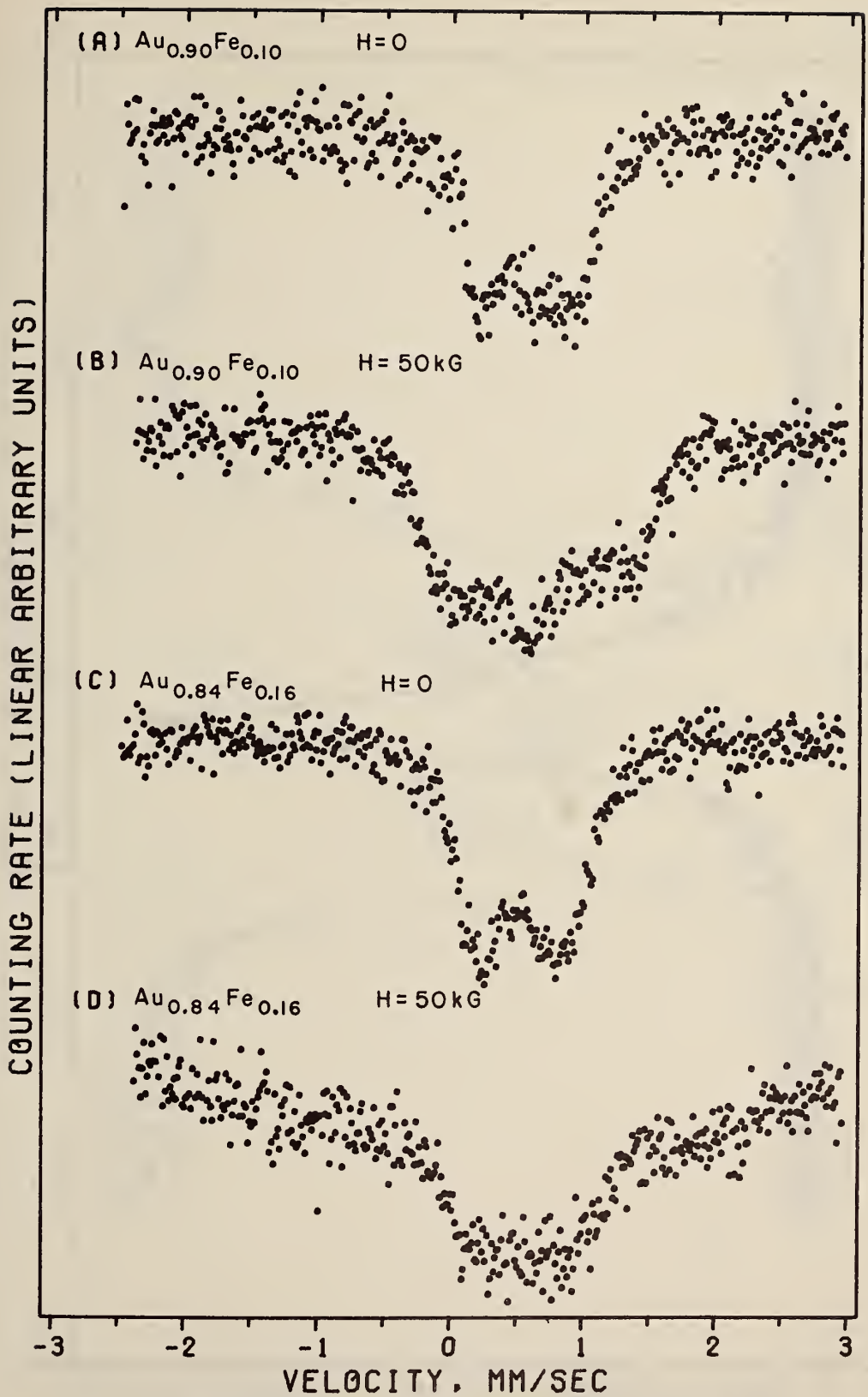

Figure IV-12. Au-Fe alloy spectra at 205°K with either zero field or an applied field of 50 kG.

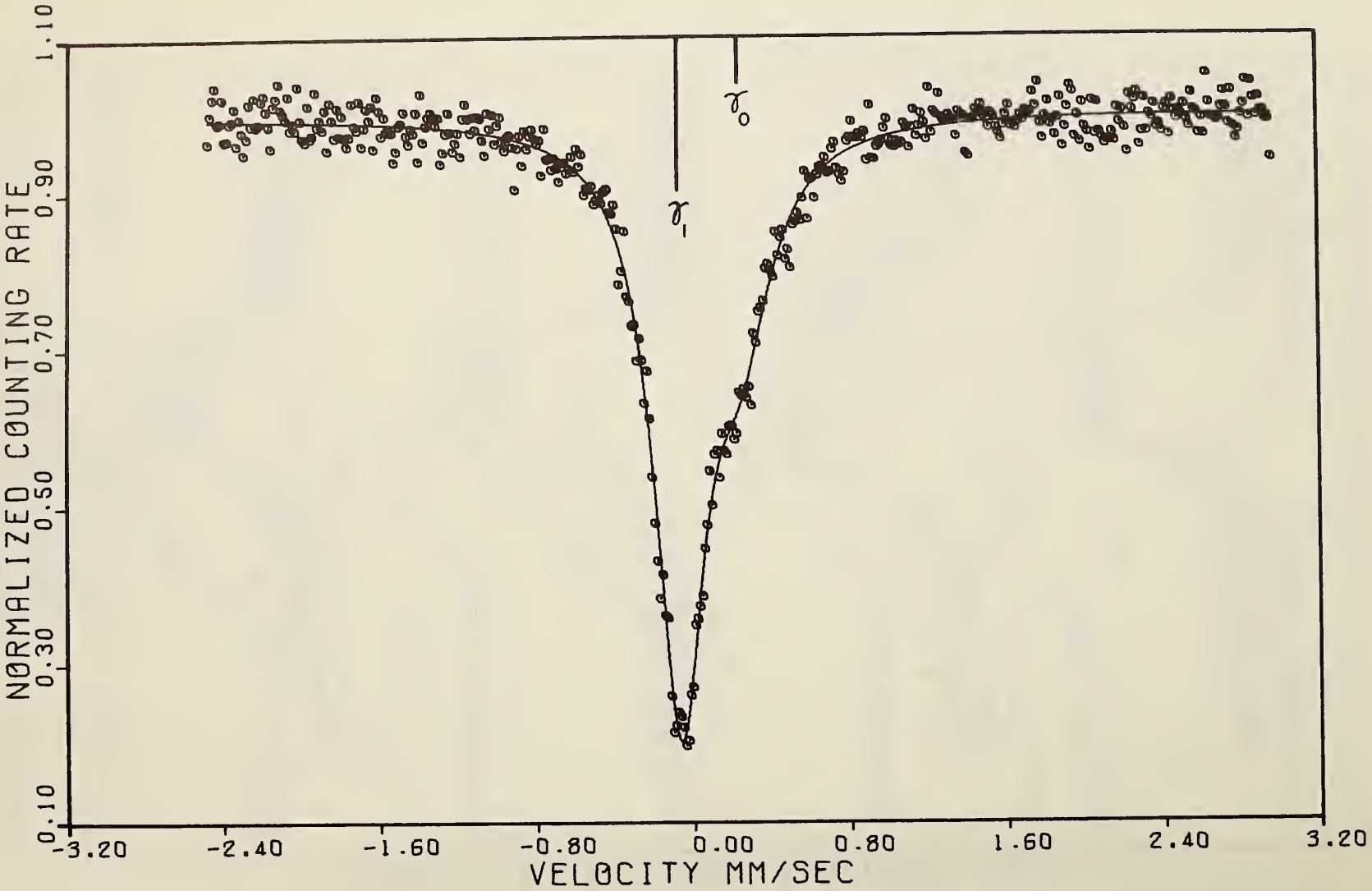

Figure IV-13(a). Annealed sample of $Cu_{0.97}Fe_{0.03}$ at 205°K taken in magnet with H = 0.

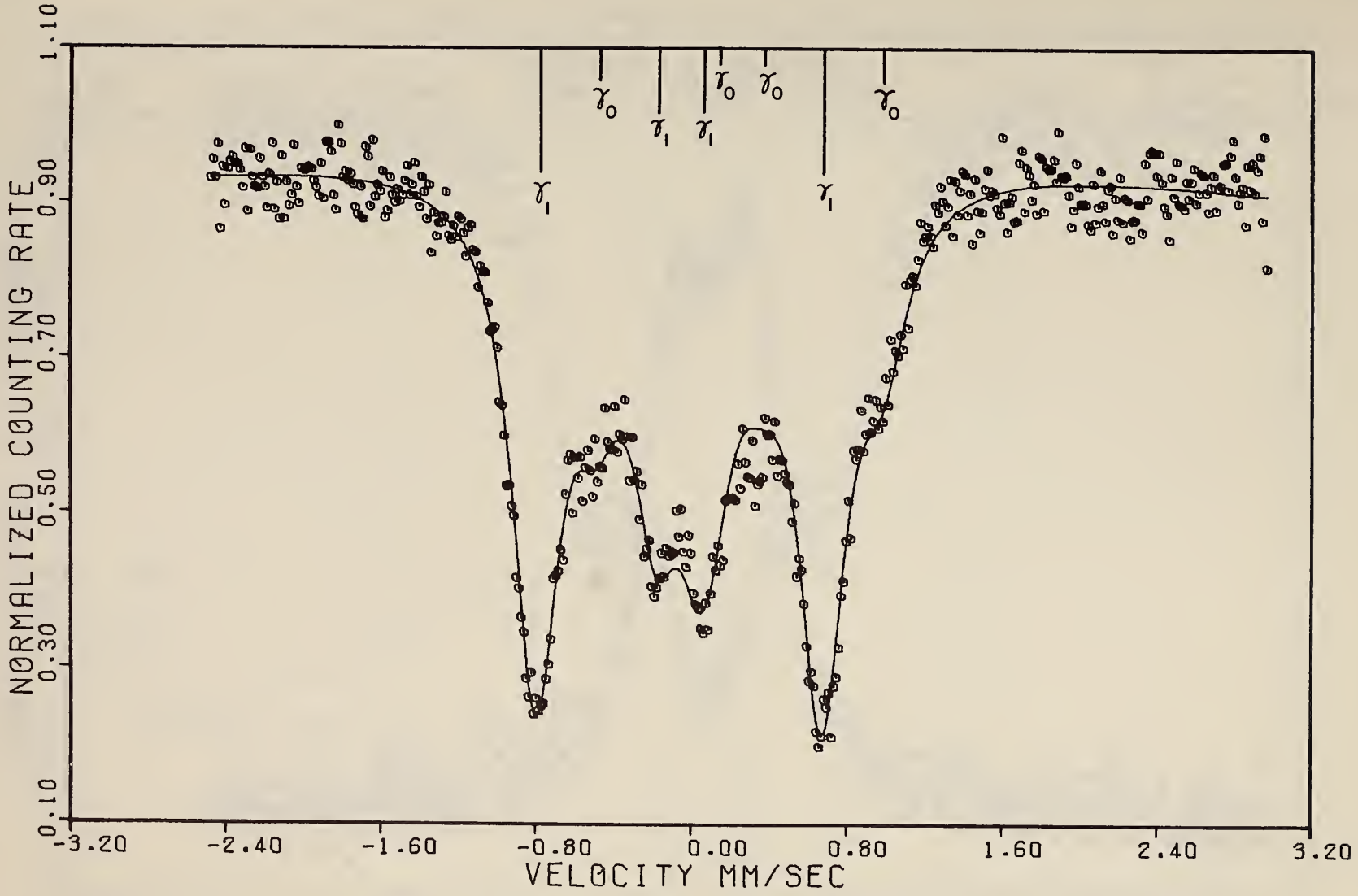

Figure IV-13(b). Annealed sample of $Cu_{0.97}Fe_{0.03}$ at 205°K taken in magnet with H = 50 kG.

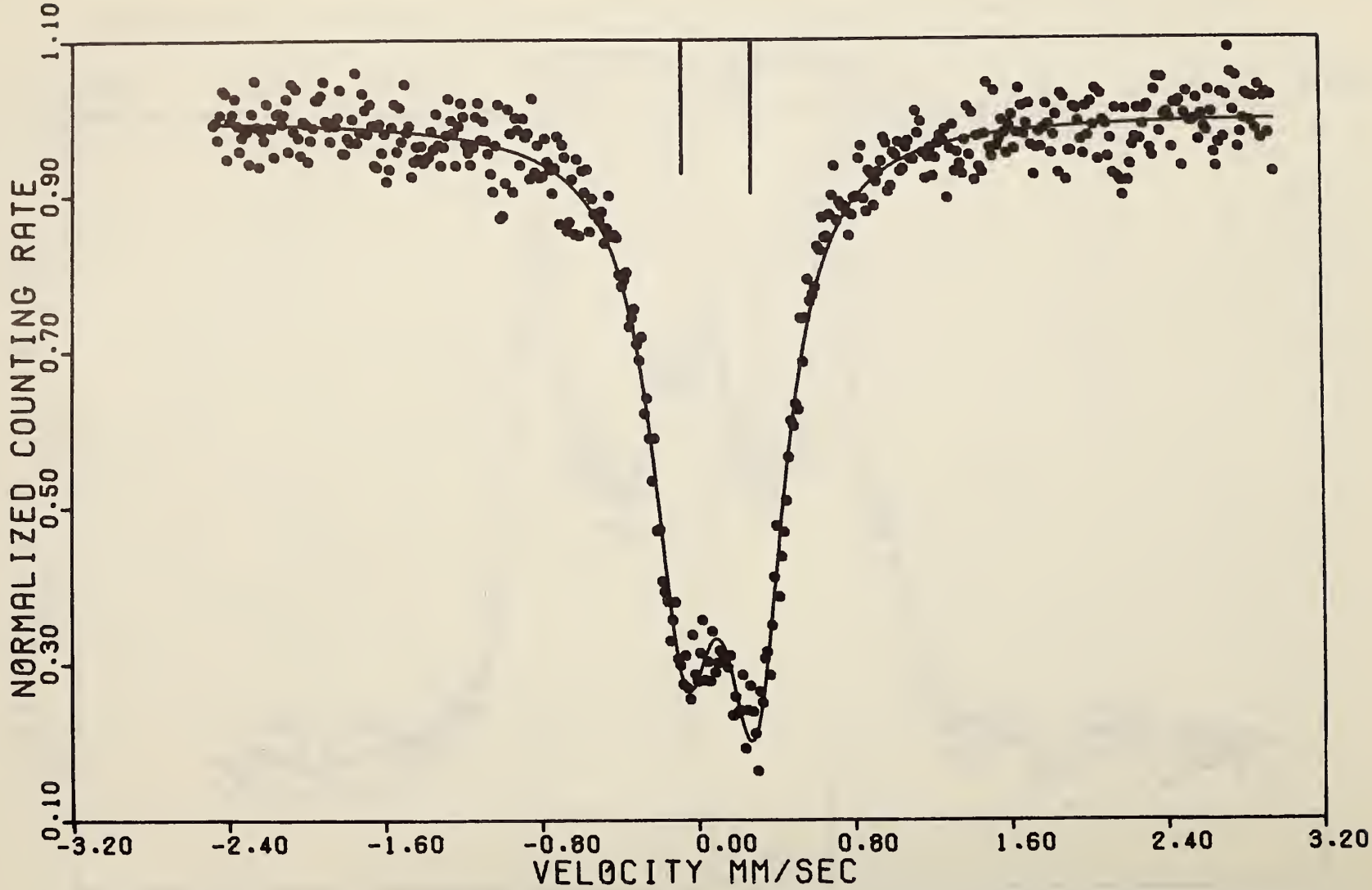

Figure IV-14(a). Quenched sample of $(Cu_{0.90}Ni_{0.10})_{0.97}Fe_{0.03}$ at 205°K taken in magnet with H = 0.

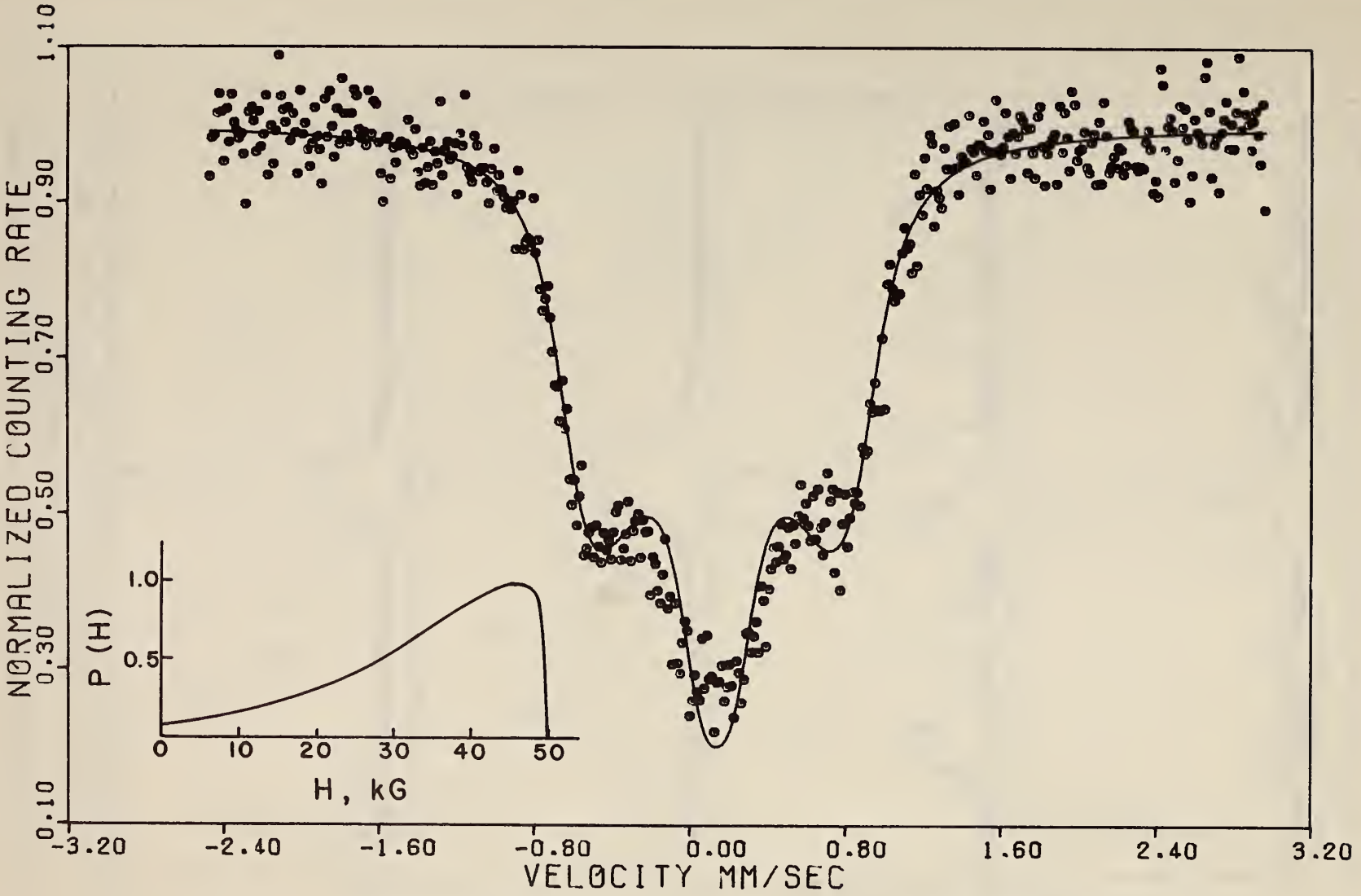

Figure IV-14(b). Quenched sample of $(Cu_{0.90}Ni_{0.10})_{0.97}Fe_{0.03}$ at 205°K with H = 50 kG.

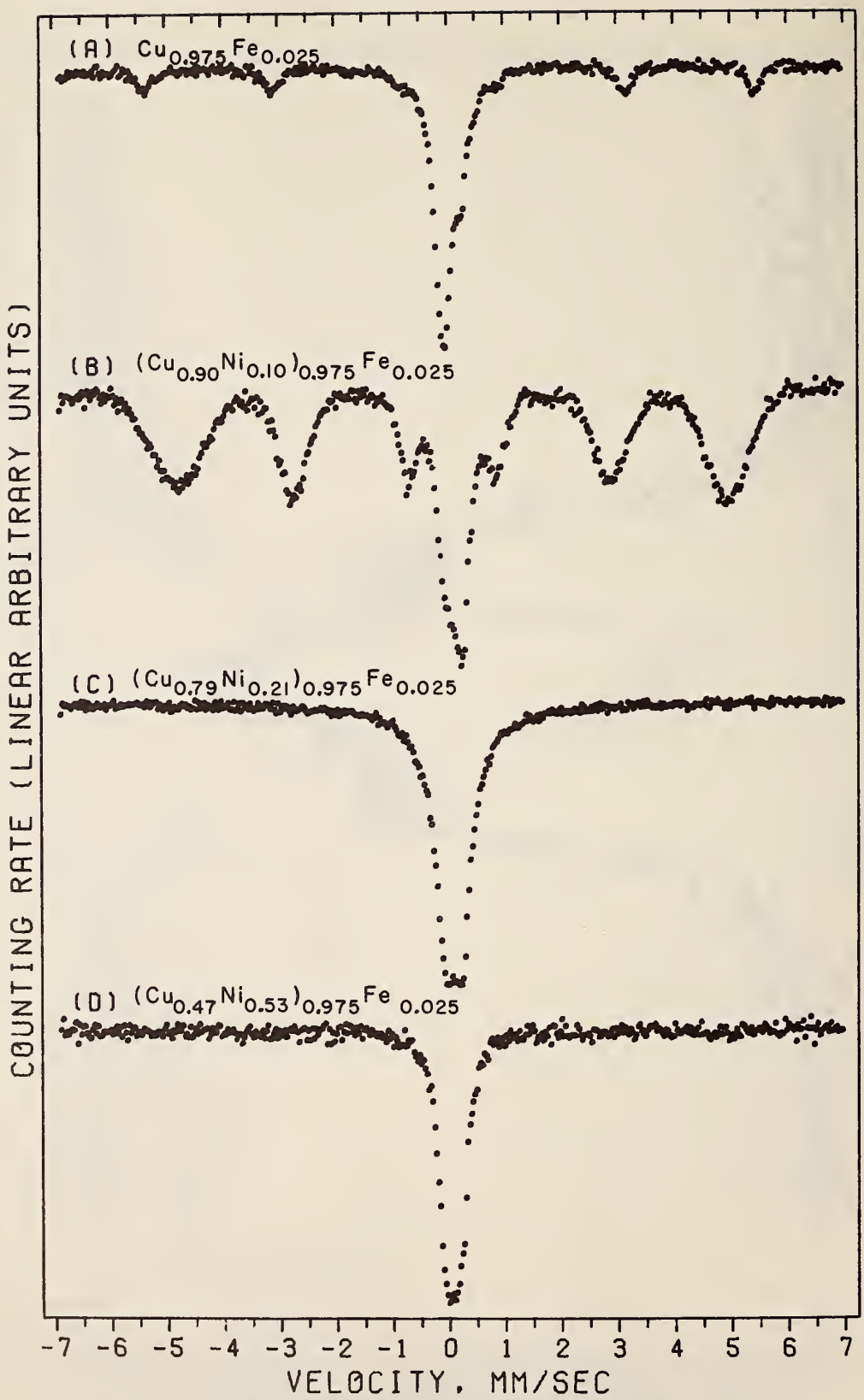

Figure IV-15. Spectra of four furnace cooled samples taken at 298°K.

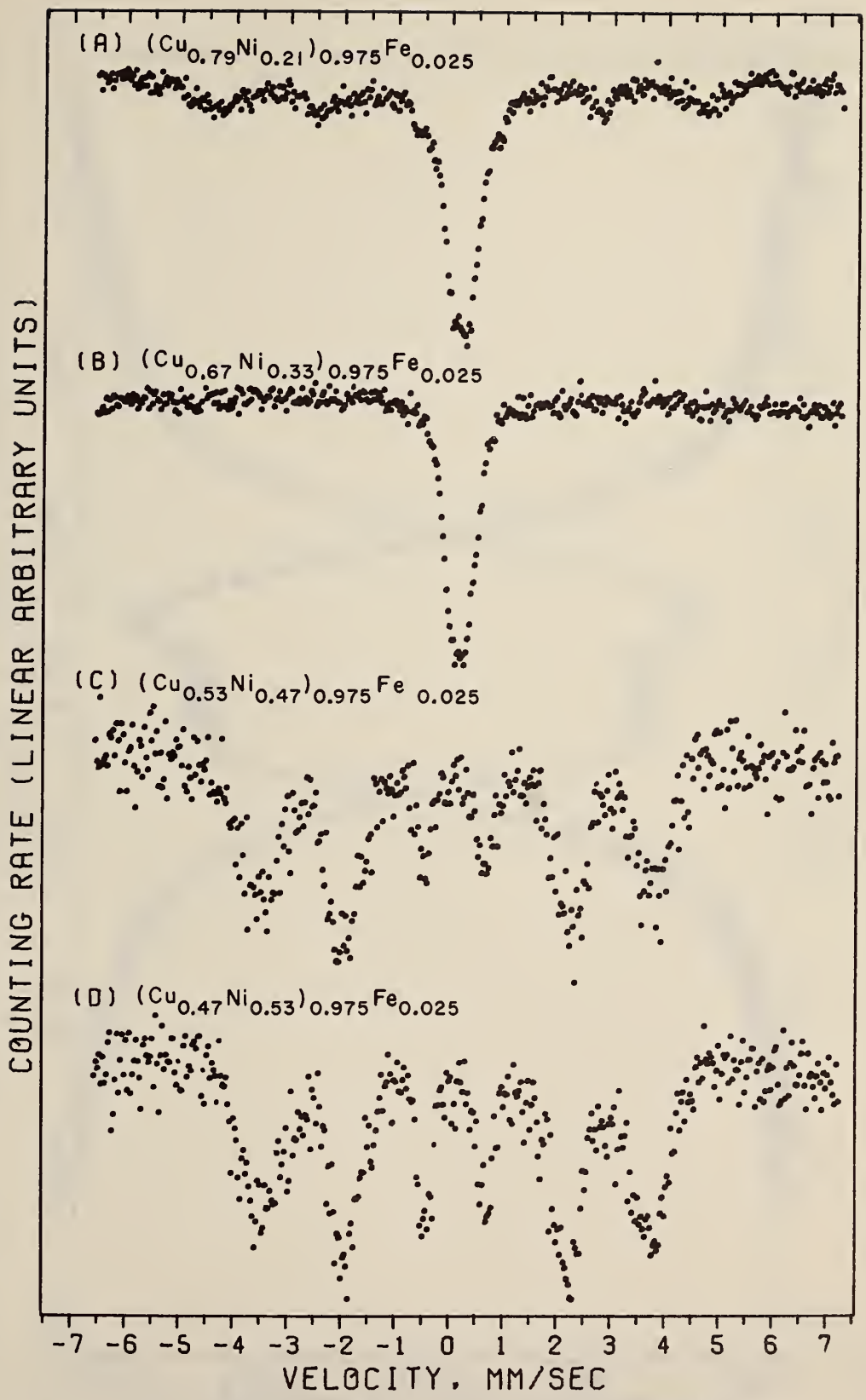

Figure IV-16. Spectra of four furnace cooled samples taken at 78°K.

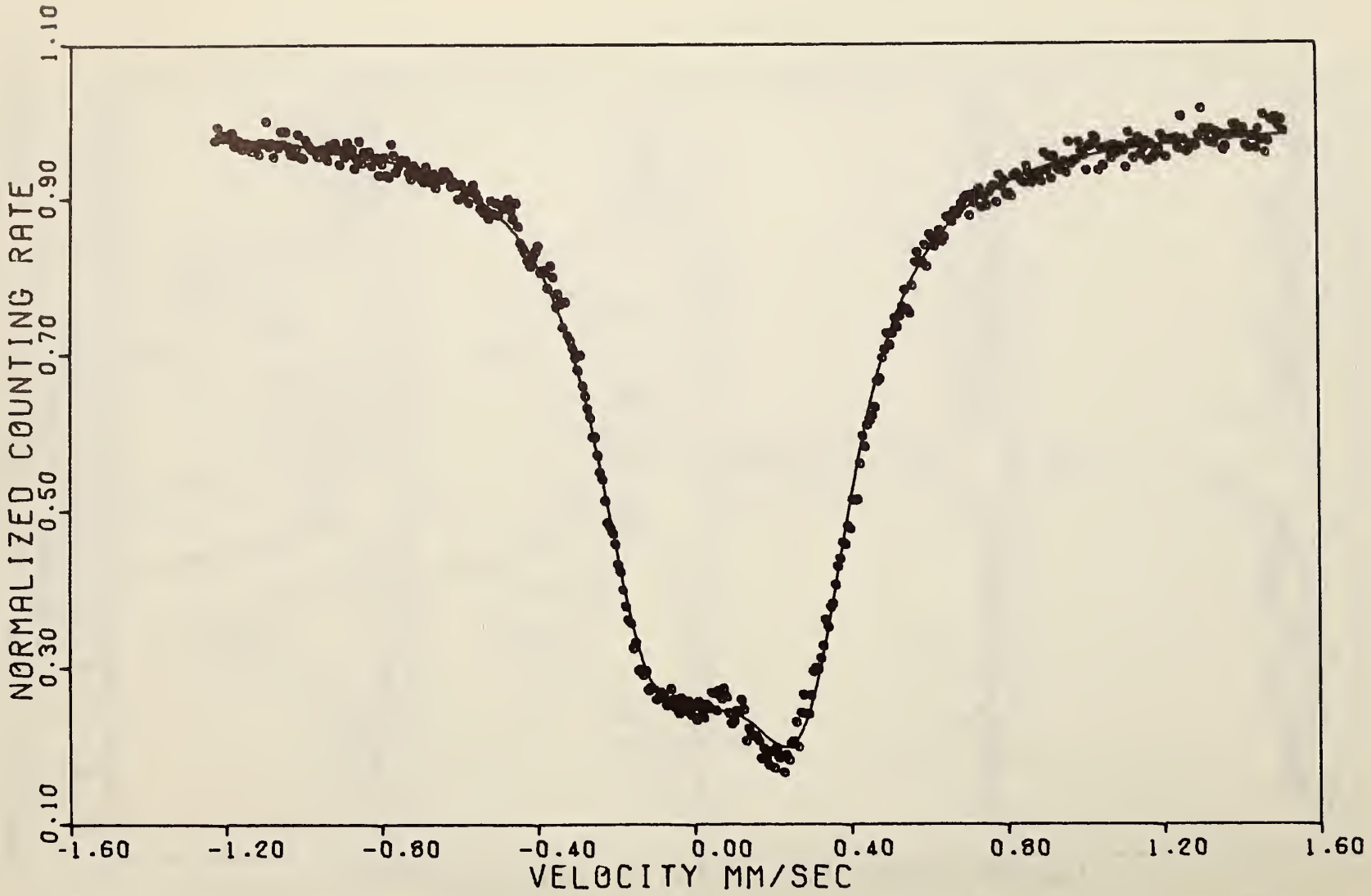

Figure IV-17(a). Spectrum of quenched $(Cu_{0.90}Ni_{0.10})_{0.97}Fe_{0.03}$ at 298°K fitted to a six-line hyperfine field pattern.

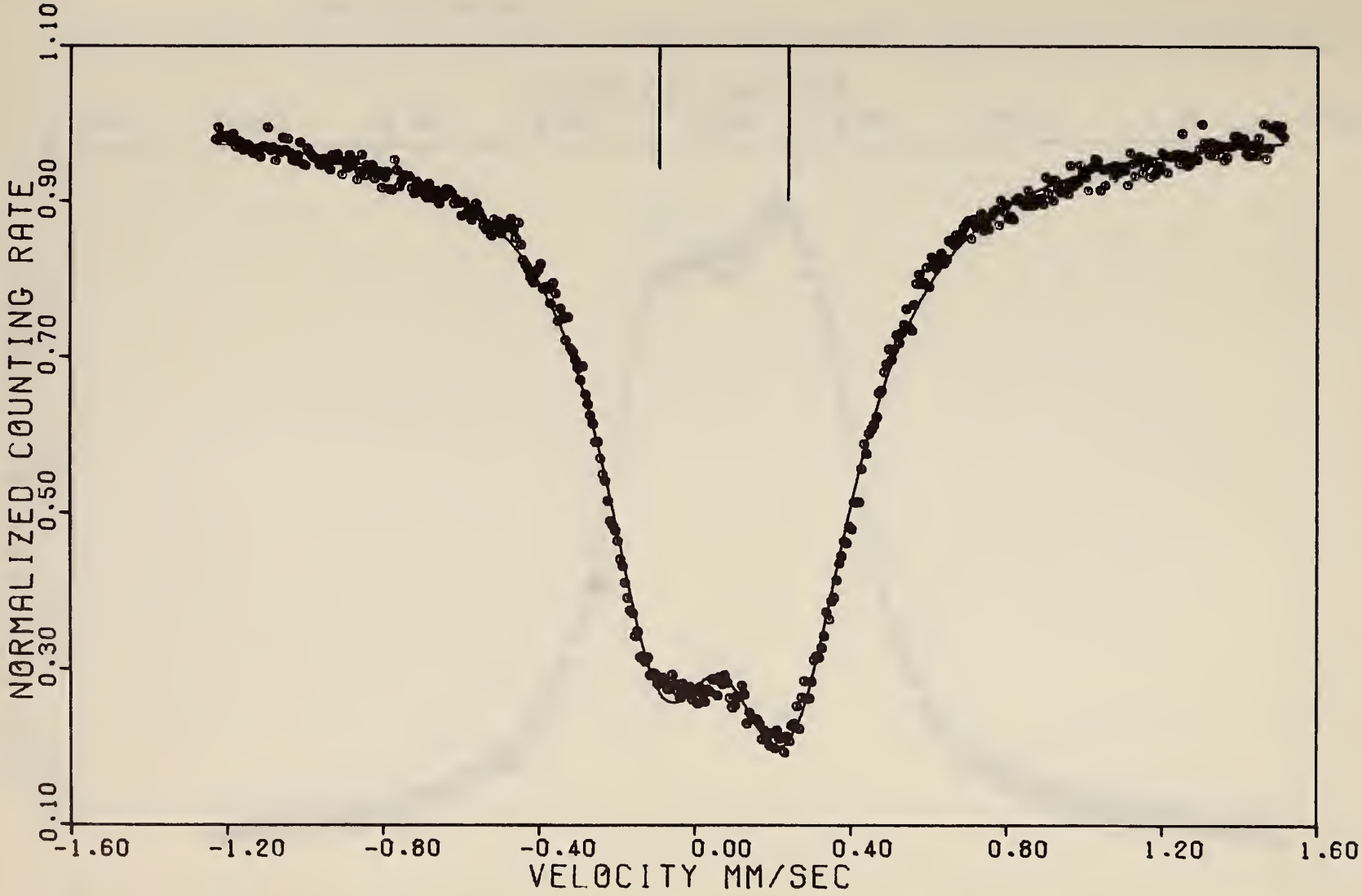

Figure IV-17(b). Spectrum of quenched $(Cu_{0.90}Ni_{0.10})_{0.97}Fe_{0.03}$ at 298°K fitted to two separate Lorentzians.

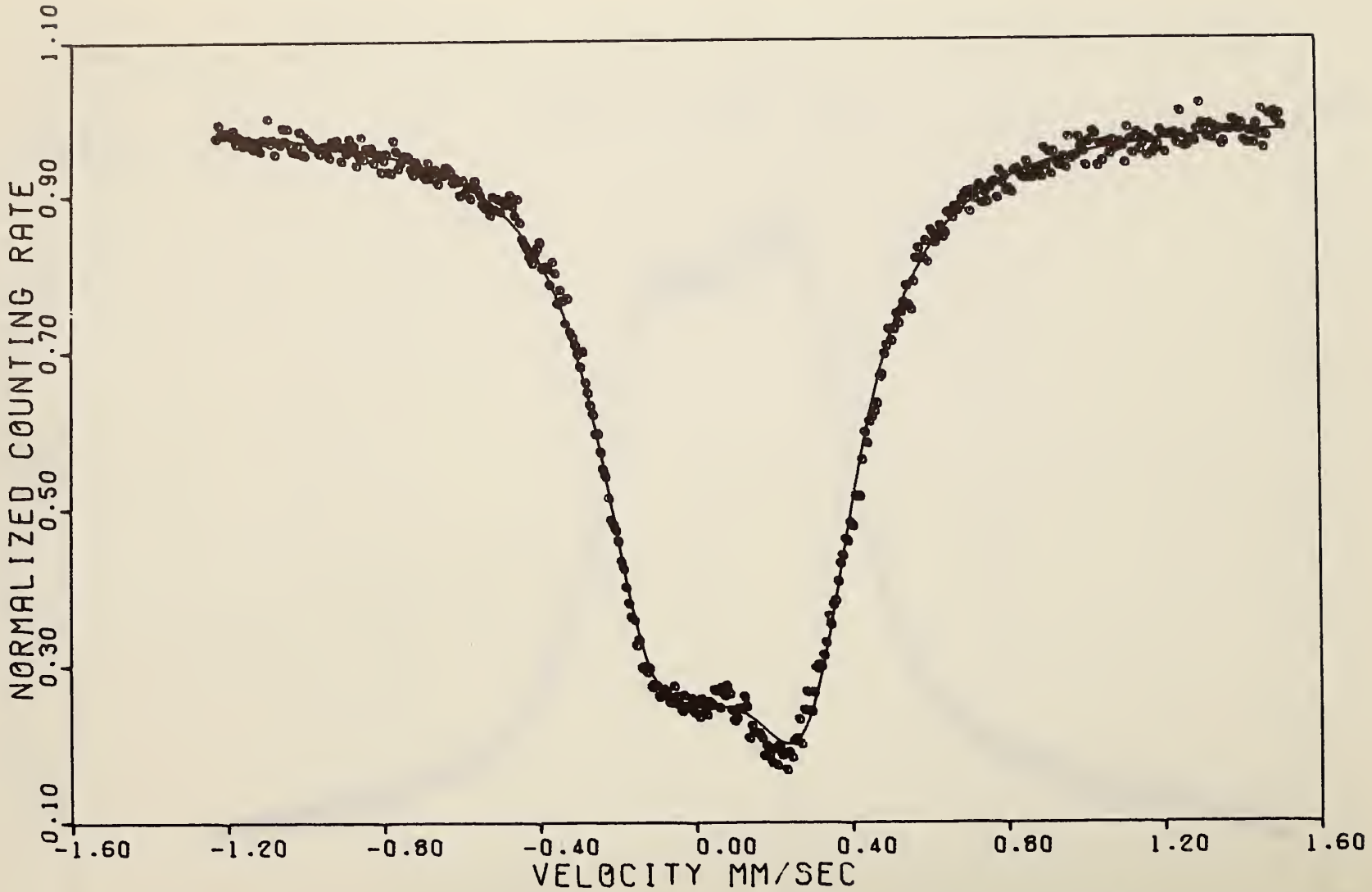

Figure IV-18(a). Spectrum of quenched $(Cu_{0.90}Ni_{0.10})_{0.94}Fe_{0.06}$ at 298°K fitted to a six-line hyperfine field pattern.

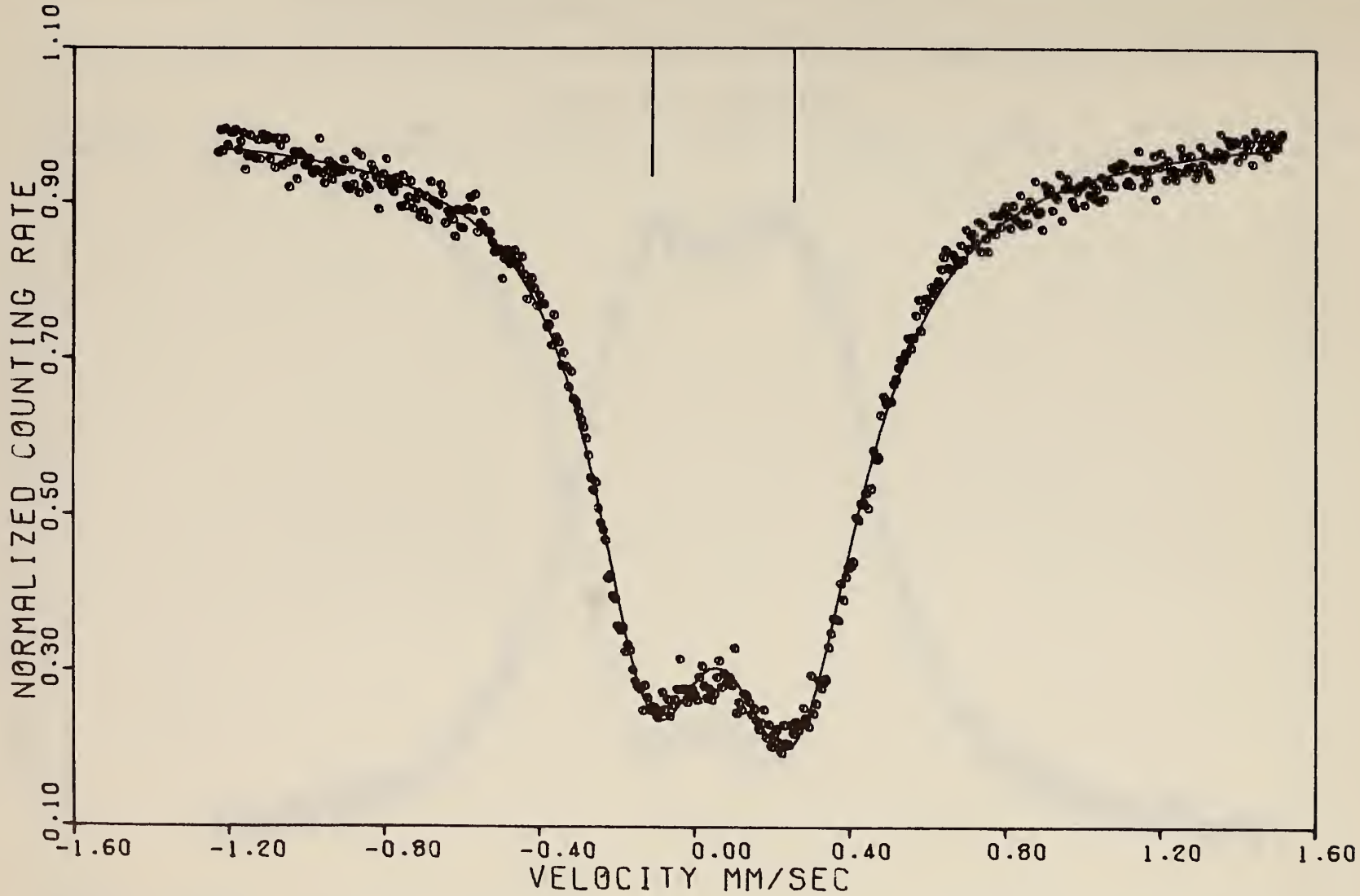

Figure IV-18(b). Spectrum of quenched $(Cu_{0.90}Ni_{0.10})_{0.94}Fe_{0.06}$ at 298°K fitted to two separate Lorentzians.

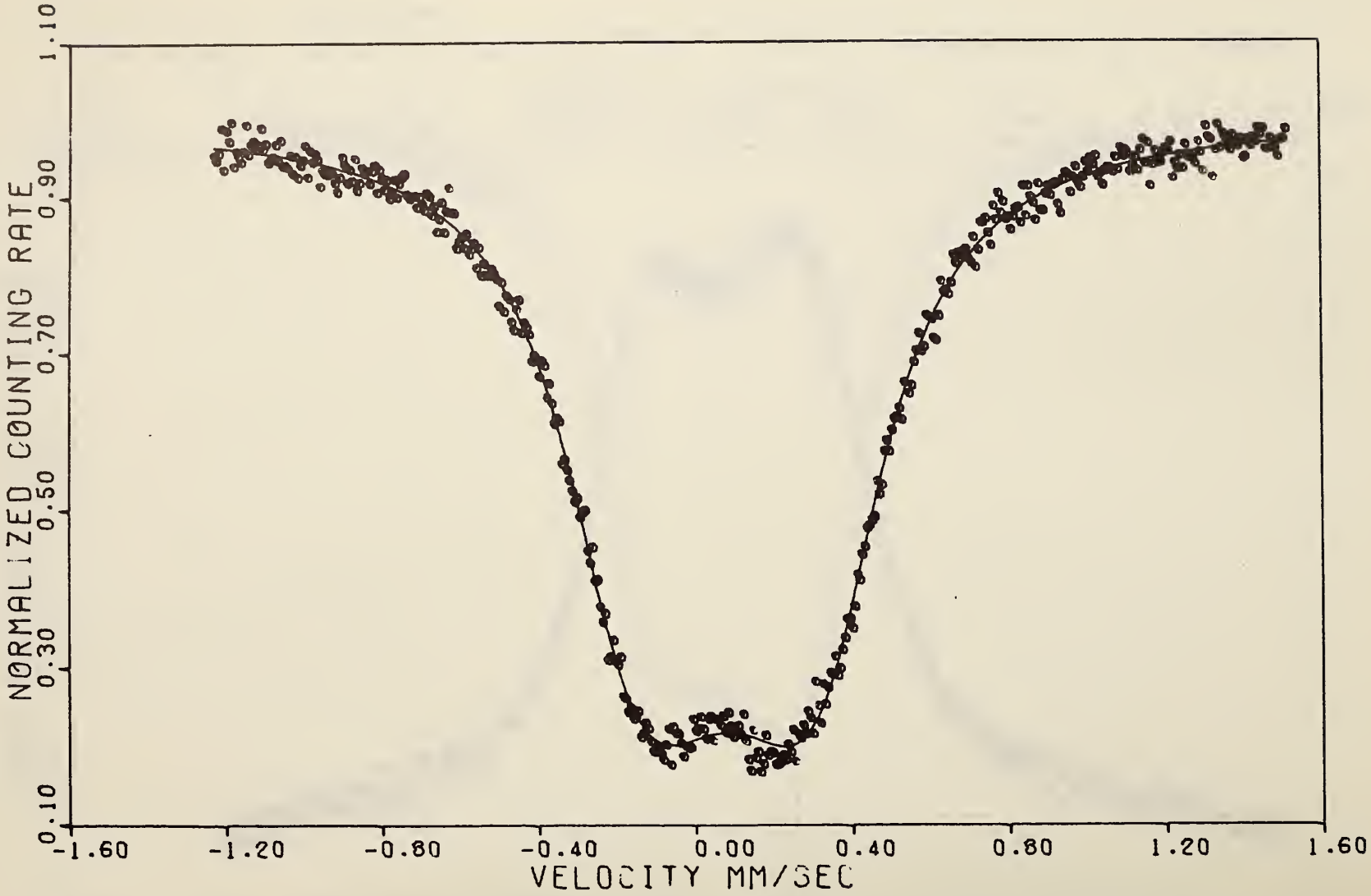

Figure IV-19(a). Spectrum of quenched $(Cu_{0.90}Ni_{0.10})_{0.92}Fe_{0.08}$ at 298°K fitted to a six-line hyperfine field pattern.

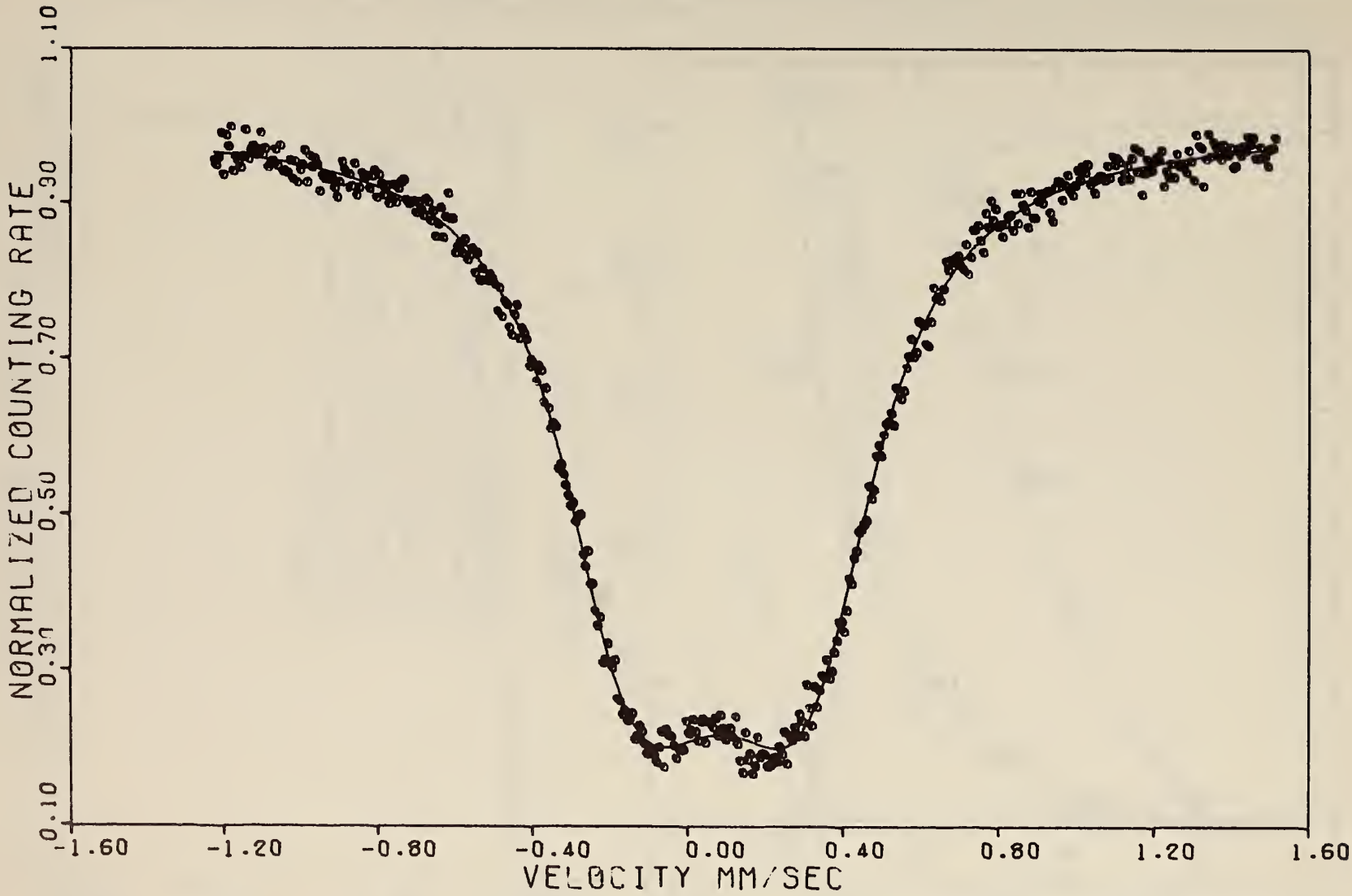

Figure IV-19(b). Spectrum of quenched $(Cu_{0.90}Ni_{0.10})_{0.92}Fe_{0.08}$ at 298°K fitted to two separate Lorentzians.

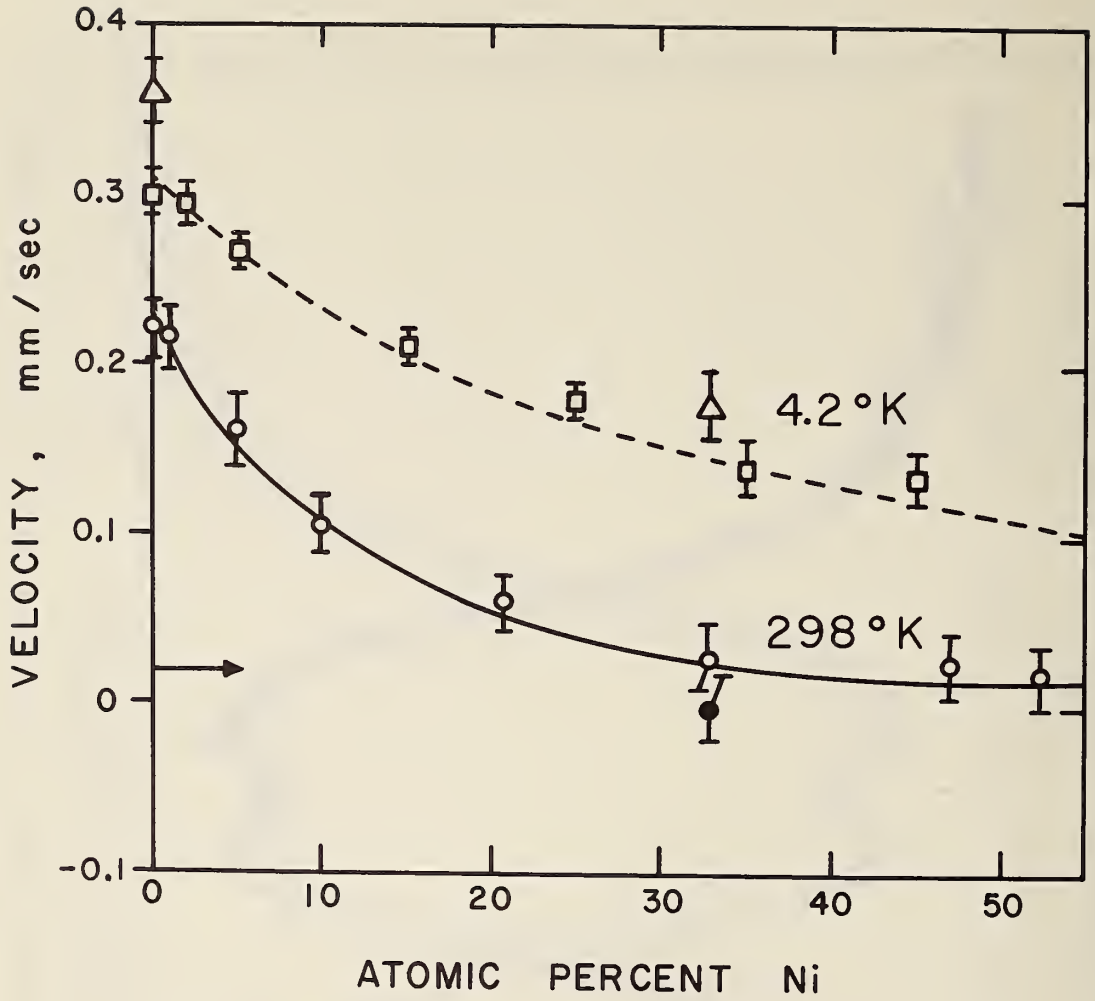

Figure IV-20. Isomer shifts in Cu-Ni alloys with respect to pure Fe metal at room temperature. Circles are for 0.5% Fe in Cu-Ni at 298°K, triangles for 0.5% Fe in Cu-Ni at 4.2°K, and solid circle for a source at 298°K. Open squares are from the results of Wertheim and Wernick[162] corrected to pure Fe as a reference. Arrow is at the value for pure Ni at room temperature given by Quaim.[106]

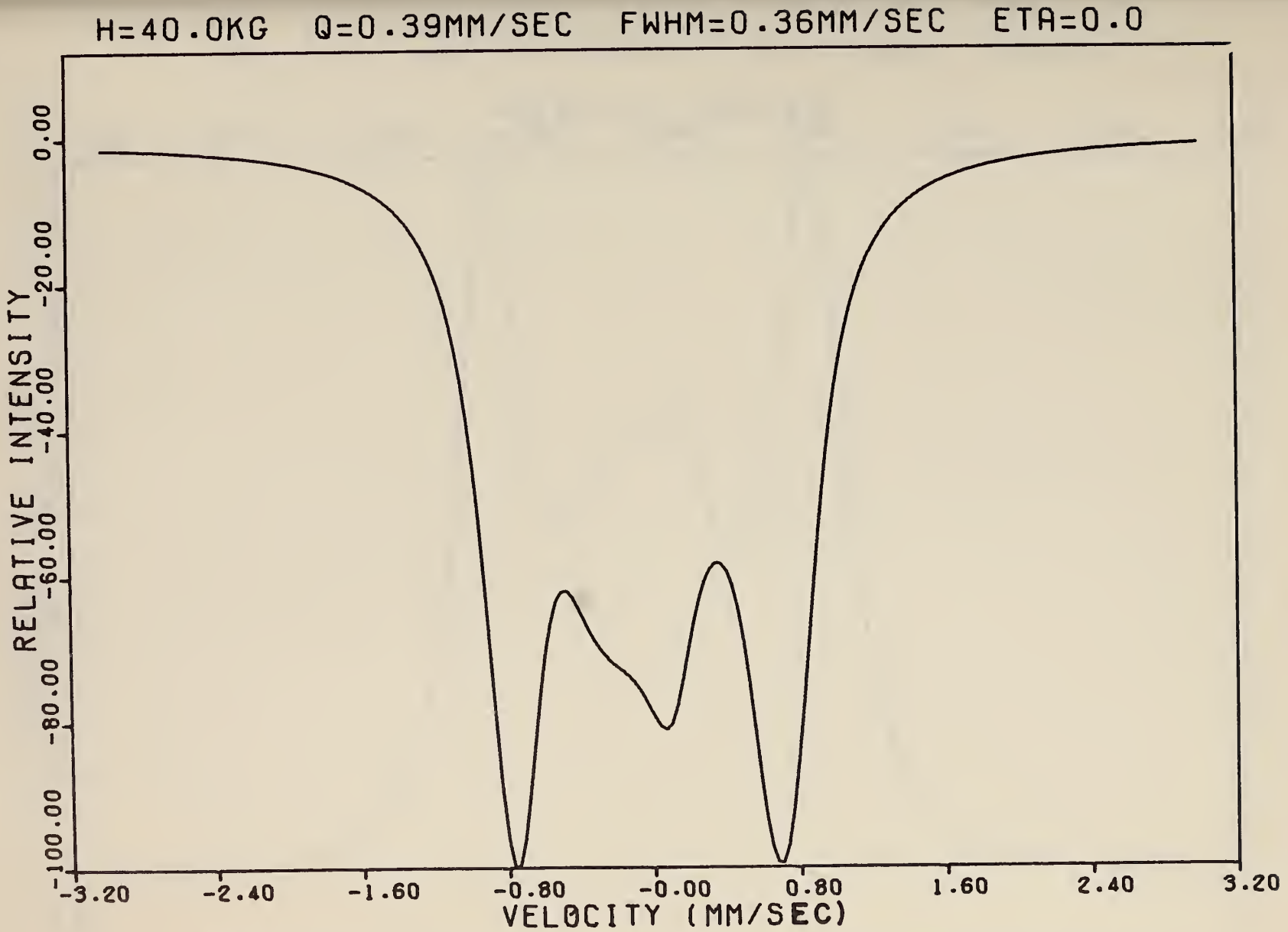

Figure V-1(a). Theoretically generated spectrum for combined longitudinal magnetic field and randomly oriented electric field gradient.

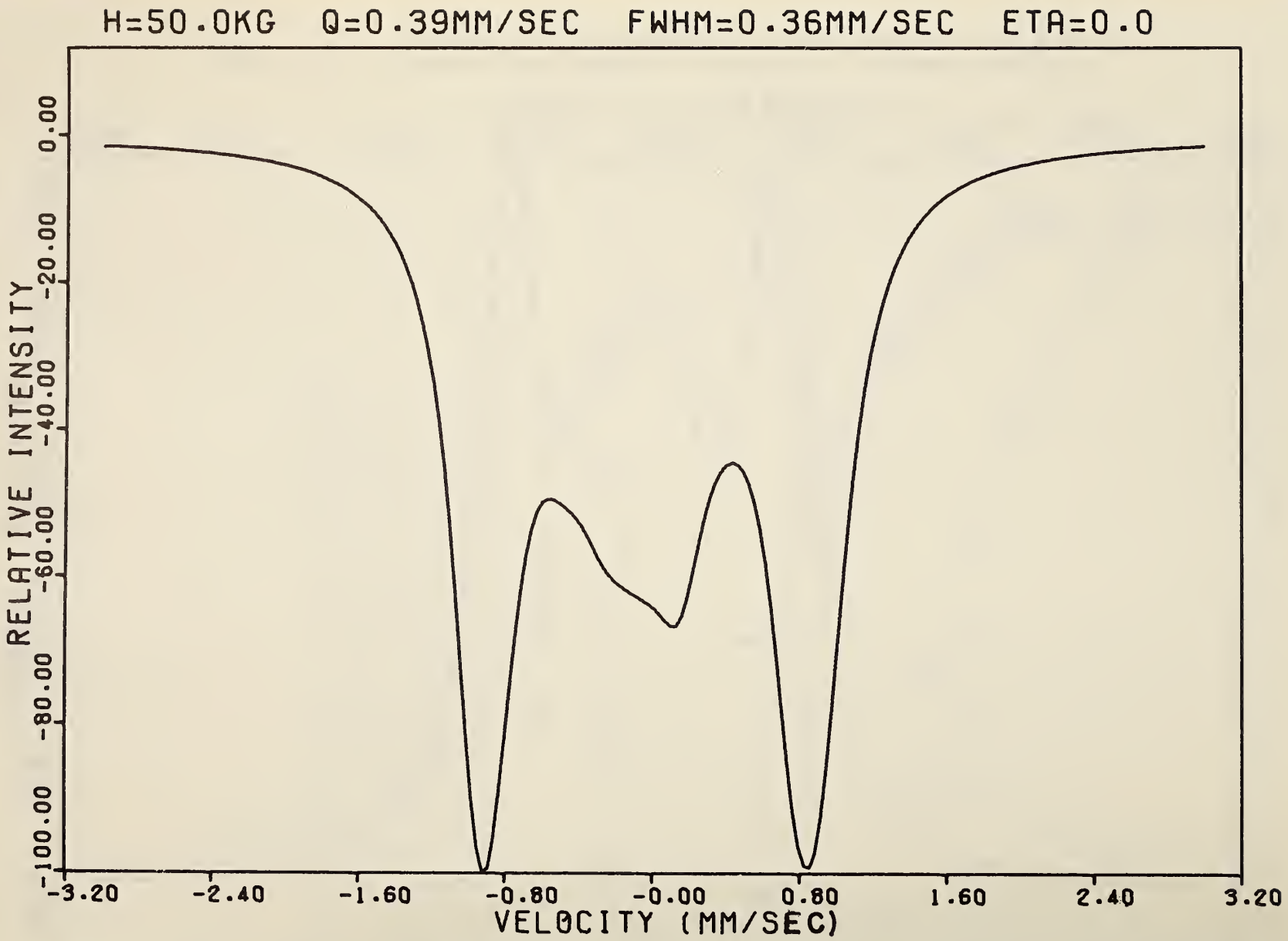

Figure V-1(b). Theoretically generated spectrum for combined longitudinal magnetic field and randomly oriented electric field gradient.

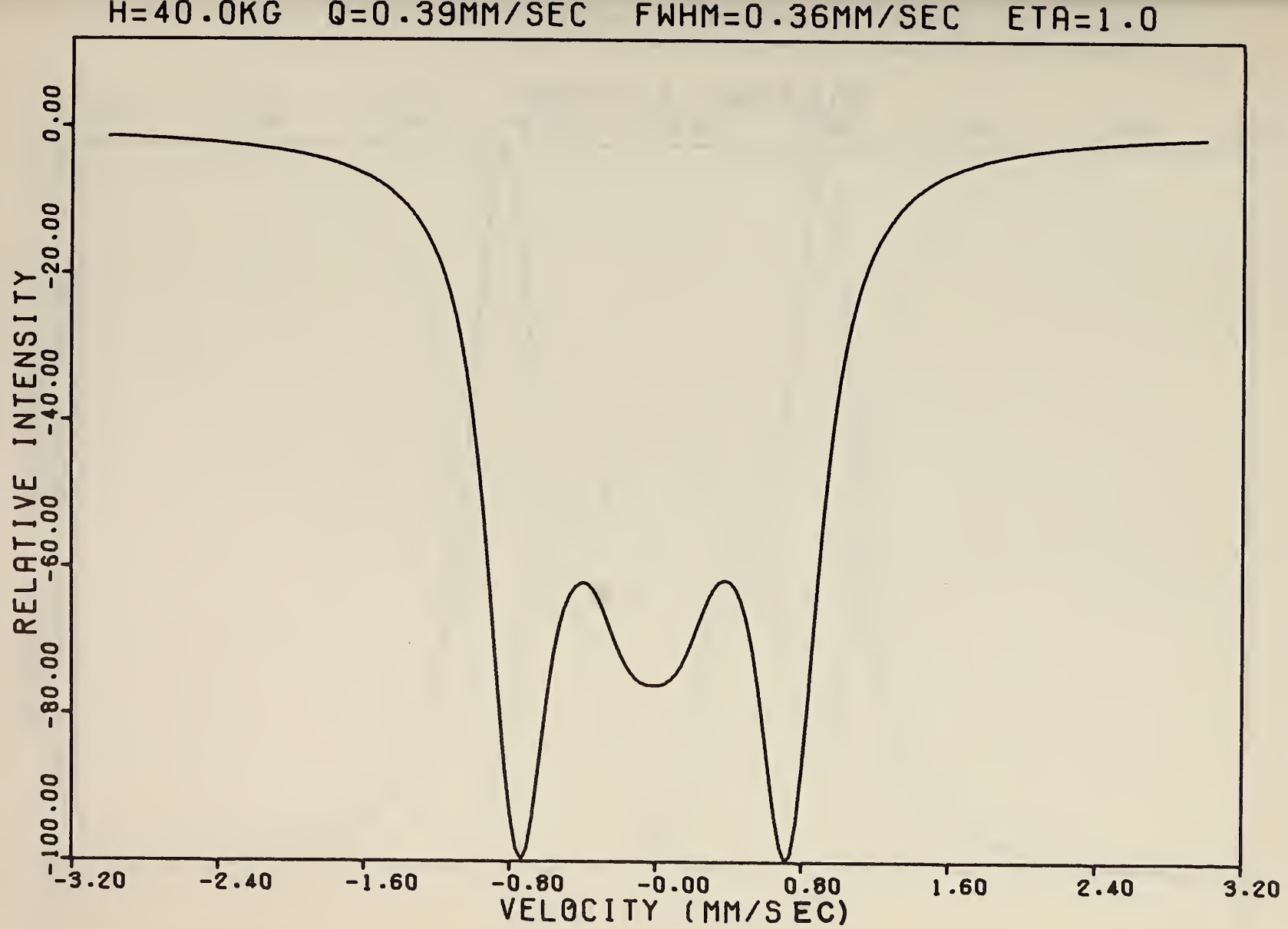

Figure V-1(c). Theoretically generated spectrum for combined longitudinal magnetic field and randomly oriented electric field gradient.

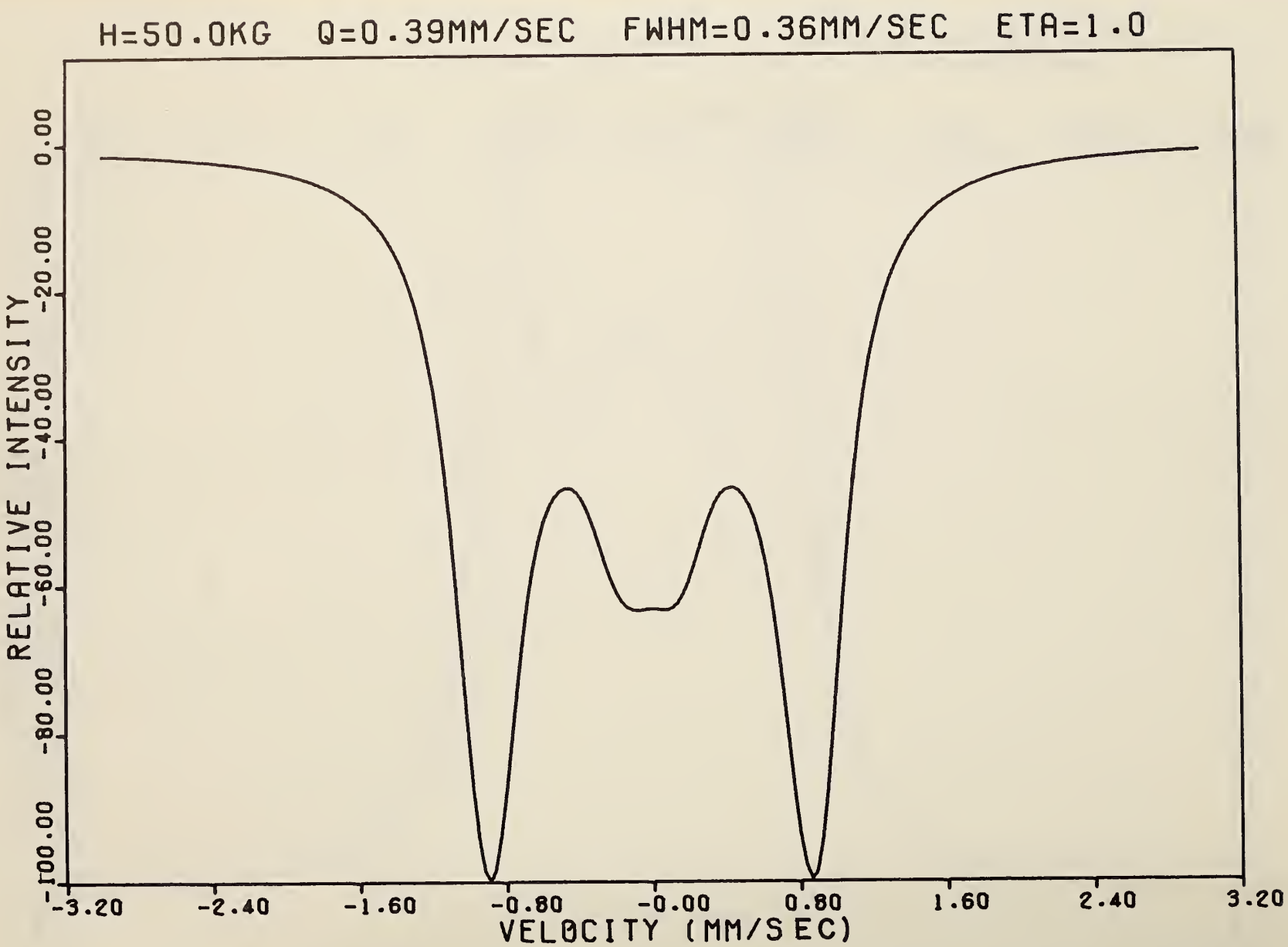

Figure V-1(d). Theoretically generated spectrum for combined longitudinal magnetic field and randomly oriented electric field gradient.

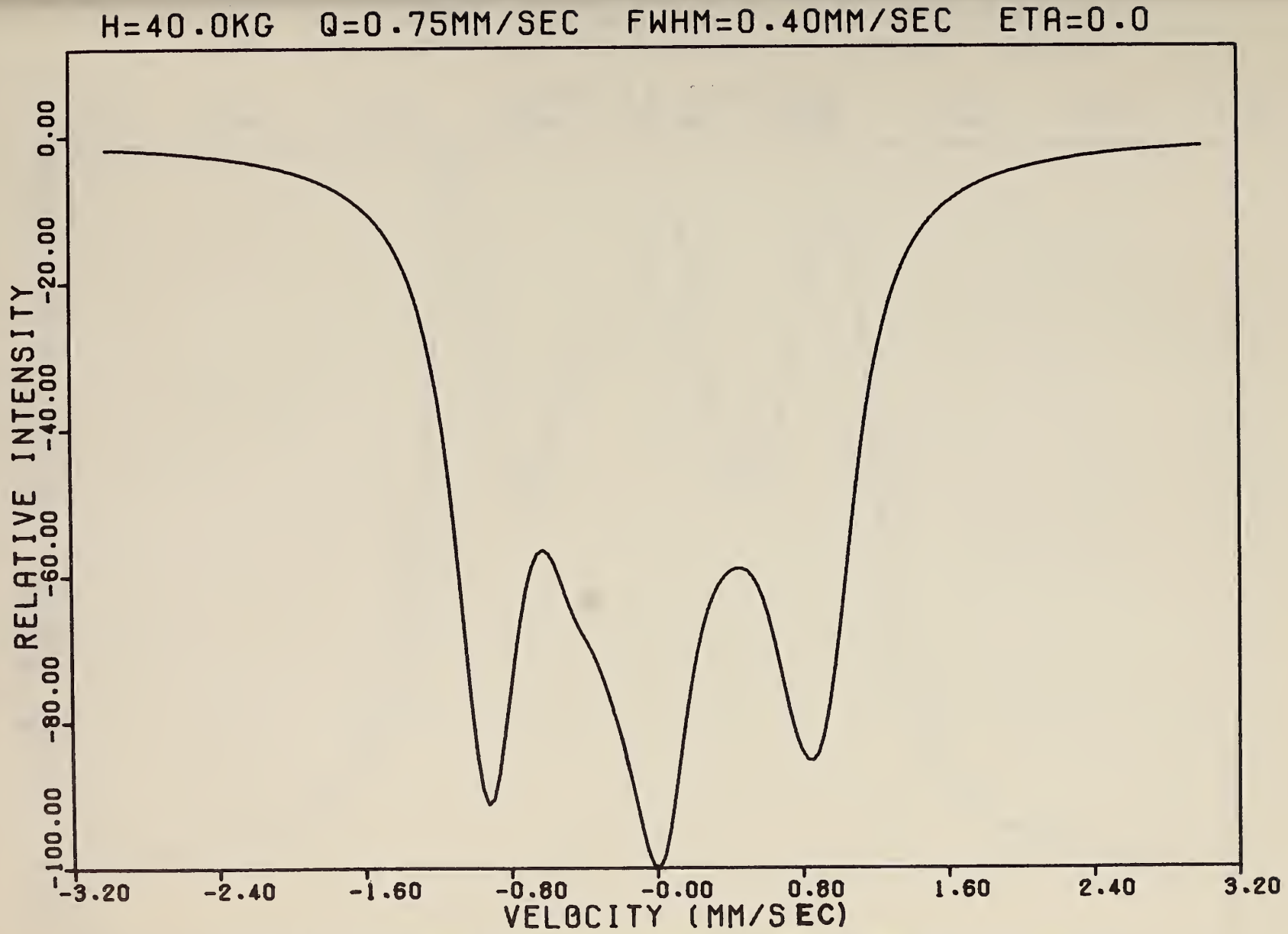

Figure V-1(e). Theoretically generated spectrum for combined longitudinal magnetic field and randomly oriented electric field gradient.

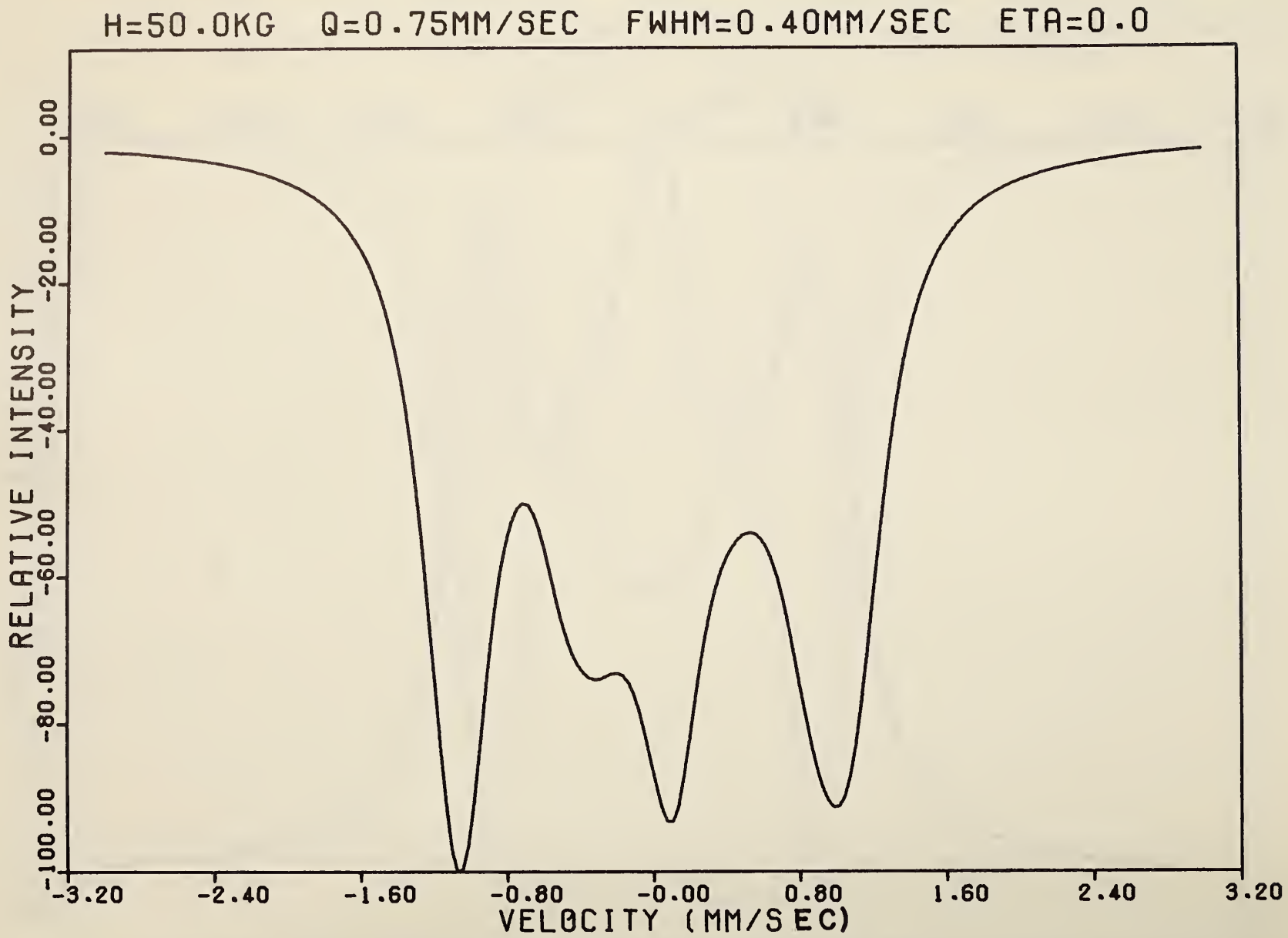

Figure V-1(f). Theoretically generated spectrum for combined longitudinal magnetic field and randomly oriented electric field gradient.

NBS TECHNICAL PUBLICATIONS

PERIODICALS

JOURNAL OF RESEARCH reports National Bureau of Standards research and development in physics, mathematics, chemistry, and engineering. Comprehensive scientific papers give complete details of the work, including laboratory data, experimental procedures, and theoretical and mathematical analyses. Illustrated with photographs, drawings, and charts.

Published in three sections, available separately:

• Physics and Chemistry

Papers of interest primarily to scientists working in these fields. This section covers a broad range of physical and chemical research, with major emphasis on standards of physical measurement, fundamental constants, and properties of matter. Issued six times a year. Annual subscription: Domestic, $5.00; foreign, $6.00*.

• Mathematical Sciences

Studies and compilations designed mainly for the mathematician and theoretical physicist. Topics in mathematical statistics, theory of experiment design, numerical analysis, theoretical physics and chemistry, logical design and programming of computers and computer systems. Short numerical tables. Issued quarterly. Annual subscription: Domestic, $2.25; foreign, $2.75*.

• Engineering and Instrumentation

Reporting results of interest chiefly to the engineer and the applied scientist. This section includes many of the new developments in instrumentation resulting from the Bureau's work in physical measurement, data processing, and development of test methods. It will also cover some of the work in acoustics, applied mechanics, building research, and cryogenic engineering. Issued quarterly. Annual subscription: Domestic, $2.75; foreign, $3.50*.

TECHNICAL NEWS BULLETIN

The best single source of information concerning the Bureau's research, developmental, cooperative and publication activities, this monthly publication is designed for the industry-oriented individual whose daily work involves intimate contact with science and technology—*for engineers, chemists, physicists, research managers, product-development managers, and company executives.* Annual subscription: Domestic, $1.50; foreign, $2.25*.

*Difference in price is due to extra cost of foreign mailing.

NONPERIODICALS

Applied Mathematics Series. Mathematical tables, manuals, and studies.

Building Science Series. Research results, test methods, and performance criteria of building materials, components, systems, and structures.

Handbooks. Recommended codes of engineering and industrial practice (including safety codes) developed in cooperation with interested industries, professional organizations, and regulatory bodies.

Special Publications. Proceedings of NBS conferences, bibliographies, annual reports, wall charts, pamphlets, etc.

Monographs. Major contributions to the technical literature on various subjects related to the Bureau's scientific and technical activities.

National Standard Reference Data Series. NSRDS provides quantitative data on the physical and chemical properties of materials, compiled from the world's literature and critically evaluated.

Product Standards. Provide requirements for sizes, types, quality and methods for testing various industrial products. These standards are developed cooperatively with interested Government and industry groups and provide the basis for common understanding of product characteristics for both buyers and sellers. Their use is voluntary.

Technical Notes. This series consists of communications and reports (covering both other agency and NBS-sponsored work) of limited or transitory interest.

CLEARINGHOUSE

The Clearinghouse for Federal Scientific and Technical Information, operated by NBS, supplies unclassified information related to Government-generated science and technology in defense, space, atomic energy, and other national programs. For further information on Clearinghouse services, write:

Clearinghouse
U.S. Department of Commerce
Springfield, Virginia 22151

Order NBS publications from:
Superintendent of Documents
Government Printing Office
Washington, D.C. 20402

U.S. DEPARTMENT OF COMMERCE
WASHINGTON, D.C. 20230

OFFICIAL BUSINESS

POSTAGE AND FEES PAID
U.S. DEPARTMENT OF COMMERCE